DOCTORAL THESIS IN BIOMEDICAL TECHNOLOGIES

(CYCLE XXVII)

UNIVERSITY OF MILANO-BICOCCA

Coordinator: Prof.ssa M. Del Puppo

PET IMAGING AS A BIOMARKER OF TUMOR RESPONSE TO THERAPY

Student: Isabella Raccagni

Supervisor: Prof.ssa Rosa Maria Moresco

2013/2014

ABSTRACT

Molecular imaging allows the non-invasive visualization and characterization of biological processes. It can be used in oncology to identify biomarkers for the evaluation of tumor progression and response to therapy. In this thesis work, the animal PET was used as a potential biomarker of tumor response to therapy focusing on altered metabolism and hypoxia in a) a model of oncogenic k-ras and b) in a model of glioma.

Metabolic alterations, such as increased glycolysis and glutamine consumption, are associated with mutations in k-ras gene. The decoupling of glucose and glutamine uptake leads to a reprogramming of their metabolism to support cell proliferation representing a target for cancer therapy. The aim of this study is to investigate metabolic alterations in k-ras transformed fibroblasts (NIH-RAS) in *in vivo* studies and to assess response to therapy.

Animals subcutaneously implanted with NIH-RAS performed [^{18}F]FDG- and [^{18}F]FLT-PET at several time points to evaluate glucose metabolism and cell proliferation, respectively. Tumors were collected and evaluated for different markers by immunohistochemistry (IHC) to confirm *in vivo* results. In the same model, the efficacy of chloroquine (autophagy blocker) and BPTES (glutaminase inhibitor) alone or in combination was monitored by [^{18}F]FDG- and [^{18}F]FLT-PET before and 48 hours after treatments. All animals developed fast growing and highly glycolytic tumors in few days that appear homogeneous for both [^{18}F]FDG and [^{18}F]FLT uptake. PET imaging showed a significant increase in [^{18}F]FDG uptake while cell proliferation remained stable over time, as depicted by [^{18}F]FLT uptake. IHC analyses confirmed the high aggressiveness of these cells.

Chloroquine and BPTES combined treatment slowed down tumor growth only if compared to vehicle, without affecting glucose metabolism or cell proliferation. The presence of alternative pathways for glutamate production and the need of higher doses of treatments may provide explanations to the lack of treatments' efficacy.

Hypoxia is implicated in many aspects of tumor progression and it is involved in the intracellular stabilization of the hypoxia regulator gene HIF-1α. Since the expression of HIF-1α is associated with poor prognosis and therapy resistance in glioblastoma, a better comprehension of its involvement in tumor response to treatment can be of great interest for clinical translation.

U251-HRE-mCherry cells expressing Luciferase under control of a Hypoxia Responsive Element (HRE) and mCherry under the control of a constitutive promoter have been used to assess HIF-1α modulation and cell survival after treatment, both *in vitro* and *in vivo*.

In vivo analyses characterized the model obtained by stereotaxic injection ofglioma U251-HRE cells in mice brain. Tumor progression was monitored comparing bioluminescence, fluorescence and PET

with [^{18}F]FAZA and [^{18}F]FLT. Afterwards, two regimens of temozolomide (TMZ) were administered starting 21 days after cells injection. TMZ efficacy was monitored by optical and fluorescence imaging, [^{18}F]FLT-PET and MRI. Bioluminescent signals provided information about tumor growth and hypoxia presence, confirmed by both fluorescence acquisition and [^{18}F]FAZA PET. IHC for Ki67 confirmed data obtained by [^{18}F]FLT-PET, showing a high rate of cell proliferation.

Both TMZ regimens showed a decrease of HIF-1α-dependent Luciferase activity at early time after TMZ administration. On the contrary, mCherry fluorescence, such as [^{18}F]FLT uptake, decreased only at the end of treatments.

HIF-1α activity reduction can be considered a biomarker of tumour response to TMZ and the U251-HRE-mCherry cell model a feasible tool to evaluate HIF-1α activity and treatment effects in *in vivo* studies.

SOMMARIO

Le tecniche di imaging molecolare permettono di visualizzare e caratterizzare processi biologici e rivestono un ruolo fondamentale in oncologia, consentendo di identificare marcatori per la diagnosi e la risposta al trattamento. In questo lavoro di tesi è stato valutato il ruolo della PET come possibile marcatore di risposta al trattamento in a) un modello con k-ras oncogenico e b) un modello di glioma, focalizzando l'attenzione sulle alterazioni del metabolismo e l'ipossia.

L'incremento della glicolisi e del consumo di glutammina sono associati a mutazioni dell'oncogene ras in diversi tumori. Il disaccoppiamento di tali processi determina una riprogrammazione del metabolismo per supportare l'aumentata proliferazione fornendo un interessante target terapeutico. Scopo dello studio è la valutazione *in vivo* delle alterazioni metaboliche e della risposta alla terapia nel modello ottenuto mediante inoculo di fibroblasti con k-ras oncogenico (NIH-RAS). A tale scopo gruppi di topi sono stati monitorati longitudinalmente mediante PET-[^{18}F]FDG e [^{18}F]FLT per la valutazione del metabolismo glucidico e della proliferazione cellulare. I tumori sono stati sottoposti ad analisi immunoistochimiche per confermare i dati ottenuti *in vivo*. Nello stesso modello è stato valutato l'effetto di un inibitore dell'autofagia (Clorochina) e della glutaminasi (BPTES) singolarmente e in combinazione mediante PET-[^{18}F]FDG e [^{18}F]FLT. Gli animali hanno sviluppato in breve tempo tumori glicolitici e caratterizzati da un'omogenea captazione di [^{18}F]FDG e [^{18}F]FLT. Le immagini PET hanno mostrato un aumento della captazione di [^{18}F]FDG nel tempo e un andamento stabile della proliferazione come mostrato dalla costante captazione di [^{18}F]FLT. Clorochina e BPTES in combinazione hanno determinato un rallentamento della crescita tumorale rispetto ai controlli, ma non sono state osservate variazioni nella captazione di [^{18}F]FDG e [^{18}F]FLT. La presenza di vie alternative per la produzione di glutammato e la necessità di dosi più elevate potrebbero spiegare l'assenza di efficacia di questi trattamenti.

L'ipossia rappresenta un fenomeno sfavorevole per la progressione tumorale. L'espressione di HIF1α, principale regolatore dell'ipossia, è associata alla resistenza alla terapia in molti tumori, compreso il glioma. Per questo, una migliore comprensione della modulazione dell'attività di HIF1α nel processo di risposta alla terapia è di particolare interesse.
Cellule di glioma U251-HRE-mCherry in grado di esprimere l'enzima luciferasi sotto il controllo di HRE (Hypoxia Responsive Element) e mCherry sotto controllo di un promotore costitutivo sono state utilizzate per valutare la modulazione di HIF1α in seguito a trattamento con Temozolomide (TMZ) *in vitro* e *in vivo*. La crescita tumorale è stata monitorata *in vivo* in animali sottoposti ad inoculo intracerebrale tramite bioluminescenza, fluorescenza, RM e PET con [^{18}F]FAZA e [^{18}F]FLT. In seguito, è stato valutato in vivo l'effetto di due diversi regimi di TMZ. Mediante bioluminescenza è stato possibile monitorare la crescita tumorale e identificare aree ipossiche. I dati ottenuti sono stati

confermati dalle immagini di fluorescenza e PET-[^{18}F]FAZA. Le analisi ex vivo per Ki67 hanno invece confermato i dati PET-[^{18}F]FLT ed hanno mostrato un'elevata proliferazione cellulare. Entrambi i dosaggi di TMZ hanno determinato una diminuzione dell'attività di HIF1α a tempi precoci. Al contrario, il segnale di fluorescenza e la captazione di [^{18}F]FLT hanno subìto una diminuzione solo a tempi più tardivi.

L'attività di HIF1α può essere considerata un marcatore di risposta al TMZ e questo modello un utile strumento per la valutazione in vivo di farmaci per il trattamento del glioma.

LIST OF SYMBOLS

[^{18}F]FAZA	[F-18]Fluoroazomycin-arabinofuranoside
[^{18}F]FDG	2-[F-18]Fluorine-2-Deoxy-D-glucose
[^{18}F]FLT	[F-18]Fluorine-Levo-thymidine
[^{18}F]FMISO	[18F]FluoroMISOnidazolo
[64Cu]ATSM	[64Cu]diacetyl-bis(N^4-methylthiosemicarbazone)
1H-MRS	Proton magnetic spectroscopy
2-HG	2-HydroxyGlutarate
a-KG	a-KetoGlutarate
ACC	Acetyl-CoA Carboxylase
ACL	ATP Citrate Lyase
AKT	Activated Kinases Theronine
AML	Acute Myeloid Leukemia
AMPK	Adenosine MonoPhosphate–activated Protein Kinase
ARNT	Arylhydrocarbon Receptor Nuclear Translocator
BBB	Blood Brain Barrier
BLI	BioLuminescence Imaging
BPTES	Bis-2-(5-Phenyleacetamido-1,2,4-Thiadiazol-2-yl) Ethyl Sulfide 3
CAIX	Carbonic Anhydrase IX
CBV	Cerebral Blood Volume
CCD	Charge-Coupled Device
CQ	ChloroQuine
CT	Computed Tomogrphy
CXCR4	C-X-C chemokine Receptor type 4
DAB	3, 3'-Diaminobenzidine
DCE-MRI	Dynamic Contrast Enhanced - MRI
dNTP	DeoxyNucleotide TriPhosphate
DFX	DeFeroXamine
DSC-MRI	Dynamic Susceptibility Contrast - MRI
dTMP	deoxyThymidine MonoPhosphate
dTTP	deoxyThymidine TriPhosphate
dUMP	deoxyUridine MonoPhosphate
DW-MRI	Diffusion Weigthed MRI
EDTA	EthyleneDiamineTetraacetic Acid
EGFR	Epidermal Growth Factor Receptor
EM	Expected Maximization
EORTC	European Organisation for Research and Treatment of Cancer
FAS	Fatty Acid Synthase
FDG	^{18}F-fluorine-2-deoxy-D-glucose
FGF	Fibroblast Growth Factor
FLK-1	Fetal Liver Kinase 1
FLIT	Fluorescence Imaging Tomography
fMRI	Functional MRI
GAP	GTPase Activating Protein
GBM	GlioBlastoma Multiforme
GC	Gas Chromatography
GC-MS	GC–Mass Spectrometry
GDH	Glutamate DeHydrogenase
GEF	Guanine-nucleotide Exchange Factors
GEF-DN	GEF Domain Negative
GLS	GLutaminaSe
GLUT	GLUcose Transporter
GOT	Glutamate Oxaloacetate Transaminase
H&E	Hematoxiline & Eosin

HIF-1α	Hypoxia Inducible Factor 1á
HK	HexoKinases
HLHZ	Helix Loop Helix Zipper
HRE	Hypoxia Responsive Element
IHC	ImmunoHistoChemistry
IDH	Isocitrate DeHydrogenase
LDHA	Lactate DeHydrogenase A
LKB1	Liver Kinase B1
LOH	Loss Of Heterozigosis
MAPK	Mitogen Activated Protein Kinase
MDH	Malate DeHydrogenase enzyme
ME	Malic Enzyme
MFA	Metabolic Flux Analysis
MGMT	MethylGuanine MethylTransferase
MMp	Metalloproteinases
MRI	Magnetic Resonance Imaging
MRS	Magnetic Resonance Spectroscopy
MS	Mass Spectrometry
mTOR	mammalian Target Of Rapamycin
mTORC	Mammalian Target Of Rapamycin Complex
NADP	Nicotinamide Adenine Dinucleotide Phosphate
NIRF	Near-InfraRed Fluorescence
NMR	Nuclear Magnetic Resonance
NTFD	Non-targeted Tracer Fate Detection
OAA	Oxalacetate
OXPHOS	OXidative PHOSphorylation
PAI-1	Plasminogen Activator Inhibitor-1
PBS	Phosphate-Buffered Saline
PC	Pyruvate Carboxylase
PDGF-B	Platelet Derived Growth Factor B
PDGFRA	Alpha-type Platelet Derived Growth Factor Receptor
PDH	Pyruvate DeHydrogenase
PDK1	Pyruvate Dehydrogenase Kinase 1
PEP	PhosphoEnolPyruvate
PET	Positron Emission Tomography
PGK	PhosphoGlycerate Kinase
PHD	Proline Hydroxylases Domain
PI3K	Phosphatidylinositol 3-Kinase
PPP	Pentose Phosphate Pathway
PTEN	Phosphatase and TENsin homolog
RB	RetinoBlastoma
ROI	Region Of Interst
ROS	Reactive Oxygen Species
RTK	Receptor Tyrosine Kinases
SD	Standard Deviation
SDF-1	Stromal Derived Factor 1
SOS	Son Of Sevenless
SREBP	Sterol Regulatory Element-Binding Protein
SUV	Standardized Uptake Value
T/B	Tumor/Background
TK1	Thymidine Kinase 1
TMZ	Temozolomide
TS	Thymidylate Synthase
TSC	Tuberous Sclerosis Complex
TSP1	ThromboSPondin-1

VEGF	Vascular Endothelial Growth Factor
VHL	Von Hippel-Lindau
WHO	World Health Organization

TABLE OF CONTENTS

1. INTRODUCTION

1.1 The hallmarks of cancer

Tumour can be considered as a complex disease arising from mutational events and altered signalling pathways that support cancer cells growth and survival.

In 2000s, in order to rationalize the complexity of neoplastic disease, Hanhan and Weinberg described six phenotypic hallmarks shared by cancer cells (Figure 1). These cancer hallmarks represent capabilities that normal cells progressively acquired during the complex process that leads them to become tumorigenic and, ultimately, malignant and include: sustaining proliferative signalling, evading growth suppressors, resisting cell death, enabling replicative immortality, inducing angiogenesis and activating invasion and metastasis [1].

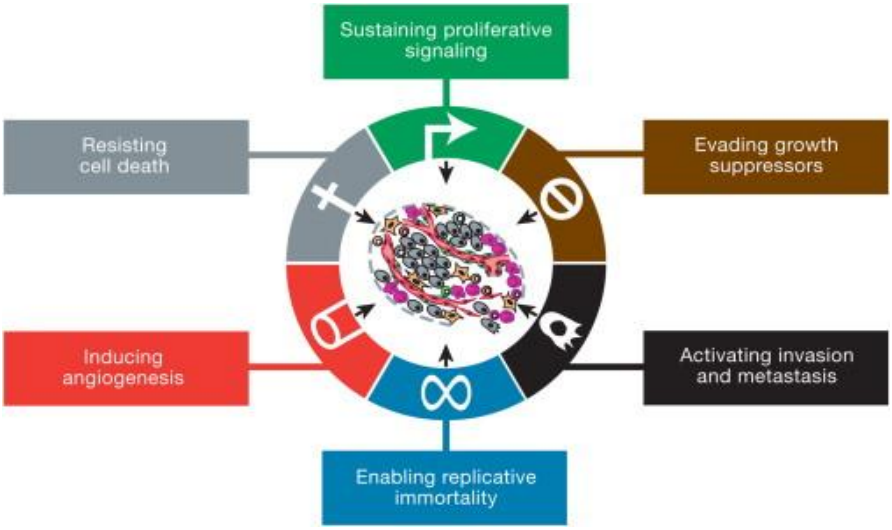

Figure 1 The hallmarks of cancer. *The six hallmark capabilities proposed in 2000 by Hanahan (Hanahan D., Hallmarks of cancer: the next generation. Cell, 2011).*

1.1.1 Sustaining proliferative signaling

The main feature of cancer cells is their ability to proliferate autonomously. Cancer cells activate an autocrine signalling pathway for proliferation through the autonomous production of growth factors. Moreover, the stimulation of normal cells of the stroma to release growth factors contributes to the sustained proliferation of cancer cells. Finally, cancer cells take advantage from the increased levels of surface receptors for growth factors and from mutations that together make components of signalling pathways constitutively active regardless the presence of ligand-binding stimulation.

1.1.2 Evading growth supressors

To maintain the high rate of proliferation, cancer cells have to contrast the pathways that negatively regulate cells proliferation acquiring the ability to evade growth suppressor. The negative regulation of proliferation depends on the role of tumour suppressors that result inactive in many cancers. RB (retinoblastoma-

associated) and p53 represent the central system of this regulation, being responsible of important circuits that lead to proliferation or, alternatively, to senescence and cells death [2]. Tumors often display defects in these genes that contribute to the uncontrolled proliferation. Moreover, while normal cells homeostasis is controlled by contact inhibition that sequesters growth factor receptors and inhibits mitogenic effects, cancer cells show downregulated expression of these pathways and adhesion molecules.

1.1.3 Resisting cell death

Resisting cells death represents another hallmark cancer cells exhibit to obtain a survival advantage.

The activation of programmed cells death is triggered by stress condition and it is mainly regulated by the tumor suppressor Tp53. Tp53 is the main critical damage sensor that, through the transcription of genes as Puma and Noxa, induces the apoptotic state when the amount of damaged DNA is too elevated to be repaired. In tumor cells the apoptotic process is limited by the loss of theTp53 function,the increase of antiapoptotic regulators (Bcl-2) and survival signals (Igf1/2).

Another way used by cells to contrast stress is autophagy. In stressful conditions and nutrient deprivation, the autophagic program enables cells to break down organelles through the formation of autophagosomes. This process allows cells to obtain catabolites useful for the biosynthesis of nutrients to support survival. How cancer cells regulate autophagy is not yet fully understood If on one hand it seems to prevent cancer progression facilitating DNA repair, on the other hand it seems to be cytoprotective for cancer cells exposed to therapies. In fact, some cancer cells reach a state of dormancy that confer to them an advantage to resist to the action of radio and chemo therapy through autophagy [3].

In contrast to apoptotic and autophagic processes, necrotic cell death does not contrast the increased proliferation, but provides cancer cells several advantages promoting tumorigenesis. Indeed, necrosis triggers the release of pro inflammatory signals in the surrounding microenvironment that facilitates the recruitment of immune cells. All together these factors can stimulate viable cells of the stroma to proliferate helping tumor progression [4].

1.1.4 Enabling replicative immortality

Differently from normal cells which pass only through limited number of growth/division cycles, cancer cells require unlimited replicative potential to proliferate and promote tumor progression. Telomeres are known to protect the end of chromosome, shortening at each division cycle until cell undergoes into its crisis phase and seem to be involved in the mechanism of unlimited replicative immortality. The immortalization capability is attributed to the activation of the DNA polymerase telomerase that is responsible for the regeneration of telomeres adding segments of nucleotides. While in normal cells this enzyme is inactivated,telomerase activity is achieved after the pre-malignant state of cancer, when the cell has accumulated an aberrant karyotype, and its activation fosters cancer progression with proliferative ability [5].

1.1.5 Sustained angiogenesis

In order to sustain nutrients and oxygen supply, cancer cells promote the formation of neo-vasculature through the angiogenesis process. Angiogenesis implies the sprouting of new blood vessels from the existing ones leading to the formation of the new vascularisation characterized by leak, distorted and enlarged blood vessels. This process, which is only transiently activated in the adult, appears constantly activated in tumor progression to help expansion and growth [6]. The angiogenic switch is mainly regulated by pro angiogenic factors like VEGF (vascular endothelial growth factor) and FGF (fibroblast growth factor) that are upregulated in cancer cells and anti angiogenic factors such as TSP1 (thrombospondin-1) that are not sufficient to counteract the pro-angiogenic process.

In tumor cells, VEGF is upregulated by the action of oncogenes or by hypoxia conditions, while FGF exerts the same function of VEGF when upregulated in cancer cells [7].

1.1.6 Activating invasion and metastasis

Cancer cells develop the ability to migrate from their primary site and disseminate and colonize other tissues in the body. Invasion and metastasis can be described as a sequence of processes that begins with the local invasion, intravasion into blood and lymphatic vessels by cancer cells, transit through the hematogenous and lymphatic systems and finally escape the lumina of the vessels into the parenchyma of distant tissues with formation of metastasis [2]. This process is associated both to mutations causing alterations in cells attachment to extracellular matrix and to the action of other molecules that allow cells to be motile and invasive such as matrix-degrading enzymes. Macrophages inducing the production of metalloproteinases (MMp) able to degrade the extracellular matrix also contribute to enhance cancer cells invasion and motility.

1.1.7 Enabling characteristics: genomic instability and tumor inflammation

The capability of cancer cells to survive, proliferate and disseminate described above depends in large part on several alterations in the genome of neoplastic cells. Genomic instability is considered as an enabling characteristic of cancer cells which triggers the acquisition of a mutant genotype that allows cancer cells to obtain a selective advantage.

Another enabling characteristic is represented by the tumor-associated inflammation driven by the immune system that is known to contribute to many hallmarks capabilities supplying molecules to the tumor microenvironment including growth factors, survival factors, pro angiogenic factors and reactive oxygen species. Inflammation in most cases becomes evident in the early stages of disease, fostering the development of cancer and representing an intriguing target for contrasting tumor [2].

1.1.8 Emerging hallmarks: energy metabolism and avoiding immunity

Recently, two new features have been considered as hallmarks of cancer: avoiding immune destruction and reprogramming cellular energy metabolism. The immune system is known to both antagonize and enhance tumorigenesis. Cancer cells develop the ability to evade from the elimination operated by immune cells

favouring their survival and proliferation [2]. Deregulating cell energy pathways cooperates to support continuous cell growth and proliferation, replacing the metabolic program that works in normal tissue and providing a promising therapeutic target, as described in the following sections.

1.2 Metabolic reprogramming

To feed the high levels of proliferation, cancer cells require large amount of nutrient, energy and biosynthetic activity. To meet this need, tumour cells reprogram their metabolism during tumor progression. Increased uptake of glucose together with enhanced glutamine uptake and metabolism supports the production of intermediates for lipids, protein and nucleotides synthesis. Moreover, genetic mutations in oncogenes as well as in oncosuppressors and environmental conditions (hypoxia or inflammation) have been shown to cooperate in generating the malignant phenotype [8].

Since cancer cells have to adjust their sources for fronting this highly energy request, metabolic activity of proliferating cells appears different from that of non-proliferating cells.

In this view, a better understanding of the differences that characterize the metabolism of cancer cells compared to that of normal ones could provide a new strategy for developing new, specific and effective anticancer drugs [9].

1.2.1 The Warburg effect

In 1920s Otto Warburg explained the first metabolic adaptation occurring in solid tumours. He observed that differently from normal, proliferating and cancer cells generate more than the 50% of energy from the metabolism of glucose to lactic acid, both in the presence and absence of oxygen (Figure 2). This phenomenon, known as aerobic glycolysis or as the 'Warburg effect", is characterized by elevated glucose uptake and increased glycolytic rate.

Although aerobic glycolysis is less efficient than the oxidative phosphorylation (OXPHOS) in terms of ATP molecules production, it has been suggested that tumour cells with glycolytic metabolism progress rapidly because of their competitive advantage over their normal counterparts [9]. Several explanations have been proposed for this phenomenon.

The enhanced glycolytic flux guarantees a high amount of resources (i.e. glucose) and allows cancer cells to do not undergo into apoptotic processes, even in the presence of such low production of ATP molecules. Hence, the production of ATP molecules reaches or also exceeds the one deriving from the oxidative phosphorylation. This would ensure the ATP levels satisfy the demands of highly proliferating cells [9, 10].

The principal end product of aerobic glycolysis, lactate, provides acidic conditions causing the environment to favour tumour invasion and suppress anticancer immune effectors. Finally, accelerated glycolysis provides a constant supply of metabolic intermediates of the glycolytic pathway necessary for anabolic reactions.

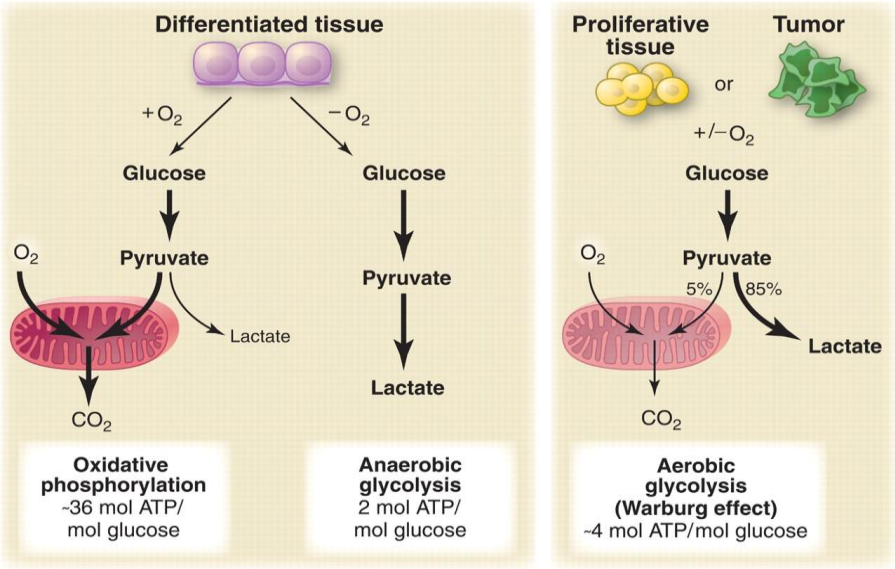

Figure 2 Metabolic differences between normal and proliferative/cancer cells. *Normal cells mainly metabolize glucose to pyruvate for growth and survival followed by oxidation of pyruvate to CO_2 through the TCA cycle in oxygen conditions (OXPHOS). When O_2 is low cells redirect pyruvate outside from TCA to generate lactate (anaerobic glycolysis). Cancer cells conver most of glucose to lactate regardless the availability of O_2 allowing glycolysis to continue with minimal ATP production. (Vander Heiden G., Science, 2009, 324, 5930 1029-1033).*

The two major biosynthetic requirements for proliferating cells are the production of ribose-5-phosphate (R5P) for nucleotide biosynthesis and fatty acid for lipid biosynthesis. For R5P generation cells divert carbon from glycolysis into the oxidative or non-oxidative arms of the Pentose Phosphate Pathway (PPP). This pathway consists in two main ways: the oxidative branch and the non-oxidative branch.

In the *oxidative branch*, G6P after few enzymatic passages is converted into ribulose-5-phosphate, producing 2 NADPH molecules and CO_2; ribulose-5-phosphate then can be used for nucleotide synthesis when converted into ribose-5-phosphate.

Tumor cells are highly replicative cells, and the higher is the proliferation, the greater is the need of nucleotide synthesis; in fact, PPP provides 2 NADPH molecules, not only required for nucleotides synthesis, but also for other biosynthetic processes, such as lipid synthesis. Moreover, NADPH is necessary for restoring one of the main antioxidant molecules, glutathione (GSH): in fact NADPH is the substrate of glutathione reductase enzyme (GSR), which reduces the oxidized form of glutathione. This is a strategy adopted by highly proliferative cells for buffering oxidative action of ROS (reactive oxygen species), mostly produced in the TCA cycle, due to the high macromolecular biosynthesis rate and O_2 consumption [11].

In the *non-oxidative branch*, ribose 5-phosphate undergoes several reactions, resulting into production of fructose-6-phosphate and glyceraldehyde-3-phosphate, which can be reintroduced in the glycolytic pathway or into PPP for more nucleotide *de novo* synthesis [11].

The PPP is particularly critical for cancers because it provides pentose phosphates for nucleotides biosynthesis and represents the main source of NADPH that is required for both the fatty acids biosynthesis and cell survival under stress conditions. In fact, the reversible reduction of glucose-6-phosphase (G6P) by G6P dehydrogenase is associated with reduction of NADP to NADPH, an important dropping agent for

several reactions including fatty acid synthesis. Beyond the NADPH productions fatty acids synthesis requires anaplerotic reactions which give cells the ability to use the TCA cycle as a supply for biosynthetic precursors. Differently from non-proliferating cells, in which the TCA serves as ATP source from oxidable substrates, in cancer cells TCA is considered a source of molecules for biosynthesis. The export of citrate from the mithocondria and its subsequently conversion into OAA and lipogenic precursor Acetil CoA for fatty acids synthesis must be compensated by the replacement of OAA molecules through anaplerosis. If this does not happen, citrate synthesis cannot continue. Cells can produce anaplerotic activity generating OAA directly from pyruvate using Pyruvate Carboxylase (PC) or, alternatively, through the metabolism of amino acids, particularly glutamine [10].

So Warburg effect seems to be the preferential strategy in cancer for its advantages in bioenergetics and biosynthetic pathways, and also for reactions' speed: the V_{max} of glycolysis and lactate production overtake the V_{max} of PDH. High glycolytic flux can provide energy and metabolic precursors to rapidly proliferating cells in a faster way if compared to a complete pyruvate oxidation; moreover, LDH-A (lactate dehydrogenase A) is the system that avoids pyruvate accumulation in this pathway by converting it into lactate, which, differently from pyruvate, can be easily secreted out of the cell.

Hence, high glycolytic flux provides ATP and biosynthetic precursors to PPP to support rapidly proliferating cells, but with the disadvantage of producing high levels of lactate [12].

Aerobic glycolysis is just one step of oncogenic metabolic transformation. Indeed, proliferating cells need to synthesize at least the double of every macromolecule in order to provide them to the daughter cell: genome replication, lipid synthesis and proteins.

Proliferating cells, as like as tumors cells, require more than glucose molecules and glycolytic intermediates for their needs to achieve the production of necessary elements [13].

In fact, in proliferating cells, glucose alone cannot be used for carbon catabolism and for ATP, because high levels of ATP would impair A-CoA production, and consequently another energy source is necessary for replenishing the TCA cycle with intermediates for biosynthesis of macromolecules.

In particular, for restoring OAA levels, which are impaired by the export of citrate from the mitochondria in order to synthesize lipids necessary for cellular and organelles membranes, tumor cells exploit a different source: glutamine [12].

1.2.2 Glutamine metabolism

Since 1950s, it is known that proliferating and tumour cells consume a large amount of glutamine, indicating the importance of glutamine as nutrient and metabolic precursor.

Glutamine is the most abundant amino acid in the plasma and its primary functions are the storage of nitrogens in the muscle and the transport of them between organs. It is traditionally considered a non-essential amino acid since tissues are able to synthesize it themselves, but during periods of rapid growth or other stress the demand for glutamine exceeds its supply and it becomes essential [12]. After glucose,

glutamine is the most prominent carbon's resource for the synthesis of the three major classes of macromolecules to support cell growth and division [12].

The metabolic fate of glutamine can be divided into reactions that use glutamine for their γ-nitrogen (i.e. nucleotide synthesis) and reactions that use glutamine for both its α-nitrogen and carbon skeleton (i.e. TCA cycle). Glutamine is able to operate as source of metabolic intermediates into TCA cycle, precursor for the biosynthesis of nucleic acids, amino acids and glutathione, but it must be primarily converted into glutamate by phosphate-dependent glutaminase enzymes (GLS) that are often over expressed in many types of cancer. Mammals express two types of glutaminases that differ for their affinity for glutamine and for the possibility to be inhibited by glutamate concentrations.

The human form, the K-type, encoded by the GLS gene, displays high affinity for glutamine and can be inhibited by glutamate. On the contrary, the L-type, encoded by the GLS2 gene, has a low affinity for glutamine and is not inhibited by glutamate. The K-type is prevalently expressed by cancer cells, although they often possess transcripts of both forms, suggesting how tumour can modulate the expression of GLS on the basis of the concentrations of glutamine or glutamate.

In tumors there is a high concentration of glutamate since it is necessary for metabolic reactions that use the α-nitrogen. On the other hand, the α-nitrogens comes from glutamine and are used for nucleotides synthesis, especially in rapidly proliferating cells with a high request of nucleic bases for DNA replication.

Glutamine's oxidation takes place into the mitochondria and represents the major source of energy in proliferating cells. As depicted in Figure 3, the first step of glutaminolysis implies the deamidation of glutamine into glutamate and ammonia as a byproduct and then the conversion of glutamate to α-ketoglutarate (a-KG) via glutamate dehydrogenase (GDH) or by glutamate oxaloacetate transaminase (GOT). α-KG is a TCA intermediate and the major source of OAA, which replaces the exported citrate for the fatty acid synthesis. The complete oxidation involves the exit of α-KG from the TCA cycle as malate, the latter conversion into pyruvate and acetyl-CoA and the re-entry into the TCA cycle. Glutamine that is not converted into pyruvate in TCA can furnish more OAA for citrate formation [12].

OAA is an essential substrate because its condensation with acetyl-coA into mitochondria produces citrate. Citrate, upon transport into the cytosol by a citrate shuttle, is utilized by action of ATP-Citrate lyase, producing OAA and above all acetyl-CoA, an essential substrate for synthesis of cholesterol and fatty acids and for the modification of chromatin structure.

Glutamine metabolism produces OAA in a process known as anaplerosis that indicates the refilling of the mitochondrial carbon pool. Replenishment of the mitochondrial carbon pool by glutamine provides mitochondria with precursors for the maintenance of mitochondrial membrane potential and for the synthesis of nucleotides, proteins and lipids [14].

Glutamine metabolism also provides precursors for the synthesis of glutathione (GSH) the major thiol-containing endogenous antioxidant which serves as a redox buffer against various sources of oxidative stress.

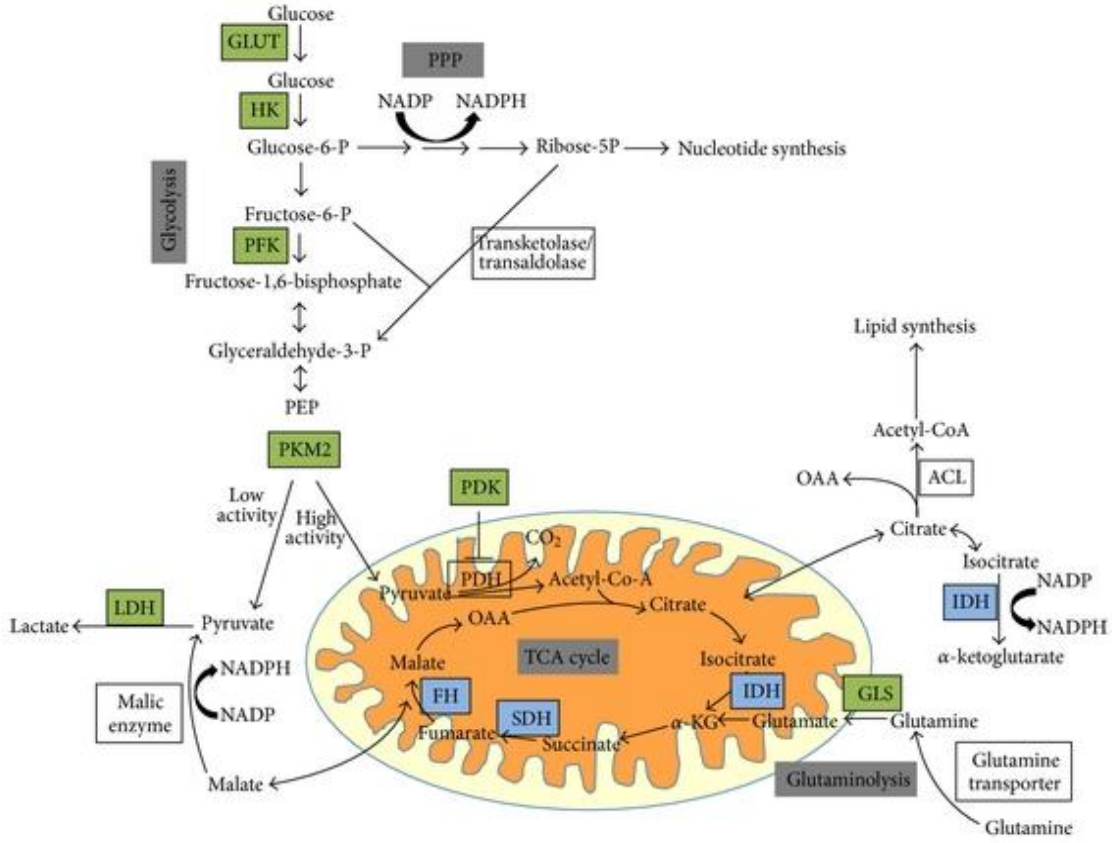

Figure 3 Glutamine metabolism. *MYC enables cancer cells to maximize glutamine uptake from the extracellular space through the upregulation of the glutamine transporter. Once glutamine enters the cell, it can be metabolized through glutaminolysis to provide glutamate. The transamination of glutamate to αKG will feed the TCA cycle (adapted from Vander-Heiden et al Science, 2009, 324, 5930 1029-103).*

An alternative way to get citrate from glutamine is through its direct conversion via *reverse reductive metabolism* by isocitrate dehydrogenase (IDH) enzyme activity (Figure 4). While normally the enzyme catalyses the oxidative decarboxylation of isocitrate into αKG, in the reductive metabolism αKG is converted into citrate (Figure 4). This IDH reverse reaction is possible in hypoxic conditions after HIF-1α (hypoxia-inducible factor 1) activation, which enables PDK1 (pyruvate dehydrogenase kinase 1) to inactivate PDH catalytic site and reduce the amount of pyruvate entering in TCA cycle. In fact, pyruvate conversion into acetyl-CoA and oxidation of glutamine into oxaloacetate requires NAD+ cofactor, which is impaired in low O_2 conditions (unbalanced NAD+/NADH ratio) [17].

It has been demonstrated that this type of catabolism improves citrate and, consequently, lipid production to supply cell growth. This reaction takes place when HIF-1α pathway is constitutively activated or in cancer cells [16].

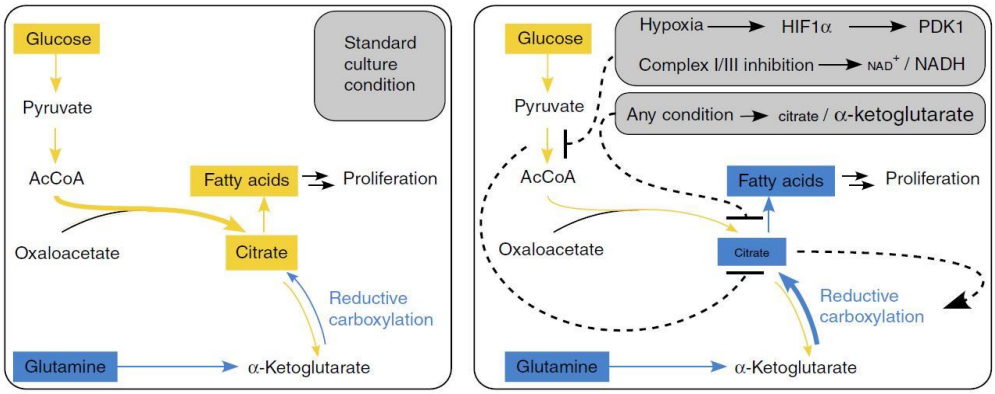

Figure 4 Glutamine metabolism. *Glutamine reductive metabolism in normal and pathological conditions (Fendt SM, Bell EL, Keibler MA et al, Nat Commun. 2013;4:2236.).*

1.2.3 Fatty acid synthesis

Fatty acid synthesis occurs at a very high rate in cancer cells. In normal cells *de novo* fatty acid metabolism takes place mainly in the liver and utilizes carbons from glycolysis. In cancer cells, instead, *de novo* fatty acids production is needed for the rapidly production of new membranes for daughter cells and new organelles [15]. The increased lipogenesis in cancer is reflected by the over expression and hyperactivity of lipogenic enzymes such as ATP citrate lyase (ACL), acetyl-CoA carboxylase (ACC), or the fatty acid synthase (FAS).

Conversion of glutamine into pyruvate is the major source of NADPH used for the reduction of αKG into citrate in reductive metabolism of glutamine and for lipid synthesis [16].

The acetyl groups for lipid synthesis are provided by citrate produced in TCA cycle and it is exported to the cytosol. In the cytosol, citrate is converted into acetyl-CoA and OAA by the cytosolic enzyme ATP-citrate lyase (ACL). Then, oxaloacetate is converted into malate by malate dehydrogenase enzyme, and just like glutamine-derived malate, it is successively converted by malic enzyme (ME) into pyruvate (producing NADPH), and finally into lactate by LDH-A enzyme. Acetyl-CoA, instead, is irreversibly carboxylated by Acetyl-CoA carboxylase-1 enzyme (ACC) into malonyl-CoA, which is further converted to long-chain fatty acid by FAS.

Proliferating cells that exhibits glycolytic metabolism convert glucose to lactate taking glucose carbon away from the TCA and fatty acid synthesis. Hence, cancer cells employ reductive glutamine metabolism to generate the Acetyl-CoA for fatty acids synthesis.

In summary, to achieve anaplerosis of citrate in TCA cycle, cancer cells use glutamine as alternative source. Thanks to glutamine reductive pathway and to glutaminolysis-derived OAA, a continuous lipids synthesis is provided furnishing citrate and producing NADPH through the conversion of glutamine into pyruvate by malic enzyme and from PPP reactions [16].

1.2.4 Role of oncogenes and oncosopressors

To maintain the high fluxes of glycolysis and glutaminolysys, increased uptake of glucose and glutamine are required. In normal cells the nutrient capture from the extracellular environment is finely regulated by

growth factor signalling. In absence of that, cells lose their capability to self-autonomous nutrient uptake for basal bioenergetics. Cancer cells often display mutations in oncogenes and oncosupressors that chronically enhance those metabolic pathways leading to the uncontrolled proliferation regardless the amount of nutrient and without a homeostatic regulation.

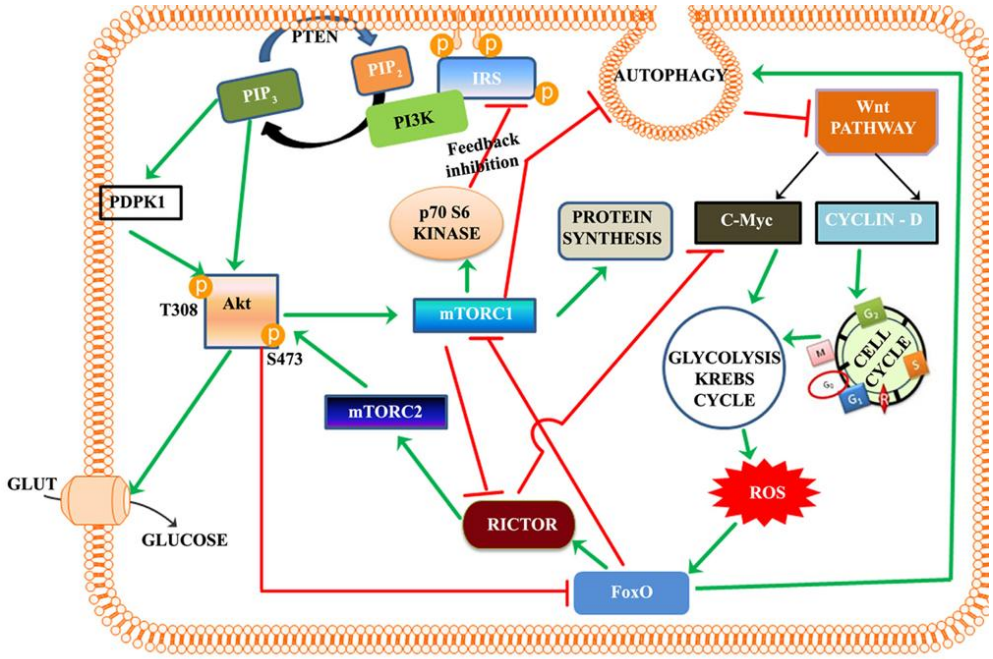

Figure 5 Oncogenes and oncosupressors. *Oncogenes and oncosupressors that modulate metabolism in cancer cells (adapted from Vadlakonda et al., Front. Oncol., April 2011).*

1.2.4.1 The PI3K/AKT/PTEN pathway

The PI3K/AKT pathway is the main regulator of glycolysis and is the most commonly mutated pathway in cancer. PI3K (phosphoinositide 3-kinase) is a heterodimer with a regulatory subunit (p85) and a catalytic subunit (p110). The p85 subunit is associated with receptor tyrosine kinases (RTK) intracellular domain which, once phosphorylated by ligand binding, activates PI3K dimer.

Once activated PI3K pathway provides strong growth and survival signal. AKT1 represents the main downstream regulator of this pathway and it is an important driver of the glycolytic phenotype and stimulator of ATP. AKT1 stimulates glycolysis, increasing the expression and membrane translocation of glucose transporters and upregulating hexokinase and phosphofructokinase enzymes. In addition, AKT stimulates the mammalian target of rapamycin (mTOR) pathway, thus promoting other metabolic reactions [18].

PI3K/AKT signalling pathway can be inhibited by the tumour suppressor phosphatase and tensin homologue (PTEN). The main functions of PTEN are the regulation of cell growth, metabolism, and survival. Loss of PTEN promotes glycolysis, while increased of PTEN levels can reverse cancer metabolic reprogramming from glycolysis to OXPHOS.

1.2.4.2 mTOR

Another downstream mediator regulated by AKT that influences protein synthesis in proliferating cell is mTOR. mTOR (mammalian Target of Rapamycin) is a serine-threonine kinase that functions as a key metabolic regulator, coupling growth signal to nutrient availability.

mTOR is composed by two multiproteic complexes, mTORC1 and mTORC2 and its activities are regulated by the tumor suppressors TSC1 and TSC2 (tuberous sclerosis complex 1 and 2 respectively) and by LKB1 (liver kinase B1).

AKT contributes to inhibit the complex TSC1-TSC2 by phosphorylating TSC2 and disrupting the complex determining the activation of mTOR. Hence, mTOR activation regulates many anabolic pathways: through the regulation of HIF-1α, mTOR activates glycolysis and the PPP, while activating the transcription factor sterol regulatory element-binding protein (SREBP1) it stimulates lipid synthesis. Phosphorylating and inhibiting mTOR, AKT1 stimulates protein and lipid synthesis and fosters growth. At molecular level mTOR stimulates mRNA translation and indirectly causes other metabolic changes through the activation of transcription factors such as HIF-1α, even in normoxic condition [18].

mTOR is inhibited in stress conditions such as nutrient deprivation or hypoxia by the adenosine monophosphate–activated protein kinase (AMPK) pathway. AMPK is a metabolic sensor that regulates energy homeostasis and it is activated in response to an increase of the ATP/ADP ratio by LKB1. AMPK can inhibit mTORC1 through the phosphorylation of TSC2 or by directly phosphorylating Raptor, a component of the mTORC1 complex. As a result, the liver kinase B1 (LKB1)/AMPK pathway acts as a metabolic check point and inhibits cancer metabolic reprogramming [18].

1.2.4.3 HIF-1α signalling

Rapidly proliferating cells need a continuous supply of nutrients and oxygen but, due to the rapid tumor growth and the insufficient and disorganized vascularisation, cells undergo into hypoxic conditions. The main mechanism that allows cells to adapt to hypoxic conditions is the induction of the transcription factor HIF-1 [19].

HIF1 is a transcription factor that consists in a heterodimeric protein, composed by HIF-1α subunit, which is regulated by O_2 concentrations, and a constitutively expressed HIF-1β subunit. In normal oxygen conditions HIF-1α is degraded by the proteasome after prolyl hydroxylation by the prolyl-4-hydroxylase domain proteins (PHDs) and the uniquitination by the tumour suppressor Von Hippel Lindau (VHL).

In hypoxic condition, proline hydroxylases cannot hydroxylate HIF-1α and the binding of VHL to HIF-1α such as the successively degradation are inhibited. In this way, HIF-1α accumulates and forms a dimer with HIF-1β. The heterodimer binds to hypoxia-response elements (HREs) within the promoters of target genes and recruits transcriptional co-activators such as p300/CBP for full transcriptional activity. In this condition HIF-1α could transcript growth factor genes initiating an autocrine signalling pathway that could be crucial for tumour progression [19, 20, 21].

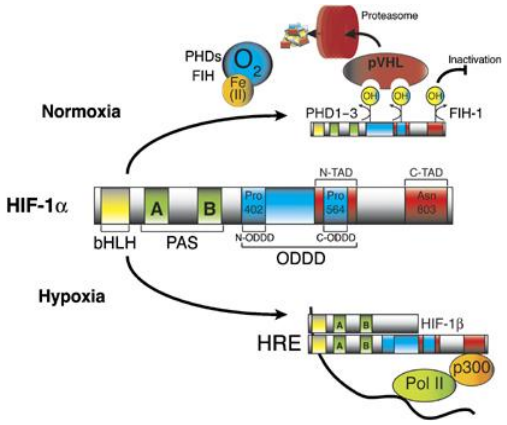

Figure 6 HIF- 1α. *Representation of HIF-1α structure and its regolation by prolyl hydroxylation and proteasomal degradation. (Weidemann A et al., Biology of HIF-1α, Cell Death and Differentiation, 2008).*

HIF-1α activation helps cells to adapt to oxygen deprivation by regulating the expression of genes involved in many cellular processes that can be grouped into 4 functional categories: proliferation, metabolism, angiogenesis and invasion/metastasis [19].

HIF-1α enhances glucose uptake amplifying the transcription of the glucose transporters (GLUT1 and GLUT3) and glycolytic enzymes (HK1 and HK2) and it upregulates the lactate dehydrogenase A (LDHA) to stimulate the conversion of pyruvate into lactate. HIF-1α is also able to enhance the expression of protein transporters that excretes lactate outside the cell and VEGF, necessary for the angiogenesis process and fundamental for the oxygen supply in low oxygen condition. Moreover, HIF-1α inhibits the pyruvate dehydrogenase kinase 1 (PDK1), which in turn inactivates the activity of the pyruvate dehydrogenase (PDH) complex reducing the entrance of the pyruvate derived from glycolysis into the TCA cycle [20].

1.2.4.4 MYC signalling

MYC pathway represents the main regulator of cell proliferation and is deregulated in many cancers. MYC is responsible for the regulation of genes involved in glucose metabolism, nucleotide, lipid, amino acid and protein synthesis.

MYC is a protein with helix-loop-helix zipper (HLHZ) structure which dimerizes with another HLHZ protein, Max. MYC-Max complex is able to bind its E-box sequence, composed by nucleotide pattern CANNTG (where N is a random nucleotide) and to begin transcription of its target genes. In cancer cells, MYC is translocated from chromosome 8 and is one of the most highly amplified oncogenes, and thus amplification of this gene increases the tranascriptional level of its target genes [22].

Regarding metabolism regulation, MYC is able to modulate glycolysis inducing the expression of almost every glycolytic gene and glutaminolysis, required for cell growth and proliferation.

c-MYC fosters the splicing of M2 isoform of PK (pyruvate kinase) enzyme that, due to its low activity if compared to PKM1, cannot convert phosphoenolpyruvate (PEP) into pyruvate, avoiding its entrance in TCA

cycle. High expression of this enzyme is advantageous in tumors, due to the accumulation of upstream intermediates of glycolysis that can be shunted into anabolic pathways such as nucleotide synthesis [22]. Like HIF-1α, MYC regulates HKs and inhibits PDH, blocking the entry of pyruvate in the mitochondria and promoting its conversion into lactate.

c-MYC also controls glutamine metabolism and can regulate nucleotide biosynthesis by transcriptional regulation of several key enzymes. c-MYC regulates mitochondrial glutaminase (GLS), whose expression is increased in c-MYC-dependent tumours also at posttranscriptional level. In fact, MYC is able to regulate different clusters of miRNA: it supresses the expression of miR-23a and miR-23b which target the GLS1 resulting in increased glutaminase expression and miR-17 cluster, which blocks the expression of PTEN. In this way, c-MYC indirectly activates AKT signalling pathway and its downstream mediators. Recently, MYC has also been associated to lipid synthesis, since many enzymes of fatty acids biosynthesis are its direct targets [22].

1.2.4.5 p53

The tumour suppressor p53 has a prominent role in the regulation of cellular metabolism exerting an important defense mechanism against tumour development. p53 is a transcription factor that regulates DNA damage response, apoptosis and senescence and its loss in many cancers determine lack of cell cycle control and inefficient DNA repair. Functional p53 promotes glucose OXPHOS and inhibits glycxolysis through its action on the transcription of glucose transporters GLUT1 and GLUT4 and the activation of PTEN. It is also known that p53 acts on glutamine metabolism activating an alternative isoform of glutaminase (GLS2/LGA) [15]. Another function of p53 is related to autophagy, on which it acts through the homologous p63 and p73. These molecules display different functions, including the regulation of metabolism. TAp63 controls fat and glucose metabolism since it is a positive regulator of Sirt1, AMPKa2 and LKB1, while Tap73 controls cell proliferation. This last can be negatively regulated by AMPK without affecting p53.

1.2.4.6 Ras

RAS belongs to a superfamily of small GTPases (monomeric small G proteins) that, together with heterotrimeric G proteins (large G proteins), composes the family of guanosine nucleotide-binding proteins (G proteins). These proteins transduce extracellular signals into intracellular changes, mediated by intracellular second messengers [23].

RAS family is the most studied family of GTPases and consists of three genes, H-*ras*, N-*ras*, and K-*ras*, which respectively encode for four homologous proteins: HRAS, NRAS, KRAS4A and KRAS4B that possess similar molecular weights of 21 kDa. These proteins share a GDP/GTP binding and GTPase activity, which is an intrinsic activity in every G protein and allows them to switch between an activated state (when they are bound to a GTP molecule) into an inactivated state (when the bond occurs with a GDP molecule) [23]. When RAS is bound to GTP, many downstream effectors are activated such as the p110 subunit of PI3K and the mitogen-activated protein kinases (MAPK) pathway (Figure 7).

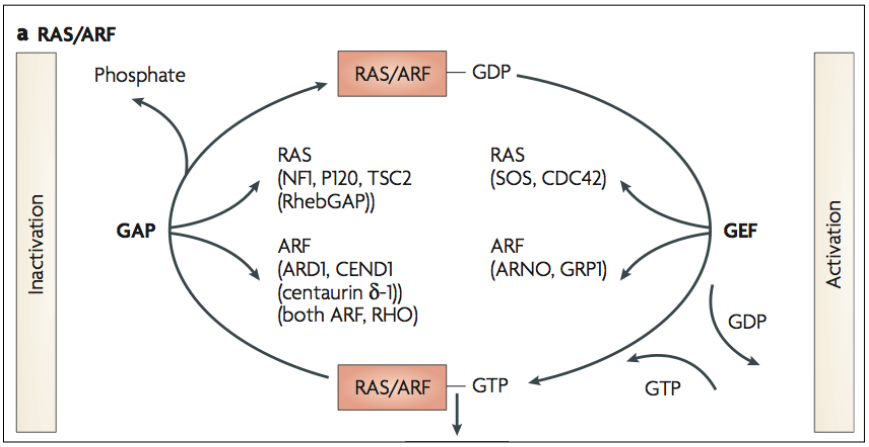

Figure 7. *Mechanism of activation/inactivation of RAS GTPases (Konstantinopoulos PA et al., Nat Rev Drug Discov. 2007;6(7):541-55).*

1.3 In vivo translational imaging to study cancer metabolism

Many efforts have been made in the last years for the investigation and evaluation of cancer hallmarks. The increasing knowledge in tumor metabolism and the development of new anticancer molecules give rise to the need of new cancer biomarkers able to early detect as well as stage tumors, evaluate treatments effects and guide patient tailored therapies.

Molecular Imaging (MI) techniques enable the non-invasive visualization, characterization and measurement of biological processes at cellular and molecular level thanks to the interaction of the specific target with a probe. MI plays a fundamental role in oncology to identify biomarkers for the evaluation of tumor progression and the response to target therapies. Due to the recent development of new imaging analysis procedures, tracers and contrast agents, molecular imaging techniques represent a fundamental tool for cancer management and study at both clinical and preclinical stages. *In vivo* imaging requires instruments with high resolution and sensitivity and includes five different modalities: positron emission tomography (PET), magnetic resonance imaging (MRI), computed tomography (CT), ultrasound and optical imaging (OI). The possibility to integrate the use of these technologies may provide synergistic advantages, overcoming the weakness of each modality and obtaining more complete information. Moreover, the emerging field of theragnostic proposing to merge therapeutic and imaging strategies to improve patients' management has increased the importance of molecular imaging in oncology [24].

Personalised and specific therapies require systems able to bridge the gap between promising *in vitro* results and their clinical application. This translation can be view as a two steps process which involves a first transfer of *in vitro* data to preclinical animal models and a following translation of knowledge gained from animal models to clinical practice [25] (Figure 8). The increasing information regarding human cancer biology and the improvement in technologies led to the development of animal models that well resemble human diseases. Consequently, molecular imaging modalities provide a link between preclinical and clinical research. In fact, the use of preclinical models is nowadays recognizes as a key strategy for non invasive and longitudinal assessment of treatments effects with several advantages:

- Permits the non invasive study of cells into their natural microenvironment;
- Enables the investigation of signaling pathways in real time;
- Gives rapid information about pharmacokinetics and pharmacodynamics to evaluate biodistribution and the efficacy potential drugs;
- Makes possible to perform longitudinal studies in the same animal, reducing the number of animals used and costs and increasing the statistical power [25].

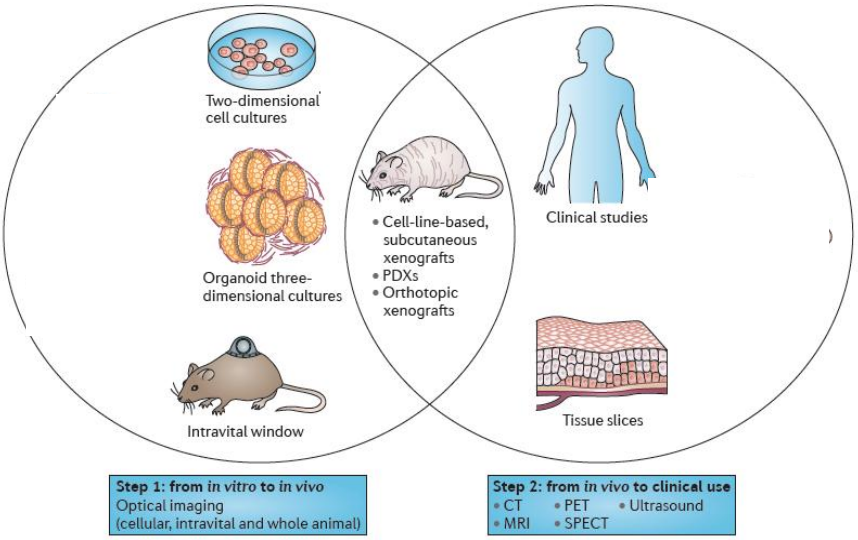

Figure 8 The two steps process required for translation of in vitro results to clinical practice. *The first step is needed to transfer in vitro results to animal models. A second step allows the transfer from animals models to clinical setting. On the basis of the research question a different model and imaging techniques are chosen. (Adapted from De Jong et al., Imaging preclinical tumor models: improving translational power. Nature Reviews, 2014).*

Nevertheless, the usefulness of preclinical models to study human diseases is still a matter of debate, *in vivo* preclinical imaging provides significant advances in the investigation of new treatment approaches that can be translate into clinical practice.

Optical imaging represents a unique tool to study tumor progression in animal models and to evaluate treatments effects due to its low cost and high sensitivity. Moreover, thanks to advancement of technology, preclinical PET machines for small-animal models have been in constant development since early 1990s with optimized parameters for small-animal models, like a small field of view and a higher resolution if compared to clinical machines. Small-animal PET tomographs are nowadays a solid preclinical tool, especially in cancer and their development and reliability have made PET imaging a translational technology [26].

1.3.1 Optical imaging

Optical imaging (OI) techniques are based on genomic, proteomics and optical technologies and enable non-invasive and whole body imaging of living small animals. At present the most used optical imaging modalities include bioluminescence imaging (BLI) and fluorescence imaging (FLI). The high sensitive and low cost render optical imaging modalities a crucial tool for the investigation of tumor progression and drug development in animal models.The required infrastructure for optical fluorescence and bioluminescence imaging is a charge-coupled device (CCD) camera and a source of filtered light, that are relatively inexpensive and easy to setup.

Taking advantage from the oxidative reaction between luciferase and its substrate (luciferine), BLI represents a reliable, sensitive and rapid method to monitor disease progression, gene expression and evaluate treatment effects. Cells transfected *in vitro* to express luciferase are then inoculated into the

experimental animal. After luciferin administration, in presence of ATP or molecular oxygen, luciferase oxidizes its substrate causing the production of light that can be visualized by the external detector (Figure 9). The usefulness of this technology has been demonstrated in tumor xenografts expressing a reporter gene (luciferase) under the control of a hypoxia responsive element (HRE) to assess cellular consequences of reduced oxygen. The use of low energy photons represent the major limit of BLI, since penetration is limited to only a few centimetres avoiding impossible the studies of large animals or human [25]. Differently from FLI, the source of light in BLI is internal and, due to the fact that tissue does not produce bioluminescence itself, the signal to background is better than FLI. In FL imaging, following the administration of a fluorescent imaging agent (fluorophore, fluorescent protein, QDot etc.), an excitation light of appropriate wavelength is used to illuminate the subject. This leads to excitation of the fluorophore/fluorescent protein and the subsequent emission of light. The light is detected via a CCD camera, collated, analyzed, and converted into an image detailing the location of emitted light (due to imaging agents) from subject (Figure 9). The use of FLI is based on the excitation of a fluorescent molecule with light with long wavelength in order to overcome limitations due to tissue deepness. Nevertheless, in the last years significant advances has been made to improving this technology in vivo using wavelength able to penetrate tissue. Near-infrared fluorescence probe (NIRF) using wavelengths in the 700-900 nm range improve the use of FLI decreasing scattering and autofluorescence of normal tissue. Fluorescence based reporter genes can provide a stronger signal and real-time images and, overall, make FLI a versatile technique with a number of advantages including its relativelow cost and the absence of a substrate administration used for preclinical evaluation of imaging agents before their translation into more expensive modalities [25].

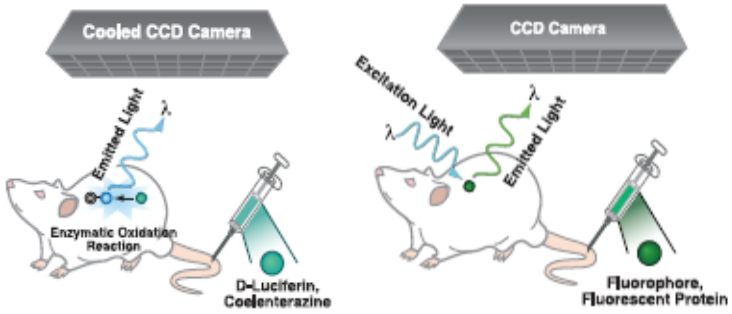

Figure 9 Optical imaging. *Schematic representation of the general principles of molecular imaging using BLI and FLI (adapted from Gambhir J et al., Molecular imaging of cancer with positron emission tomography. Physiol Rev, 2012).*

1.3.2 Positron Emission Tomography, PET

Positron emission tomography (PET) and magnetic resonance (MRI) represent the most used techniques used to obtain structural and molecular information from biological system due to their direct application in clinical settings that allows to compare studies performed on animal models to clinical studies.

The most powerful molecular imaging technique used for the study of cellular metabolism and biochemical processes is Positron Emission Tomography (PET). Because of its high sensitivity and limitless depth of penetration, PET represents a powerful diagnostic tool extensively used in clinical and preclinical settings [26, 27].

PET imaging is based on the measurement of signals originated from the radioactivity decay of radiotracers injected in microdoses intravenously into the body. Radiotracers are chemical compounds labelled with positron-emitting radioisotopes that tend to decay for their nuclear charge instability. Positron particles are highly interactive with the surrounding material, especially with tissues electrons. This interaction, known as annihilation, generates a pair of 511 keV photons emitted in opposite directions (at 180° from each other) and captured by PET detectors installed around the subjects under observation. PET detectors are scintillators composed by crystals whose different sizes determine PET resolution. Their goal is the conversion of photons in electrical signals that are subsequently converted into sinograms via photomultiplier tubes. Each sinograms is then reconstructed into tomographic images following corrections for dead time, detector normalization, substraction of random coincidences and scatter and attenuation correction (Figure 10). Information provided by PET images is a sort of "map" of distribution of the annihilation points in the scanned tissue [28, 29].

Since molecular changes generally occur before anatomical modifications, PET displays a clear advantage compared to other anatomical modalities in diagnosis.

Major limits of PET are represented by the low spatial resolution and the lack of anatomical information. To overcome this last limit, recently almost all clinical PET are associated to computed tomography (CT) or MR (Magnetic Resonance) system. The integrate use of these technologies provide synergistic advantages and overcome the weakness of each modality obtaining combined and more complete information.

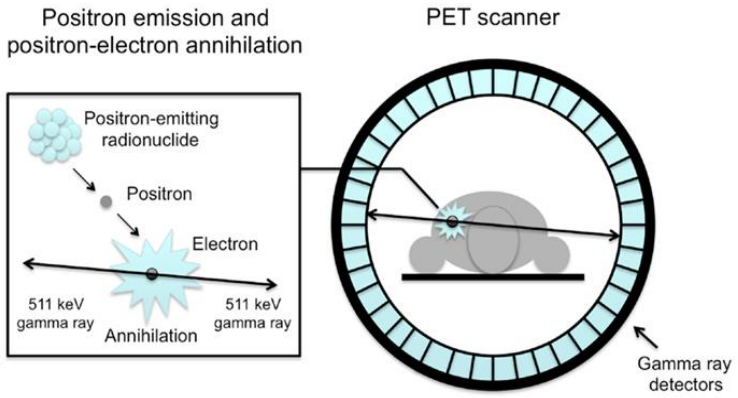

Figure 10 Annihilation reaction and coincidence detection representation. *Released positrons annihilate with tissue electrons, emitting two coincidence photons. Coincidence detection and photons processing make possible to localize the annihilation source (van Der Veldt, Front. Oncol., 2013).*

1.3.3 PET imaging of cancer's hallmarks

Several radiopharmaceuticals have been applied in clinical practice and research to follow biochemical and metabolic processes that characterize cancer (Figure 11).

^{18}F is the most used radionuclide in PET imaging for both chemical and radiochemical properties. Its short half-life (109.8 minutes) ensures synthesis and studies that can be carried on for longer times and the distribution to different PET centres. Its chemical reactivity allows the introduction also in small structures through nucleophilic substitution without affecting pharmacological properties [29].

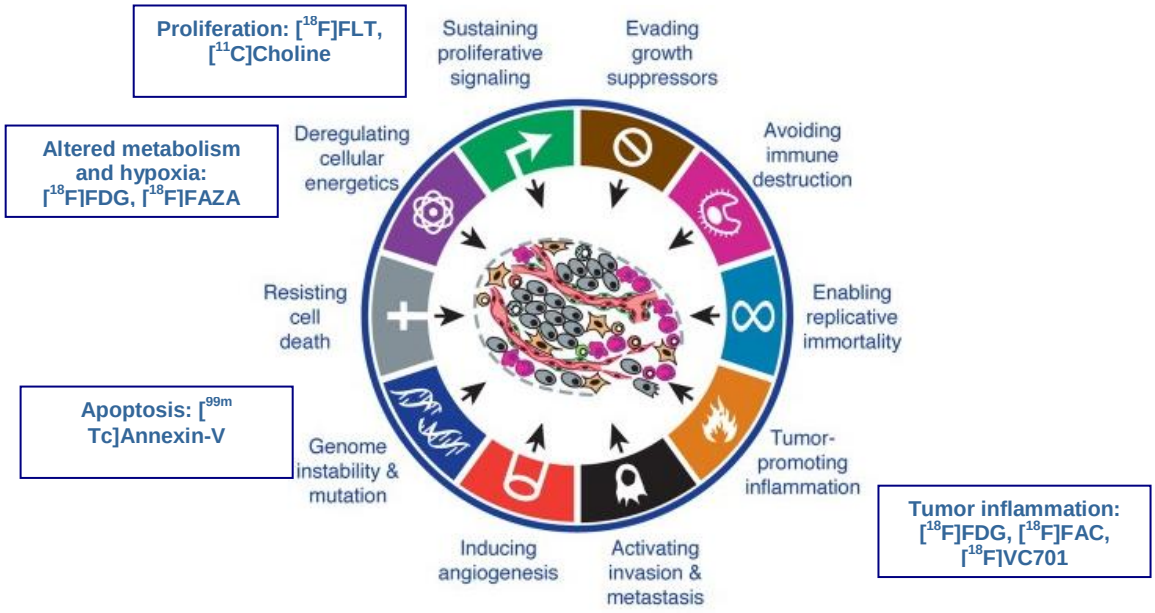

Figure 11 Cancer hallmarks and PET tracers. *Specific targets and the corresponding nuclear probes already used in clinical setting (bold) and in development (adapted from Hanahan D. et al, 2011).*

^{18}F-fluorine-2-deoxy-D-glucose (FDG) represents the most common used radiotracer in oncology. It has been synthesized for the first time in 1978 through the substitution of the 2-carbon hydroxyl group of the glucose with a radioactive fluorine atom ^{18}F. [^{18}F]FDG accumulation reflects the activity of hexokinases (HK) enzymes and, more generally, the cells demand of glucose. [^{18}F]FDG, like glucose, is taken up by the cells thorough glucose transporters and phosphorylated by hexokinase II to form FDG-6-PO4. The lack of the 2-carbon hydroxyl avoids further metabolism and, differently from glucose, [^{18}F]FDG remains trapped into the cells accumulating over time and providing a measurement of cells metabolic glucose requirement [30].

It is well known that neoplastic tissues show a higher metabolism of glucose as well as an upregulation of glucose transporters (GLUTs) compared to normal cells. As demonstrated by the Warburg effect, cancer cells consume massive amount of glucose because of the progressive loss of the tricarboxylic acid cycle and the consequent activation of the pentose phosphate pathway. In this way, [^{18}F]FDG displays a higher uptake in cancer cells if compared to the surrounding tissues with the exception of the brain because of the physiological uptake.The high sensitivity renders PET with ^{18}F-FDG a unique tool in the diagnosis of most types of tumours including non-small cell lung carcinoma, colon and breast carcinoma, melanoma and head-neck tumours.Moreover, [^{18}F]FDG PET is routinely used in clinic for cancer staging and for the identification of distant metastasis.

Recent preclinical studies showed how [^{18}F]FDG PET can monitor tumor progression and response to treatments in cancer models. Several works demonstrated a correlation between decrease in [^{18}F]FDG uptake and response to therapies using preclinical models of cancer, such as breast cancer [32], ovarian cancer [33] and B-cell lymphoma [34].

Moreover, different clinical studies focused on the role of [^{18}F]FDG PET to assess the metabolic response to treatment in some types of cancer, in particular breast cancer, lymphoma and lung cancer. More specifically, it was observed that [^{18}F]FDG uptake reduction is correlated to response to treatment in locally advanced breast cancer [35] and esophageal cancer [36].

Despite its wide use, some lesions are not characterized by high glucose demand and, in addition, in brain tumors the low signal to noise ratio due to the physiological use of glucose by the brain tissues limits the use of [^{18}F]FDG. Moreover, the presence of inflammation and brown fat cells cause aspecific [^{18}F]FDG uptake and false positive results.

To explore other metabolic pathways involved in cancer, new radiotracers have been developed. These tracers are aimed to investigate different metabolic and molecular aspects of cancer such as proliferation, hypoxia, amino acids transports and receptor over-expression [37, 38].

The thymidine analogue, [^{18}F]3'-deoxy-3'-fluorothymidine ([^{18}F]FLT) has been recently validated in clinical setting for the evaluation of cell proliferation, which represents one of the most common features of cancer. In order to sustain proliferation, cancer cells rely not only on energy deriving from glucose metabolism, but also on deoxynucleotides (dNTPs) for DNA replication whose production can be achieved from both *de novo*

and *salvage pathway* (Figure 9).In the *de novo* pathway, thymidylate synthase (TS) enzyme synthesizes thymidine monophosphate (dTMP) from uridine monophosphate (dUMP), for the subsequently tri-phosphorylation to be incorporated in DNA. On the contrary, in *salvage pathway*, exonegous purines and pyrimidines are imported by nucleoside transporters (ENT and CNT) and phosphorylated by thymidine kinase 1 (TK1) enzyme into dTMP, dTDP and ultimately to dTTP. Being an analogue of exogenous nucleosides [^{18}F]FLT is imported in the *salvage pathway* and phosphorylated into [^{18}F]FLT-monophosphate ([^{18}F]FLT-MP) by TK1 enzyme. Differently from thymidine, [^{18}F]FLT lacks of an OH group at the 3-position that avoids its incorporation into DNA and causes its accumulation providing a measure of the proliferative state of the cell [39]. The high-levels of proliferation that characterized cancer cells increase TK1 expression in S-phase elevating both the uptake of exogenous thymidine and its phosphorylation by TK1. [^{18}F]FLT uptake reflects the activity of the timidine kinase-1 (TK-1) enzyme, thus representing a direct indicator of DNA synthesis and indirect marker of cell proliferation. [^{18}F]FLT PET more interesting role is the early assessment of tumor response to therapy [39, 40]. Changes in cell proliferation seem to occur earlier than changes in glucose uptake, indicating [^{18}F]FLT as a better tool to assess treatment efficacy compared to [^{18}F]FDG. Moreover, differently from [^{18}F]FDG, [^{18}F]FLT uptake is less influenced by the inflammatory component that normally increase after treatments.

[^{18}F]FLT has been compared to [^{18}F]FDG uptake in different xenograft models in which PET images showed an earlier and more pronounced decrease in [^{18}F]FLT uptake compared to [^{18}F]FDG after treatments [41]. In clinical settings [^{18}F]FLT seemed to be more sensitive for the assessment of cancer and evaluation of treatment in non-small cell lung cancer [42], glioma [43] and breast cancer [44].

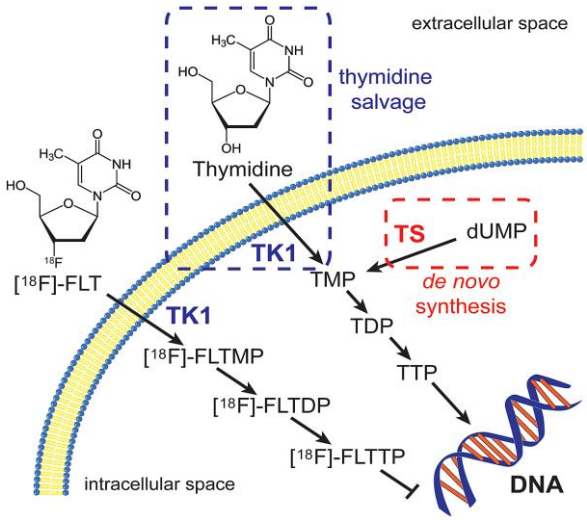

Figure 12 [^{18}F]FLT mechanism of retention. *Salvage and de novo pathways of thymidine for nucleotide synthesis (McKinley et al., Plos one 2013).*

Nevertheless the first positive results obtained and the good correlation often found with the immunohistochemical marker of proliferation Ki67, important issues remain to be considered regarding the use of [^{18}F]FLT. Measuring the activity of TK-1, FLT provides information only about salvage pathways and tumors that rely only on *de novo* pathway for nucleotides synthesis cannot be evaluated with [^{18}F]FLT, and, moreover thymidine levels in different tumor types seemed to be variable (Figure 12) [45].

Despite their limits, [^{18}F]FDG and [^{18}F]FLT can be used together as complementary tracers to have a more reliable in vivo metabolic information about cancer.

Another tracer routinely used in clinical oncology is represented by [^{11}C]Choline as a substrate for choline kinase used mainly to image prostate carcinomas. Choline is an important precursor of phosphatidylcholine and sphingomyelin, two classes of phospholipids that are abundant in cell membranes [45].

Prostate cancer cells, like other cancer cells, show increased phosphocholine levels and elevated turnover of the cell membrane phospholipid, phosphatidylcholine. Moreover, the key enzyme in choline metabolism, choline kinase, phoshporylates choline once it enters into the cell and it is up-regulated in prostate, such as other cancers [45].

The presence of hypoxic areas associated to tumor has a great clinical relevance because of its negative predictive value and overall prognosis. Moreover, tumor cell hypoxia has a negative effect on anticancer treatment as hypoxic cells display a major resistance to both chemo and radiotherapy compared to normal cells. To date there are two different approaches for noninvasive imaging of hypoxia. The first is based on the intracellular retention of nitroimidazoles following transmembrane diffusion and reduction to radical, such as [^{18}F]fluoromisonidazole or [^{18}F]fluoroazomycin arabinoside. In contrast to nitroimidazole compounds, the reduction of Cu(II) to Cu(I) has been identified as the crucial step of [^{64}Cu]diacetyl-bis-N4-methylsemicarbazone [37, 45].

Contributing to tumor's immune escape, inflammation creates a proper environment for neoplastic growth.

The possibility to investigate and image inflammation is a challenge not only for oncology but also for neurodegenerative disease. The traslocator protein, TSPO, is a 18 kDa protein located in the outer mitochondrial membrane present in almost all healthy tissue. The physiological role of TSPO is mainly related with steroidogenesis but its involvement in the regulation of apoptosis, proliferation, differentiation and more recently mitochondrial-related cell death processes, makes it a potential novel target for therapy [106]. Under physiological conditions, TSPO is present at high concentration in peripheral organs such as kidney, lung, heart, spleen and adrenal while lower levels are detectable in brain parenchyma. However, thanks to its overexpression on activated macrophages and microglia, this target has been widely used for the *in vivo* imaging of immune system activation in different brain disorders [106].

Several radioligans for *in vivo* visualization of highly expressing TSPO tissues have been developed. Moreover, beyond TSPO upregulation during inflammation, it has been demonstrated that also cancer cells overexpressed TSPO. In the late 1980s PET imaging of human gliomas using TSPO has been developed with the isoquinoline derivative ^{11}C PK11195, even if it showed numerous limitations concerning the high level of non-specific binding and poor signal-to-noise ratio [107, 108].

Indeed, despite the large numbers of preclinical and clinical findings resulting from its use, this compound is characterized by a low signal to noise ratio and short half life limitation. For this reason, recently, a number of promising tracers with high affinity for TSPO have been developed and validated and, among these, Fluorine-18 labeled compounds have the advantage of a longer half life (109.8 min) that facilitate radiopharmaceutical distribution. The analogue of PK11195, 2-quinolinecarboxamide derivative named VC701 labelled with ^{18}F, demonstrated a favourable *in vivo* profile in biodistribution studies and high affinity for TSPO representing a new compound able to investigate inflammation.

2. OBJECTIVE OF THE WORK

The general aim of this work is the evaluation of changes in biochemical processes occurring in cancer such as glucose metabolism, cell proliferation and hypoxia as potential biomarkers of tumor response to therapy by using *in vivo* molecular imaging in preclinical models.

The possibility to early detect changes in metabolism and proliferation after treatment represents an intriguing challenge for the management of aggressive tumors since it allows to select responder from non responder subjects avoiding ineffective treatments and tailoring therapies to each patient. PET with specific radiopharmaceuticals represents a potential biomarker of tumor response to therapy that can be used in preclinical setting and it can be easily transferred in clinic. For these reasons, we focused our studies on two aggressive types of cancer: a) a k-ras transformed model and b) a glioblastoma model.

a) k-ras mutations have been found in several human cancers characterized by high aggressiveness and resistance to therapy. We chose the NIH-RAS model harboring a k-ras mutation that represents an established cell model to study transformation *in vitro* to evaluate *in vivo* the potential role of [^{18}F]FDG and [^{18}F]FLT as biomarkers of response to metabolism-targeted therapies. Mice injected with NIH-RAS fibroblasts were treated with a glutaminase inhibitor and an autophagy blocker and assessed with PET before and early after treatment.

b) U251-HRE-mCherry glioblastoma cells expressing Luciferase under control of a Hypoxia Responsive Element (HRE) and mCherry under the control of a constitutive promoter have been used to generate the murine model of glioblastoma and to assess HIF-1α modulation after treatment. Tumor progression and Temozolomide effects were monitored *in vivo* comparing bioluminescence, fluorescence, MRI and PET with [^{18}F]FAZA and [^{18}F]FLT. Imaging data were supported by histological and immunohistochemical analyses.

3. K-RAS MODEL

3.1 RAS signalling

Ras belongs to the superfamily of small GTPases (monomeric small G proteins) that, together with heterotrimeric G proteins, composes the family of guanosine nucleotide-binding proteins (G proteins). These proteins transduce extracellular signals into intracellular changes, mediated by intracellular second messengers. Ras family is the most studied family of GTPases and consists of three genes: H-*ras*, N-*ras*, and K-*ras*, which respectively encode for four homologous proteins: HRAS, NRAS, KRAS4A and KRAS4B [47]. These proteins share a GDP/GTP binding site and GTPase activity which allows them to switch between an activated state when they are bound to a GTP molecule into an inactivated state when the bond occurs with a GDP molecule. Under physiological condition, these two activated/inactivated states are mediated by different molecules. Guanine-nucleotide exchange factors (GEFs) with the function of exchanging GDP with GTP, such as Son of sevenless protein (SOS), and GTPase activating proteins (GAPs) which stimulate intrinsic Ras GTPase activity hydrolyzing GTP to GDP, are all molecules responsible to the modulation of Ras states of activation. Once activated, Ras proteins signal through PI3K pathway or through MAP kinases which control cellular processes such as growth, proliferation, differentiation, migration and apoptosis.

Mutations in Ras proteins have been found in about 20% of human cancer and result in a constitutively activated GTP-bound Ras protein and, as a consequence, in a continuous activity of downstream pathways. Although Ras has been extensively studied, many issues remain to be clarified about the biological function of single Ras mutation and the contribution of each Ras isoform in cancer. However, the overall biological effects in the cell due by oncogenic activation of the majority of Ras mutations have been widely described. Indeed it is well known that activating Ras mutations mediate some processes involved in proliferation, resistance to apoptosis and metabolism [47].

There are several mutations of RAS and, even if these mutations are known, it is not completely understood if there is a correlation between the kind of mutation and a RAS specific biological effect. In fact, in patients with acute lymphoblastic leukemia (ALL) and with bladder cancer, different mutations in RAS isoforms lead to similar outcome [48].

In the same way, KRAS mutations found in gastrointestinal and pancreatic tumors are different, but lead to the same outcome; in this case the difference between RAS mutations is due to the etiology that caused these mutations, and the causes have to be found in mutagenic agents (for example exposure to chemicals or errors in DNA replication), which concur differently in tumors.

Despite RAS has been increasingly studied more and more in the years, there is still a lot to clarify about the biological function of every single RAS mutation and the contribution of each RAS isoform in cancer. However, the overall biological effects in the cell due by oncogenic activation of the majority of RAS mutations have been widely described.

Activating RAS mutations mediate some processes involving proliferation, resistance to apoptosis and metabolism.

3.1.1 Metabolic changes driven by RAS

In cancer cells RAS activation can drive metabolic changes mainly upregulating HIF-1α. HIF-1α is one of the downstream targets of mTOR, which is hyperactivated in RAS mutated cancer cells.

To support metabolic reprogramming, K-ras has also been found to be a promoter of autophagy conferring to cancer cells an "autophagy addicted" phenotype. Autophagy is a conserved survival pathway that consists in the degradation of cytoplasmic constituents like organelles and proteins aggregates inside the cell. In basal levels in normal cells, it occurs for normal proteins and organelles turnover, but it is also highly activated when cells need a high amount of energy in stressful conditions, such as in lack of nutrients or in hypoxia [49]. In this way, cells maintain their bioenergetics providing to themselves necessary substrates by degrading their internal organelles and by using them to replenish TCA intermediates and to synthesize ATP. In the meantime, cancer cells eliminate damaged organelles, like hypoxia ROS-damaged mitochondria, that can mine cellular homeostasis [49].

Essentially, autophagic process consists in the passages shown:

- Vesicle nucleation, which is the vesicle membrane formation, mediated by lipid kinase signalling complex, composed by Atg6 (also known as Beclin-1, one of the main initiators of autophagy, encoded by BECN1 gene), Atg14, Vps34 (bound to Beclin-1), and Vps15 proteins;
- Vesicle elongation and closure for its formation (autophagosome);
- Fusion with a lysosome (vesicle which contains lysosomal enzymes, activated by acidification of the phagosome, necessary for degradation in the vesicle) and formation of autolysosome, where occurs the molecule and organelle breakdown [50].
- Recycling pathway that makes Atg proteins (Atg2, Atg9, Atg18) to detach from mature autophagosomes and being reused for further autophagosome formation.

Basal autophagy, assessed with LC3 measurements, was demonstrated higher in K-ras mutated cells if compared to wild type Ras prostate cells; inactivation of autophagy genes decreased tumorigenicity and survival in Ras-mutated cancer cells, but had a weaker or null opposite effect on WT Ras prostate cancer cells; finally, Ras mutated and autophagy-competent cells have a greater TCA cycle functionality than autophagy-deficient cells, suggesting that autophagy in cancer cells can supply energetic demand by maintaining mitochondrial function (while eliminating the damaged ones) and by producing substrates through the catabolism of its target [51].

In early stages, autophagy can also prevent tumorigenesis and protect cells from DNA damage due to ROS accumulation caused by protein aggregates. Despite this finding, it has been showed that in tumors this process can also be one of the most supportive strategies for survival and homeostasis in hypoxic and starvation conditions, especially if it's associated with oncogene activation. This reveals that autophagy has a controversial function in oncogenesis representing nowadays a not fully understood process.

3.1.2 NIH-RAS fibroblasts: a model to study cancer metabolism

K-ras transformed NIH3T3 (NIH-RAS) cells are a genetically well-defined immortalized cell line established as a model cell line for the study of cell transformation, largely used for their indefinite growth in culture, serum independence and retention of contact inhibition. As other cancer cells, k-ras transformed fibroblasts display high rate of glucose consumption, mitochondrial dysfunction and altered transcription of several genes involved in cell metabolism. A single amino acid change in the catalytic domain of GEF has been demonstrated to convert this molecule into a dominant negative protein (GEF-DN) able to displace the wild-type GEF from oncogenic k-ras in NIH3T3 fibroblasts, stabilizing the inactive form. In this way GEF becomes unable to provide the GDP/GTP exchange, reverting the phenotype to that of normal fibroblasts. As a consequence, the tumorigenic phenotype could be attenuated, with the consequent loss of tumour capabilities such as independent growth ability and contact inhibition [52].

Compared to normal and GEF-DN NIH3T3 cells, the K-ras transformed NIH3T3 cells showed alterations in their metabolism, already assessed with transcriptional profile analysis. Genes encoding glycolytic and fatty acids biosynthesis proteins are upregulated, leading to a higher consumption of glucose and production of lactate even in low-glucose conditions. Moreover, K-ras transformed fibroblasts display down regulation of transcriptional regulators involved in the expression of nuclear and mitochondrial respiratory genes that are associated with mitochondrial dysfunction and tumour progression [53].

In a recent work Gaglio et al. observed that NIH-RAS fibroblasts are characterized by an addictive glutamine metabolism. In normal cells glutamine shortage slows down the G_2/M transition, suggesting a role of glutamine in cell cycle and not a total dependence from it. On the contrary, in NIH-RAS cells, the continuous activation of Akt pathway and cyclin D1 lead them to enter into S-phase and in this condition glutamine deprivation triggers a cell-cycle arrest in abortive S phase. Moreover, deprivation of glutamine impairs nucleotides production, and thus affects RNA and DNA *de novo* synthesis, which is needed for high rate replication [54].

Gaglio and colleagues also assessed glucose and glutamine metabolism in NIH3T3 K-ras^{G12V} mutated cells with two specific techniques: ^{13}C metabolic flux analysis (MFA) of ^{13}C-labelled glutamine and glucose metabolism and the non-targeted tracer fate detection (NTFD) of ^{15}N-labeled glutamine. In this way, they followed the metabolic fate of glutamine-derived nitrogen and assessed the carbon utilization from both glucose and glutamine. In particular, they observed that citrate formation was mainly due by [^{13}C]glutamine, deriving from both its oxidative and reductive pathways, and less from [^{13}C]glucose, which mainly ended into lactate [55].

Moreover, a higher expression of PDK genes matched with low pyruvate contribution in TCA cycle, together with an upregulation of some positive regulators of TCA cycle such as IDH2, that fuels reductive carboxylaton of glutamine.

Finally, Gaglio and colleagues observed how glutamine-derived α-nitrogen contributed to biomolecules anabolism. They found that glutamate, aspartate and alanine had more labelled nitrogen than control cells

and transcriptional analysis confirmed these results showing an increase of genes involved in glutamine utilization [55].

All together these findings demonstrated that, as in cancer, in NIH-RAS cells the majority of consumed glucose is diverted into lactate, while the oxidation of Pyruvate to AcCoA is consistently decreased. In this way, TCA cycle flux resulted decrease, presumably because of the expression of Pdk genes. The decrease in glucose utilization through the TCA cycle is replaced by glutamine that becomes the more major source of both carbon and nitrogen for cellular biosynthesis, through aminotransferase and glutamate dehidrogenase activity (Figure 13).

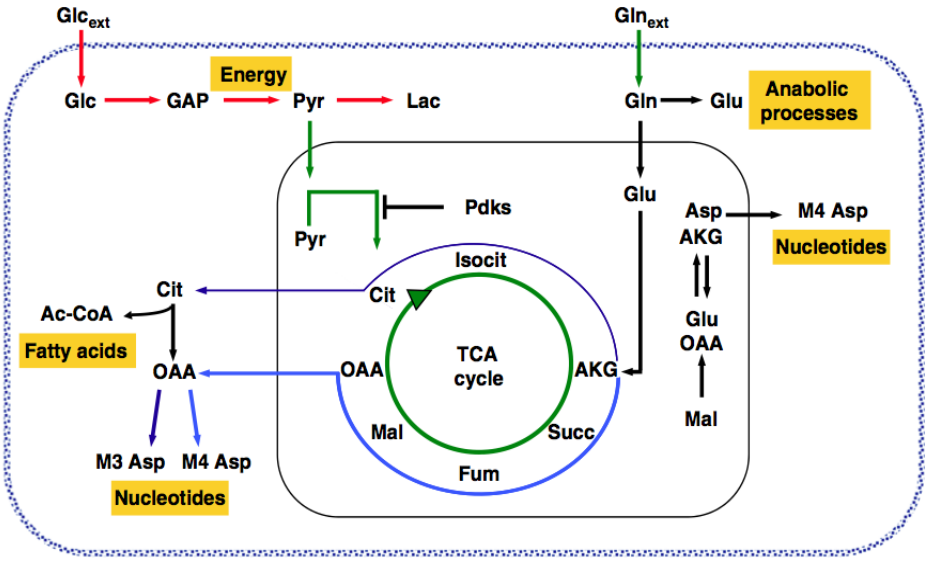

Figure 13 Metabolic rewiring. *Schematic representation of the metabolic reprogramming occurring in transformed k-ras fibroblasts. Red arrows indicate enhanced fluxes, green arrows indicate unchanged fluxes, thin blue arrow indicates glutaminolysys while light blue arrow indicates glutamine reductive carboxylation. (Gaglio D et al. Mol Syst Biol. 2011;7:523.).*

In conclusion, NIH-RAS cells match the classical metabolic phenotype observed in the majority of K-ras driven cancer cells with elevated glycolytic flux for ATP production and decoupling of glycolysis due to an impaired mitochondrial function from the pathway of glutamine, representing a feasible and useful tool to investigate new treatment approaches.

3.1.3 Imaging cancer cell metabolism

A better comprehension ofcancer metabolism may provide great support to tumor diagnosis and treatment. Metabolites are complex molecules showing different physiochemical properties with no direct link to the genetic code. Since metabolites can be view as the product of enzymes action, even a small variation in enzyme activity can cause significant changes in metabolites. For the reason above, the study of metabolites represent a highly specific and sensitive measurement of the biochemical state of the cell. The easiest way to

measure metabolites fluxes is the determination of precursors and their end products such as the evaluation of glucose consumption and lactate production to estimate the glycolytic flux [56].

The study of metabolites involves the combined use of analytical techniques and multivariate statistics analysis among which nuclear magnetic resonance spectroscopy (NMR), gas chromatography–mass spectrometry (GC-MS) and liquid chromatography-mass spectrometry (LC-MS) represent the most important techniques. Both NMR spectroscopy and MS are used as preferential tools to profile metabolism in a systemic way for tumor prognosis and diagnosis, through analysis of fluids, such as blood plasma and urine [57]. NMR and MS methodologies allow to follow variations of metabolite concentrations in normal and pathological conditions. Nevertheless, the same techniques can be exploited in order to identify new metabolites, whose production is a consequence of metabolic alterations. NMR is based on 1H and 13C NMR spectroscopy and allows the detection of all the metabolites present in a sample at concentrations detectable by the instrument. It allows to obtain information in a non-invasive manner maintaining the integrity of tissues, with the limitation due to the low sensitivity.

GC-MS and LC-MS provide the separation of metabolites thorough two different steps. At first, metabolites are separated through chromatographic methods and then, after ionization, according to their mass to charge ratio which can be used for their identification. Nevertheless these techniques allow a higher sensitivity, not all the metabolites can be ionized.

An emerging technique for the in vivo evaluation of cancer metabolism and glutamine utilization is Magnetic Resonance Spectroscopy (MRS) that allow the quantification of different metabolites including glutamine and glutamate. Although MRS indicates only the global level of metabolites in a tissue without giving information about fluxes, it is widely used in vitro using labelled compounds.

Hyperpolarized ^{13}C MR represents another tool to monitor reactions in metabolic pathways. Molecules are labelled with NMR-active nucleus and then hyperpolarized using dynamic nuclear polarization. [5-13C]-glutamine, [1-13C]-glutamate, and [5-13C-4-2H2]-glutamine have been successfully used in cells, but their implementation *in vivo* at preclinical stage remains limited [58].

As already stated, modifications in cell metabolism can be measured *in vivo* through the use PET. Several radiopharmaceuticals have been developed and validated to evaluate modifications in cell metabolism that characterize cancer like glucose or fatty acid metabolism, cell proliferation, tissue hypoxia and molecular target like epidermal growth factors or integrin receptors, as already described in previous paragraphs.

[^{18}F]FDG uptake specifically reflects the levels of glucose transporter GLUTs and HK activity and remains the most widely used tracers in oncology. Nevertheless, there is a large portion of low glycolytic tumors that remain undetectable, suggesting the presence of a switch in their metabolism and energy consumption from glucose to glutamine as alternative nutrient. The possibility to evaluate glutamine metabolism represents and interesting alternative for tumor diagnosis also in association with [^{18}F]FDG. Since glutamine metabolism plays an important role in the metabolism of proliferating cells, many efforts have been recently dedicated to the development of PET radiotracers for the in vivo imaging of glutamine metabolism. 18F-(2S,4R)4-fluoroglutamine and l-[5-11C]-glutamine have been described and validated at preclinical level [59].

Although these tracers are taken up and specifically retained by cancer cells giving good signal to noise ratios, more preclinical studies are needed to better understand if the accumulation mechanism really reflects glutaminolysis.

The potential use of [^{18}F]FLT as a biomarker of therapy efficacy has been evaluated at both preclinical and clinical level as described in the previous chapter. [^{18}F]FLT provides a measure of TK-1 activity and, indirectly, it allows to monitor alterations in metabolic pathways that affect tumor growth including glutaminolysis. Although it provides only indirect measure of glutamine metabolism, [^{18}F]FLT represents an interesting tool in monitoring metabolic alterations because of its almost consolidated use in clinical practice and its demonstrated capability in early predicting therapy efficacy in cancer models and in clinical setting.

3.1.4 Metabolism as target for cancer therapy

Tumor cells exhibit altered metabolic behavior due to both cell-intrinsic properties and tumor microenvironment. Despite the incomplete understanding of cancer metabolism, the recent insights have generated interests in studying new class of therapeutic agents that target altered pathways in cancer, now referred as "metabolic therapies".

Regarding the model of NIH-RAS oncogenic fibroblasts, one of these therapeutic strategies may be based on the great addiction of these cells to glutamine metabolism. BPTES (Bis-2-[5-phenylacetamido-1,2,4-thiadiazol-2-yl]ethyl sulfide) is a potent and selective non-competitive allosteric inhibitor of GLS, in particular the K-type isoform. It binds the allosteric sites of the enzyme and reduces its affinity with phosphate, impairing its phosphate-dependent activation, in both free and substrate-bound enzyme [60].

This drug was successfully used in several studies for blocking conversion of glutamine to glutamate in different glutamine-addicted cancers cells. Emadi and colleagues showed a reduction of primary AML (acute myeloid leukemia) cells with IDH mutations that makes them particularly addicted to glutamine metabolism after BPTES treatment [61]. In another study, Lee and colleagues used a MYC-inducible human Burkitt lymphoma model p593 and showed the effects of BPTES administration in aerobic and hypoxic conditions *in vitro*. They observed a reduction of cancer cells growth and proliferation in aerobic condition after BPTES, demonstrating that the inhibition of glutaminase kills preferentially hypoxic cells and suggesting the importance of glutamine metabolism in supporting cell bioenergetics and oxidative stress. Moreover, BPTES administered *in vivo* in mice significantly decreased tumor progression of P593 tumors [62].

Another possible target for NIH-RAS fibroblasts can be autophagy. Autophagy represents a fundamental process for maintaining cells homeostasis, especially when ROS production damages mitochondria or in hypoxic conditions [63]. Expression of oncogenic k-ras has been demonstrated to render cells particularly susceptible to autophagy inhibition, giving rise to the hypothesis that RAS cancer cells are "autophagy-addicted". Targeting tumor cells with autophagy inhibitors may be a useful way to treat aggressive cancers. Although the role of autophagy in RAS cancer cells is not still completely clear, chloroquine represents another candidate drug for NIH-RAS cells, where Ras metabolic alterations and metabolic stress lead to an increase in the level of basal autophagy [64].

Chloroquine (CQ) is an FDA-approved antimalarial drug, well tolerated as already demonstrated and used to treat autoimmune diseases due to its low immunosuppressive properties [64]. Nowadays, CQ represents the only drug acting against autophagy approved in clinical use. CQ diffuses itself into lysosomes of cells and, being a weak base with hydrophobic characteristics, it is protonated and remains trapped. Within the lysosomes, CQ leads to a rise in pH, avoiding the fusion with autophagosomes and blocking autophagy at a late stage.

Recently, many studies have been performed to evaluate the efficacy of CQ in combination with other drugs in contrasting tumor progression.

In a syngeneic model obtained with cancer cells with no p53 induction, CQ treatment showed an impaired tumor growth, but not a regression. Conversely, conditional p53 activation with tamoxifen showed a high percentage of regression, with accumulation of autophagosomes assessed with GFP-LC3 fluorescence, demonstrating tumor dependence on autophagy as adaptation strategy for survival in apoptotic state [65].

Another study by Kaneko et al., used human colorectal cancer cell lines (CaR-1 and HT-29) and murine colorectal cancer cell line (Colon26).

In *in vivo* xenograft models of colorectal cancer the combination of CQ and Temsirolimus - a rapamycin-derived chemotherapeutic drug known to block mTOR and thus activate autophagy - increased the expression of LC3 and p62 proteins, indicating an accumulation of autophagic vesicles in the cytoplasm of the cells. Moreover, the synergic treatment showed an increased BAX/BCL-2 ratio and a reduced tumor growth, if compared to TEM monotherapy. This remarks the importance of autophagy in cancer resistance to anti-mTOR drugs [66].

Taken together, these results clearly suggest that, as a consequence of apoptosis and other processes inducing stress like chemo/radiotherapy, cancer cells try to maintain their homeostasis through autophagy. Hence, the use of CQ may represent a strategy to improve therapy and better counteract cancer cells growth for these type of tumors with high levels of basal autophagy.

3.2 Materials and methods

3.2.1 Cell line

Mouse embryonic fibroblast NIH3T3 and NIH3T3 K-ras transformed cell lines (NIH-RAS) were routinely grown in Dulbecco's modified Eagle's medium containing 10% newborn calf serum, 4 mM L-glutamine, 100 U/ml penicillin and 100 mg/ml streptomycin (normal growth medium) (all from Invitrogen, Carlsbad, CA, USA) at 37°C in a humidified atmosphere of 5% CO2.

For treatment studies, cells were plated at the density of 3000 cells/cm^2 in complete growth medium. After 18 hours, cells were washed twice with phosphate-buffered saline (PBS) and incubated in a media with different glutamine concentrations (4 and 0.5mM glutamine). Cells were treated for 54 hours with 50 μM Chloroquine (CQ) or different concentrations of BPTES (4, 6 and 8 μM) (Sigma-Aldrich Inc.).

To measure cell proliferation, harvested cells were counted by Burker chamber.

3.2.2 Animal model

To generate the orthotopic model, 250000 NIH-RAS cells were injected subcutaneously on the right flanks of 8 weeks old nu/nu male mice (Harlan Laboratories). Animals were housed under specific pathogen-free conditions and handled and kept in accordance with the Ethic Committee regulations. After cells injection, mice were monitored twice a week for body weight and tumor volume. Tumor volume was measured using a digital calliper and calculated following the formula:

tumor volume = (long side*(short side)^2)/2).

At the end of the studies mice were sacrificed and tumors collected for post mortem analysis.

3.2.3 Study design

The study has been performed in three phases:

Phase 1: longitudinal study for the identification of the optimal window of tumor growth and evaluation of the feasibility of using [^{18}F]FDG and [^{18}F]FLT PET to monitor tumor progression in mice injected with NIH-RAS cells (n=20).

Phase 2: metabolic study to correlate *in vivo* with ex vivo data. NIH-RAS tumor bearing mice (n=6 per imaging and time-point group) performed [^{18}F]FDG and [^{18}F]FLT PET at pre-established time points from cells injection (7, 9 and 13 days) followed by the immediate sacrifice and collection of tumors to correlate the metabolic information obtained *in vivo* with post mortem metabolomics and immunohistochemistry analyses (Figure 14).

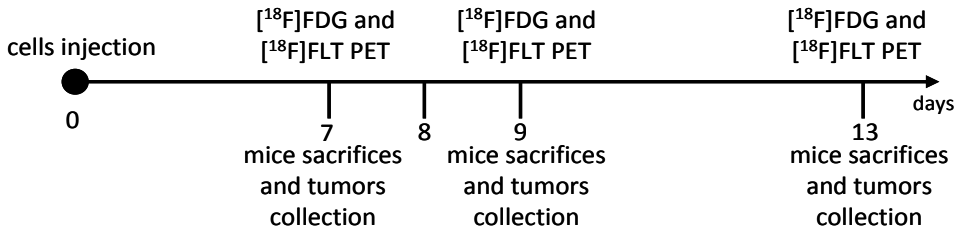

Figure 14 Study design. *Time course of animal model characterization.*

Phase 3: evaluation of tumor response to the pharmacological approach aimed to block glutamine metabolism and autophagy with [^{18}F]FDG and [^{18}F]FLT PET (Figure 12). Mice were divided into 4 groups (n=4) of treatment (Vehicle, Chloroquine, BPTES, Chloroquine + BPTES) and monitored with [^{18}F]FDG and [^{18}F]FLT PET before and 48 hours after treatment (Figure 15). Mice received PBS as vehicle, Cholorquine (5 mg/kg), BPTES (10 mg/kg) and Chloroquine plus BPTES at the same dosage. Each treatment was administered intraperitoneally.

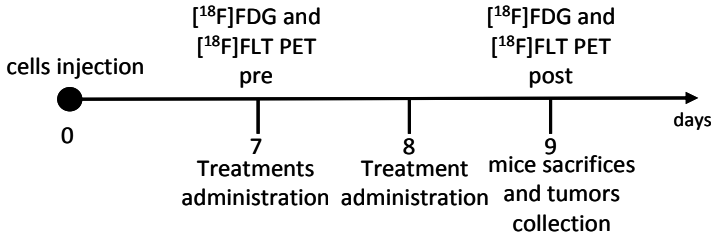

Figure 15 Study design. *Time course of treatment study.*

3.2.4 PET studies

Mice were studied using a YAP-(S)-PET II small animal scanner with [^{18}F]FLT and [^{18}F]FDG to monitor tumor growth and therapies efficacy. [^{18}F]FDG was prepared at San Raffaele facility for clinical use (European Pharmacopeia VIII Edition), while [^{18}F]FLT was obtained as previously described [67]. Both radiopharmaceuticals were injected with a purity > 99%. Animals in fasting condition were injected with an average of 44.4 MBq of [^{18}F]FDG and [^{18}F]FLT. Mice under slight ether anaesthesia were positioned prone on the bed scanner with the tumor centred in the field of view. Dynamic acquisitions start after 60 minutes of tracers uptake and lasted 30 minutes (six scans of 5 minutes each). Throughout the scan mice were maintained sedated with a mixture of Isoflurane and air (1:2). Images were acquired in 3D mode and reconstructed using the expectation-maximization algorithm (EM). Images were calibrated by dividing them with phantom image to transform count per voxel values in MBq/g, and were corrected for ^{18}F half-life (109.8 min). The radiotracer uptake of tumoral and background region were measured using ROI analysis using Pmod and ImageJ software as follows: circular ROIs were drawn on the tumor mass using the automatic isocontour tool of the software; background regions were manually defined, drawing circular ROIs on three consecutive transaxial slices on a region with a low and constant uptake of the tracer (the thoracic

muscle for [^{18}F]FDG images and the contro-lateral region for [^{18}F]FLT studies). Radioactivity concentration was calculated as maximum standardized uptake value (SUVmax), corrected for the injected dose and animal weight according to the formula:

SUVmax = (max radioactivity measured in the ROI/injected radioactivity)*animal weight.

Uptake data were also calculated as tumor-to-background ratio (T/B) dividing the SUVmax of the tumor to the SUVmean of the background. Moreover, volume of radioactivity accumulation (metabolic volume) was calculated as follows. In order to extract lesion signal from the background we established a range considering as minimum threshold the minimum uptake value of the tumor and as maximum threshold the average between the maximum tumor uptake and the mean background uptake. We hence apply this range to automatically extract the only areas of tumor metabolically active from each PET study using PMOD software.

3.2.5 Post mortem analyses

For immunohistochemistry (IHC) studies mice were sacrifice byCO2 asphyxiation and tumors were removed for histologicalanalysis.Harvested tumors were embedded in optimumcuttingtemperature compound (OCT) and frozen in liquid nitrogenfor hematoxylin and eosin (H&E) staining. Sections were fixed andimmunostained with anti-Ki67 antibodyand anti-TK1 (Novusbio). The immunoreactions were revealed usingrabbit-on-rodent horseradish peroxidase-polymer (BiocareMedical) and using 3,3 diaminobenzidine (DAB) as chromogen(Biogenex). Slides were counterstained with hematoxylin.Photomicrographs were taken usingthe AxioCam HRc (Zeiss) with the AxioVision System 6.4(Zeiss).

3.2.6 Statistical analysis

Results are expressed as mean value +/- SD. Experimental differences were tested for significance with the Student T Test or, when possible, with the One Way ANOVA test. A p-value of 0.005 or less is considered statistically significant.

3.3 Results

3.3.1 Preliminary study

We initially verified whether the NIH-RAS model was suitable for PET studies with [^{18}F]FDG and [^{18}]FLT. To this aim, a preliminary study was performed to monitor tumor growth by calliper and with PET scans performed when tumors became visible detectable.

Tumor growth results comparable and homogeneous in mice injected with oncogenic NIH-RAS fibroblasts. All mice developed fast growing tumors starting from day 7 from cell injection that reached an average of 1090 mm^3 after two weeks (Figure 16). Animals underwent a PET scan with [^{18}F]FDG and [^{18}F]FLT 10 days after cells injection when tumor volume was approximately of 172 mm^3 (+/- 46 mm^3). PET images showed the presence of glucose avid tumors with a homogeneous distribution of [^{18}F]FDG within the tumor. [^{18}F]FLT uptake, although homogeneous in each mouse considered, showed lower values in terms of both SUVmax and T/B ratio, if compared to [^{18}F]FDG. Due to the extremely fast tumor growth, no other PET scans could be performed to assess potential changes in tumor metabolism.

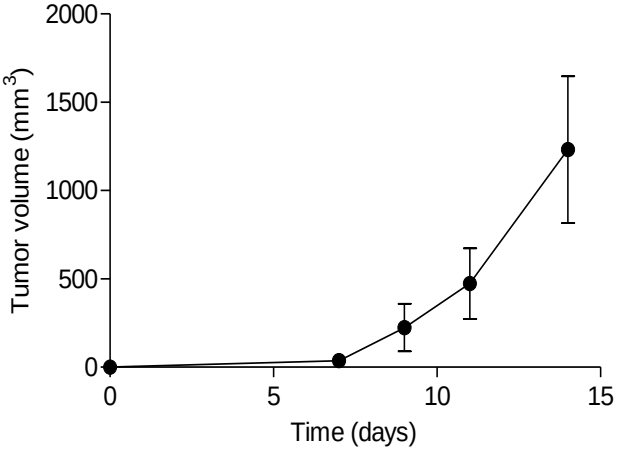

Figure 16 Tumor growth curve. *Tumor growth over time of NIH-RAS tumors; tumors displayed aggressive and fast growth rate reaching large volumes in few days.*

3.3.2 Metabolic study

Given the rapid growth of NIH-RAS cells observed in the preliminary study, it was decided to set up a longitudinal study to better monitor changes in tumor metabolism scanning animals at established and very close time points (7, 9 and 13 days after cell injection). To compare *in vivo* metabolic results with ex vivo analysis we relied on several groups of mice (a group for each tracer and for each time point) that were sacrificed immediately after imaging for tumor harvesting.

Tumour growth was monitored every day by calliper showing a trend comparable to that of the preliminary study and homogeneous among the different groups of animals. Starting from the 7th day after cells injection, mice showed a high uptake of [^{18}F]FDG and a moderate uptake of [^{18}F]FLT, as expected. A significant

increase of [^{18}F]FDG uptake was observed in terms of both SUVmax ($p = 0.00004$) and T/B ($p = 0.00022$) from day 7 to 9 after cells injection revealing a switch in glucose metabolism (Table 1 and Figure 18). On the other hand, cell proliferation remained constant as indirectly depicted by [^{18}F]FLT uptake.

At the last time point (13 days after cells injection) small areas of necrosis and/or hypoxia were detectable within all tumors influencing the uptake of both tracers. [^{18}F]FDG and [^{18}F]FLT SUVmax, as well as T/B ratio, decreased compared to the first scans.

		7	9	13
SUVmax	[^{18}F]FDG	0.769 ± 0.36	2.217 ± 0.37	2.336 ± 0.50
	[^{18}F]FLT	1.031 ± 0.59	1.359 ± 0.18	1.233 ± 0.18
T/B	[^{18}F]FDG	2.302 ± 1.20	7.845 ± 1.87	8.146 ± 1.85
	[^{18}F]FLT	2.121 ± 0.58	2.812 ± 0.91	2.226 ± 0.51

Table 1 PET quantification. *[^{18}F]FDG and [^{18}F]FLT uptake values measured as SUVmax and T/B ratio at 7, 9 and 13 days after cells injection. Red squares indicate the significant increase in [^{18}F]FDG uptake from day 7 to 9.*

Moreover, tumor metabolic volumes were evaluated observing their increase over time in parallel with volumes calculated by calliper. However, a correlation at day 9 after cell injection for both radiotracers was detected (Figure 17). The lack of correlation at the other time points can be probably due to the small volume of lesions at the earliest time point that determines the spill over effect of PET scan and the presence of wide areas of necrosis/hypoxia at the last time point that influence tracers uptake.

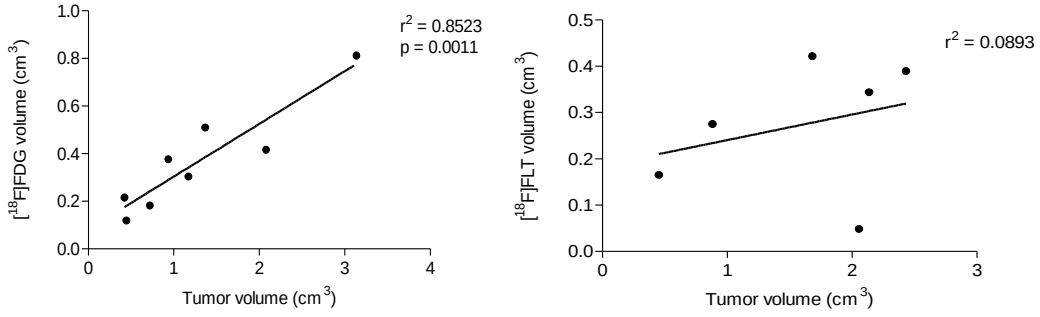

Figure 17 Correlation plots of NIH-RAS tumors. *Correlation between [^{18}F]FDG (left) and [^{18}F]FLT (right) volume measured by PET and tumor volume measured by calliper .*

A

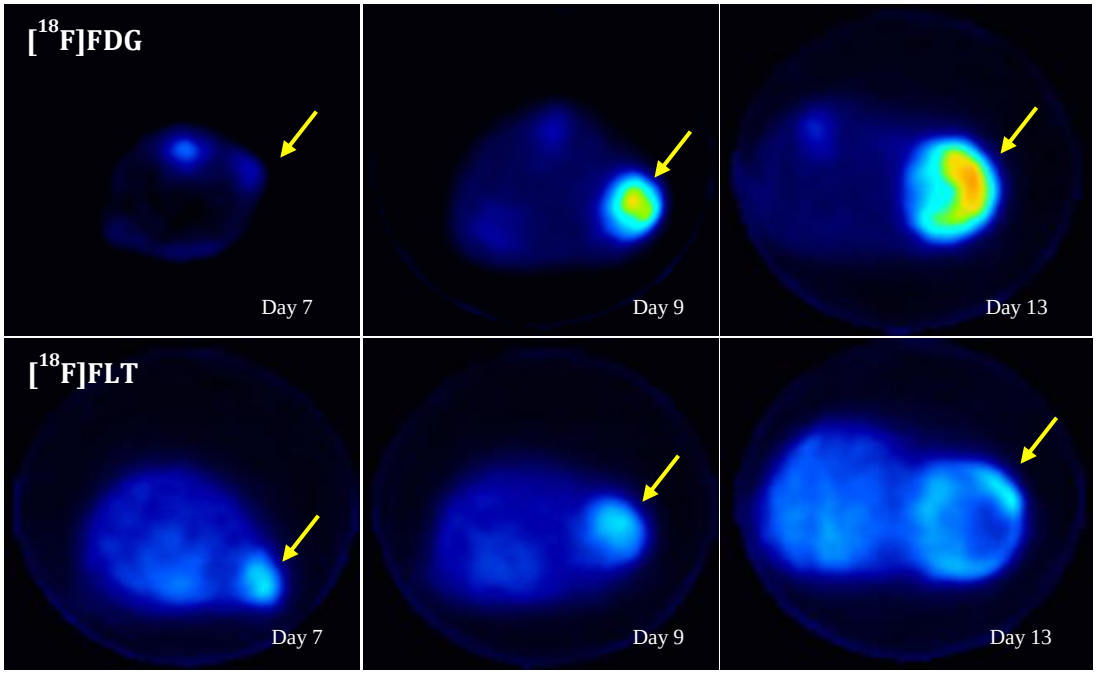

B

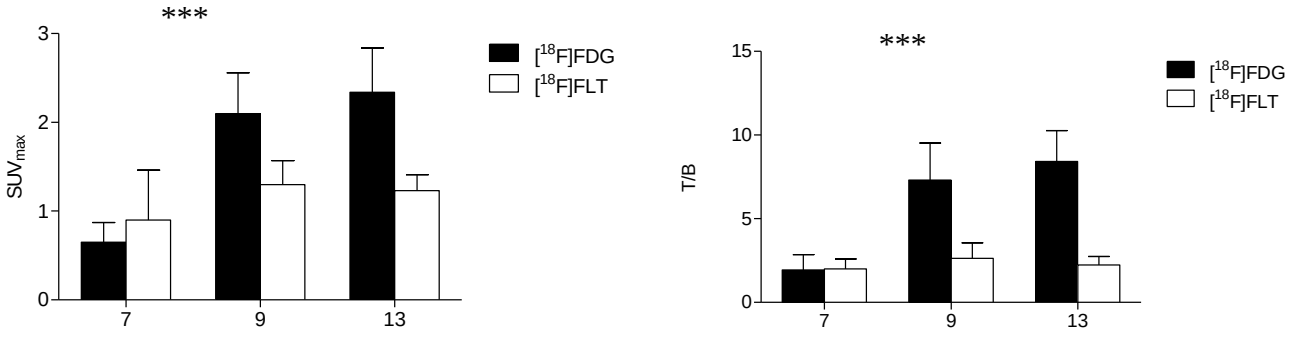

Figure 18 PET imaging. A) *Transaxial [^{18}F]FDG and [^{18}F]FLT PET images of representative NIH-RAS mice. [^{18}F]FDG and [^{18}F]FLT PET scans were performed at 7, 9 and 13 days after cells injection. Yellow arrows indicate tumor. Other [^{18}F]FDG signals are to be referred to spinal cord not-specific uptake.* ***B)*** *Radiopharmaceuticals uptake expressed as SUVmax (left) and T/B ratio (right) at different time points in NIH-RAS mice. [^{18}F]FDG uptake displays a significant increase from 7 to 9 days after cells injection while [^{18}F]FLT remained mainly constant (*** $p < 0.005$).*

3.3.2.1 Histopathological analyses

Immediately after imaging mice were sacrificed and tumors collected for post mortem analyses to investigate morphological features and correlate *in vivo* data with proliferation markers. The high aggressiveness of NIH-RAS tumors was confirmed by both H&E and immunohistochemistry. Samples displayed high mitotic activity regardless the time points, with only small necrotic areas found at the last time point after cell

injection (13 day) as depicted by H&E staining (Figure 19). IHC staining revealed tumors with homogeneous and high positivity that slowly increased over time for both Ki67 and TK-1 antibodies at each time points, confirming [^{18}F]FLT PET data and suggesting the presence of highly proliferative cells.

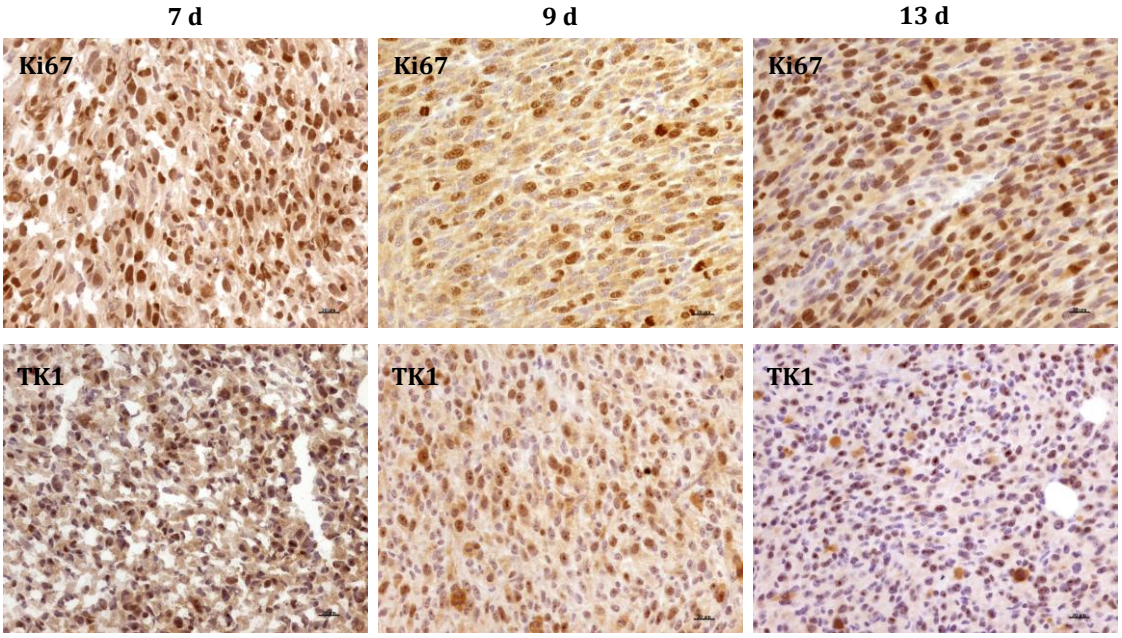

Figure 19 Post mortem analyses*. IHC staining for Ki67 and TK1 in samples collected from animals at 7, 9 and 13 days after cells injection.*

3.3.3 Treatments evaluation

3.3.3.1 *In vitro treatments*

Metabolic alterations previously demonstrated in NIH-RAS cells suggested that ras oncogenic activation together with metabolic stress could lead to autophagy activation, necessary for cancer cells growth.

NIH-RAS cells displayed a significant increase in AMP levels and ROS production essential for the induction of autophagy compared to wild type NIH3T3 cells, as measured by GC/MS. Moreover, by electron microscopic analysis of cell morphology we have observed an increased number of mithocondria within lysosomes in NIH-RAS cells compared to normal cells (data not shown).

NIH-RAS cells have been treated with with the inhibitor of autophagosomal degradation chloroquine (CQ) or with the glutaminase inhibitor BPTES. NIH-RAS grown in normal growth medium (4mM Gln) treated with 50 µM CQ have shown a high cell death with 53% of trypan blue positive cells compared to NIH3T3 that have shown a marked accumulation of vacuololi with basal (3.7%) percentage population of trypan blue positive. Moreover, since the physiological role of autophagy increase during nutrient starvation we performed co-treatment with CQ autophagy inhibitor and nutrient starvation. In NIH-RAS a larger cell death

(97.2% of trypan blue positive cells) was observed with the simultaneous treatment of CQ and glutamine deprivation as compared to normal ones (Figure 20).

Taken together, these evidences demonstrated that the basal autophagy mechanism supports cells growth in NIH-RAS cells.

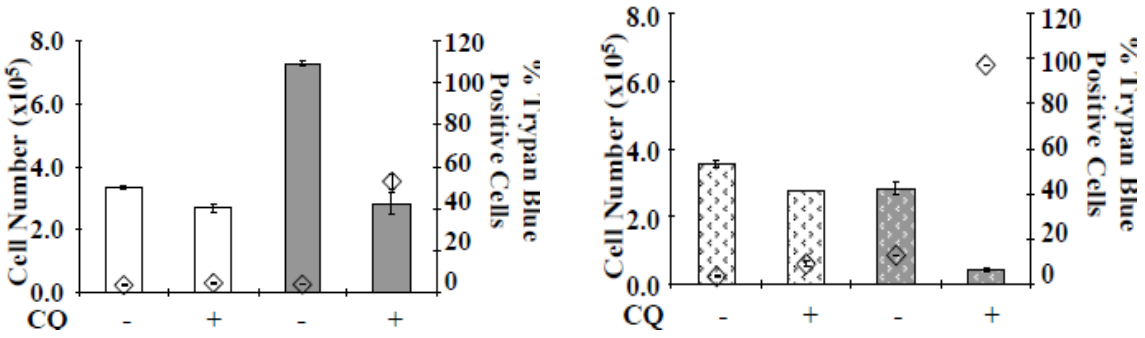

Figure 20 CQ treatment in vitro. *NIH3T3 (white columns) and NIH-RAS (grey columns) treated (+) or not (-) with CQ. CQ treatment triggers a significant reduction of cell number in both normal condition (left) and glutamine deprivation (right).*

As shown in Figure 21, only NIH-RAS proliferation was inhibited by BPTES. Moreover, cells inhibition was directly proportional to BPTES concentrations, with the highest dose determining the highest inhibition of cells proliferation.

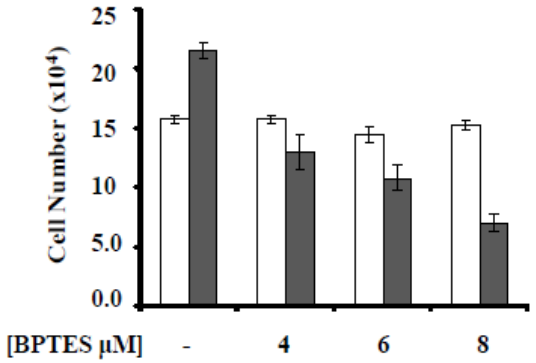

Figure 21 BPTES treatment in vitro. *NIH3T3 (white columns) and NIH-RAS fibroblasts (grey columns) plated at 3000/cm^2 treated with different concentrations of BPTES (4, 6 and 8 µM).*

3.3.3.2 In vivo treatments: effects on tumor size

The metabolic shift revealed by [^{18}F]FDG PET from 7 to 9 days after cells injection represented an intriguing therapeutic window to maximize the effects of treatments that targeted cell metabolism. We decided to design a therapeutic schedule of 48h aiming to counteract the metabolic shift started at day 7 and completed the following day. Animals were monitored for changes in tumor volume with calliper every day

and performed PET scans with [^{18}F]FDG and [^{18}F]FLT before treatment beginning and 48h after. Although we failed to observe any reduction of tumour volume after treatment, a significant difference in tumor volume between Control and Combined treated mice at the end of treatment ($p<0.05$) was found (Figure 22), indicating a delay in tumor growth due to treatments. Value rates of tumor volume's increase were 3,702 ± 1,174 in control group, 3,371 ± 0,977 in chloroquine-treated group, 2,661 ± 0,527 BPTES treated and 2,548 ± 0,416 in combined group with a p-value between control and combined treatment groups of 0,04 (Figure 22).

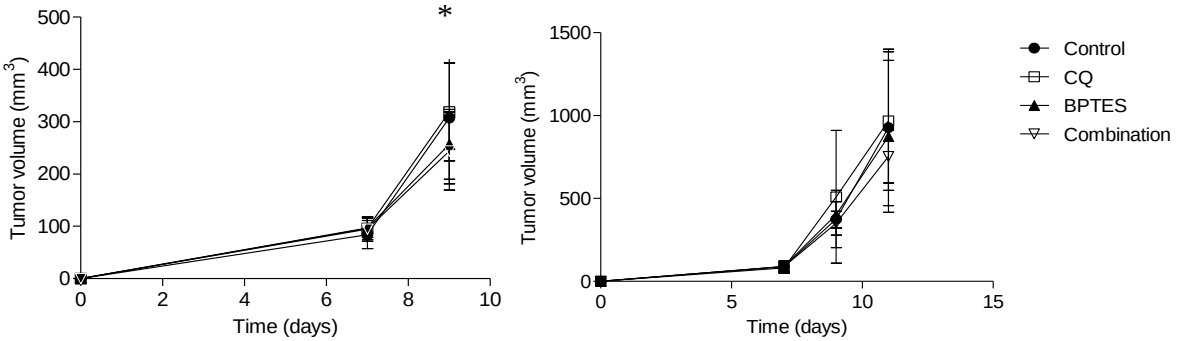

Figure 22 Evaluation of tumor size after treatment. *Analysis of changes in tumor size measured at calliper in mice treated with 2-days scheduled (left) and 4-days scheduled treatment (right). Mice received daily vehicle (Control), 50 mg/kg chloroquine (CQ), 10 mg/kg BPTES and chloroquine and BPTES in association (Combination). All results are expressed as ratio values of n=4-5 animals per group (* p < 0.05).*

Moreover, we decided to apply a prolonged treatment schedule measuring tumor size every two days starting from therapy's beginning. Irrespective of treatments, tumors showed highly aggressive and fast growth rate. Growth curves showed a slight and temporary effect of BPTES and combined treatment at day 9 after cell injection, but with no statistical significance (Figure 22). On the other hand, CQ alone seemed to worsen cell phenotype accelerating tumor progression.

3.3.3.3 In vivo treatments: effects on metabolism

In parallel, we evaluated the variation of [1^{8}F]FDG and [^{18}F]FLT uptake, expressed as ratio between the T/B values measured at day 2 and at day 0 from starting therapy (day 9 and 7 after cells inoculation respectively). No significant differences in glucose metabolism or in proliferation rate were observed in treatment groups when compared to control group as depicted by PET images as depicted by graphs in Figure 23. [^{18}F]FDG rate of increase in T/B uptake was 1,423 ± 0,398 in control group, 1,763 ± 0,787 in chloroquine group, 1,253 ± 0,113 in BPTES group and 1,314 ± 0,255 in combined group; [^{18}F]FLT rate of increase was 1,982 ± 0,771 in control, 1,769 ± 0,895 in chloroquine group, 2,083 ± 0,486 in BPTES group and 1,886 ± 0,492 in combined group.

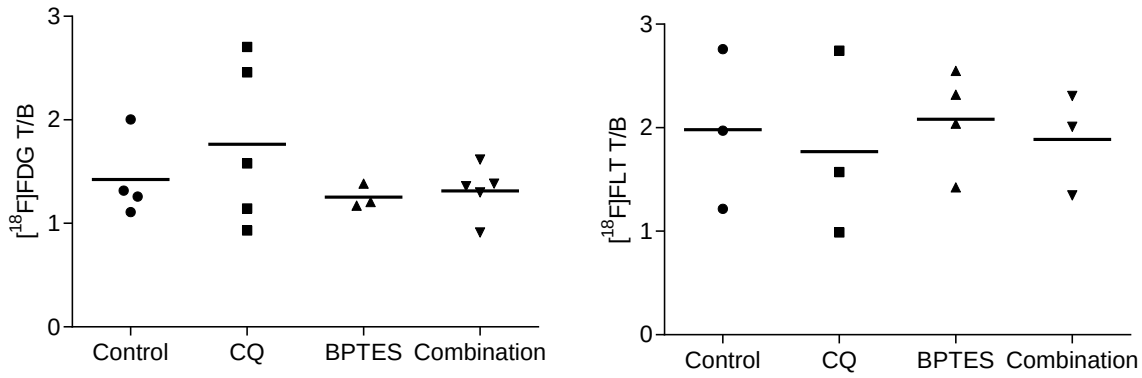

Figure 23 PET quantification after treatment. *Quantitative analysis of changes in [^{18}F]FDG (left) and in [^{18}F]FLT T/B ratio (right). Values are calculated as ratio between T/B pre and 48h post treatment in vehicle (Control), 50 mg/kg chloroquine (CQ), 10 mg/kg BPTES and chloroquine and BPTES in association (Combination) groups.*

3.3.3.4 Post mortem evaluation of treatments effect

To better investigate treatments effect and validate in vivo data, glutamate levels have been evaluated on tumors harvested after imaging. Analysis performed revealed no differences in glutamate levels between Control and BPTES treated mice as depicted in Figure 24, confirming metabolic findings obtained with PET imaging.

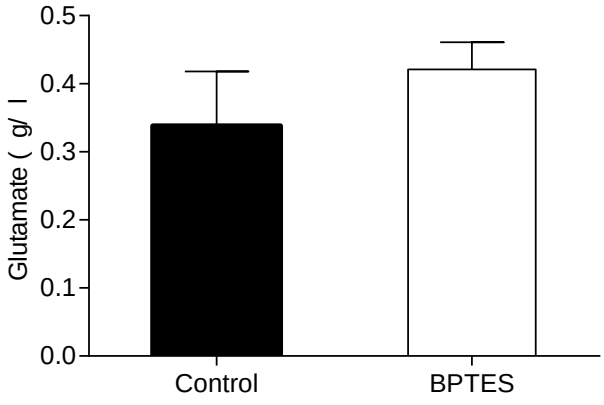

Figure 24 Evaluation of glutamate levels. *Amounts of glutamate quantified with spectrophotometry at ë = 450 nm in tumors collected from representative control and combined-treated mice.*

3.4 Discussion

Cancer cells differently from normal cells rely on glycolysis for energy production even in aerobic conditions as demonstrated by Otto Warburg in 1920s. In addition to the glycolytic dependency, cancer cells display other metabolic alterations such as increased fatty acid synthesis and glutamine consumption. Glutamine is efficiently used for mitochondrial metabolism and is decoupled from glucose metabolism providing an alternative source for energy supply and anabolic processes. Hence, glutamine becomes an important source that supports tumor growth. In this thesis work, such alterations have been investigated *in vivo,* taking advantage from the NIH-RAS fibroblasts model harboring an oncogenic k-ras gene. It has been demonstrated that k-ras oncogene expression enhanced glucose uptake and decrease its consumption in the TCA cycle that becomes fueled by glutamine. Moreover, in these cells Ras activation and metabolic stress lead to an increase of basal autophagy, contributing to the development of the aggressive phenotype by recycling damaged organelles and providing metabolic precursors from them. Overall, these evidences make the NIH-RAS an interesting model to investigate aggressive types of cancer expressing oncogenic Ras gene such as colon, pancreatic and lung.

Translating *in vitro* data to animal models of disease that can be *in vivo* investigated using PET imaging provides a translational bridge for the identification of new strategies for cancer treatment. Modifications in cell metabolism or tissue environment such as glucose metabolism, proliferation and hypoxia can be detected *in vivo* by the use of PET imaging with specific radiotracers.

The former part of this work is focused on the characterization of tumor growth of NIH-RAS fibroblasts *in vivo* by measuring tumor volume with caliper and monitoring glucose metabolism and cell proliferation using PET with [^{18}F]FDG and [^{18}F]FLT, respectively. As previously demonstrated by Bossu and colleagues [52], this cell line gave rise to measurable tumors in 100% of animals in 7 days.

Within the current work, PET imaging has been shown to be a useful tool to characterize the NIH-RAS model *in vivo* allowing the identification and monitoring of tumors during time with [^{18}F]FDG and [^{18}F]FLT already at 7 days after cells injection.

[^{18}F]FDG PET performed at a very close time points revealed a sudden increase in glucose consumption from 7 to 9 days after cells injection. On the other hand, [^{18}F]FLT uptake remained stable over time. Although [^{18}F]FLT uptake can provide only an indirect evaluation of glutamine metabolism measuring TK-1 activity and, thus, nucleotides production, it confirmed the glutamine's dependence for growth already found *in vitro* in these cells. Hence, it was assumed that the time interval of 7-9 days would correspond to the *in vivo* time point in which glucose and glutamine metabolism decouple and glutamine becomes the primary biosynthetic source for NIH-RAS replication. Finally, IHC analyses performed on tumor samples collected after imaging confirmed *in vivo* results. The elevated mitotic activity of NIH-RAS cells have been shown at each time points and only small portion of necrosis have been found, confirming the high aggressiveness and proliferative ability of these cells. The high and stable proliferation rate has been confirmed by Ki67 and TK-1 positivity of NIH-RAS tumors at each time points.

Since the high glutamine addiction of NIH-RAS cells provides a significant advantage in terms of survival and proliferation, the inhibition of glutamine conversion into glutamate would be harmful for these cells. However, hindering several pathways involved in cancer progression can be a stronger strategy for cancer treatment.

For this reason, given that NIH-Ras cells also displayed a significant increase in basal autophagy *in vitro*, a pharmacological approach that would inhibit both glutamine consumption and autophagy - based on BPTES and CQ - was adopted, investigating how it could affect glucose metabolism and cell proliferation.

Treatments with BPTES and CQ began 7 days after cells injection with the aim to maximize their effects hindering the metabolic shift. After 2 days of treatment, a slight slowdown of tumor growth in animals which received combined therapy was observed with respect to the Control group. Analogue results were obtained prolonging the treatment regimen for 4 consecutive days. The same dose of treatments for more days did not improve drugs' efficacy being unable to slowdown the fast tumor growth of NIH-RAS tumors. Regarding treatments' effects on metabolism, no differences in [^{18}F]FDG and [^{18}F]FLT uptake have been shown after 48h of treatment, indicating that treatments did not influence glucose metabolism and proliferation.

The use of BPTES to counteract cells growth has been evaluated in several previous *in vitro* studies. In the current NIH-RAS model, BPTES seems to fail in inhibiting either tumor growth *in vivo* or GLS activity, as resulted by ex vivo analyses of tumor samples.

Ex vivo assays demonstrated that glutamate production rate is comparable in Treated and Control tumors, indicating that glutamine metabolized by GLS may be not the only source of glutamate production. The existence of alternative pathways for glutamate production independent from GLS activity may represent a potential explanation of BPTES lack of efficacy. It is for instance likely that NIH-RAS cells may use transaminases enzymes to produce glutamate instead of GLS. These data confirmed in part the findings of Gross and colleagues who found a partial inhibition of glutamine consumption in the T47D breast cancer cell line after treatment with a glutaminase inhibitor analogue to BPTES, probably due to the presence of a glutaminase-independent pathway for glutamine metabolism [68]. Moreover, they indicated that glutaminase inhibitors display a short half-life and, once drug administration is suspended, glutaminase activity would restart quickly.

A great efficacy of BPTES was observed in primary AML cells with mutated IDH enzyme which are strongly addicted to glutamine *in vitro*, although, once translated *in vivo*, BPTES effects did not revealed the same efficacy in terms of reduction of volume or delay of tumor growth [61]. In the *in vivo* study of Le et al., mice inoculated with lymphoma B cells with MYC-inducible activation daily treated with BPTES for 20 days displayed smaller tumor volumes when compared to controls at the end of therapy. In the same mouse model after 7 days of daily treatment no changes in tumor volume between treated and control mice were detected by Dutta and colleagues, but only a reduction in glutamate pool [62].

The results of our current study show a similar trend, where *in vivo* results do not confirm *in vitro* BPTES effects. Moreover, differently from other works found in literature, it was decided to use a highly aggressive cell line. Although it would be representative of tumors with k-ras oncogenic mutations and resistance to

treatment and since GLS inhibitors display short half-life, higher doses of BPTES may be needed for a significant glutaminase inhibition.

Regarding autophagy, different types of cancer expressing Ras mutation have been reported to be particularly susceptible to autophagy inhibition [64].

CQ alone does not show effectiveness but reveals a valid anti-tumoral action when coupled to other agents such as chemotherapeutic drugs, radiotherapy or apoptosis induction [69, 70, 71].

Previous studies show that the addition of CQ improve Bcl-2 inhibitors' efficacy in patient-derived xenograft models of small cell lung cancer, since it decreases autophagy triggered by treatment [70]. Furthermore, the association of CQ with rapamycin was tested *in vitro* and *in vivo* in two breast cancer models where it failed to further sensitise tumors to mTOR inhibition. However, the association was effective only in the later stage of tumor growth, at a given tumor size when tumor displayed large hypoxic areas [71]. This can be a possible explanation of the lack of efficacy of CQ for NIH-Ras tumors that quickly grow, reaching massive volumes already at the beginning of therapy, but that do not display hypoxic and/or necrotic portions, as demonstrated by IHC analyses.

The observation of any effects of CQ treatment is not possible with this model, even in combination with BPTES. K-ras mutation may not trigger an exclusive addiction to autophagy and GLS activity, allowing cancer cells to avoid BPTES and CQ inhibitory activity. Finally, CQ efficacy could also have been limited because of BPTES, which do not induce a strong dependence on autophagy in NIH-RAS cells.

4. GLIOMA MODEL

4.1 Glioma

Gliomas are the most frequent cancers of the Central Nervous System and comprise low and high-grade tumors that originate from the glia, the brain tissue providing support functions to neural cells and involved in signal transduction and neurotransmission. Gliomas belong to neuroepithelial tissue cancers as established by the World Health Organization (WHO) and form a heterogeneous group of tumors that can be histologically divided into three subtypes: astrocitomas, oligodendrogliomas and ependynomas. Astrocitomas represent the most frequent form of gliomas and are graded from I to IV by the WHO: diffuse astrocytoma (WHO grade II astrocytoma), anaplastic astrocytoma (WHO grade III astrocytoma) and glioblastom amultiforme (WHO grade IV astrocytoma), the most lethal and frequent form [72].

Glioblastoma multiforme (GBM) accounts for 50% of all astrocitomas and is characterised by rapid growth and diffuse invasiveness of the adjacent brain parenchyma. Histopathological features of glioblastoma include cellular polymorphism, nuclear atypia, mitotic activity, microvascular proliferation and necrosis. Despite the many efforts, treatment of glioblastoma remains palliative and the prognosis for a patient with diffusely infiltrating GBM is dismal with a median progression-free survival of 6.9 months and a median overall survival of 14.6 months [73].

Glioblastomas can be divided into two morphologically identical subtypes based on the presence of a previous lesion: primary and secondary GBM. Primary GBM constitute the 90-95% of all GBM and are defined as de novo tumors without precursor lesions. They are highly aggressive and progress fast. Secondary GBM, instead, are rare tumors and derived from previous GBM that accumulate mutations over time and develop a higher state of malignancy and histological grade [72].

4.1.1 GBM biomarkers

Glioblastoma represents a type of tumor emblematic for inter- and intra-tumor heterogeneity and resistance to treatment. The identification of molecular biomarkers of GBM has led to a better management of patients both in terms of diagnosis and classification. In particular, several molecular biomarkers have been validated as predictive markers with a prognostic significance for the progression free-survival of GBM patients. The most well-known and common activating oncogenic changes in glioma are those involving receptor tyrosine kinases (RTK). Gene encoding epidermal growth factor receptor (EGFR), located on chromosome 7p12, is amplified and/or mutated in approximately 60% of de novo glioblastomas and rarely amplified in secondary glioblastomas [74]. Aberrant EGFR activity seems to play an important role in tumorigenisis and several therapeutic approaches have been developed targeting it. The most common product of the mutated gene is the EGFRvIII mutant protein that can homodimerize and autophosphorylatere becoming constitutively active. EGFRvIII promotes glioma cell proliferation and invasion and represents a target antigen for immunotherapy strategies [74]. In a similar way, amplification of the platelet-derived growth factor receptor gene (PDGFRA) is also present, although in a smaller proportion of adult GBM patients. Loss of the oncosuppressot Phosphatase and TENsin homolog (PTEN) gene, due to LOH of chromosome 10q and

mutations, occurs in 60-80% of GBM cases with similar frequencies in primary and secondary glioblastomas. PTEN loss results in activation of the serine/threonine-specific protein kinases (AKT)/mammalian target of rapamycin (mTOR) pathway and has been implicated in proliferation, migration and invasion [75]. Clinical studies show a correlation between PTEN loss and poor prognosis, even if the clinical relevance of PTEN as a prognostic biomarker is still unclear.

Another feature of glioblastoma is represented by the methylation of MGMT, a DNA repair protein that removes alkyl groups produced by the action of O-6-Alkylating agents. In the course of tumor development, MGMT can be silenced by the methylation of its promoter, preventing the repair of the DNA damage. MGMT has gained clinical relevance since several clinical studies report a predictive value of MGMT absence in patients undergoing treatments with alkylating agents. Although several studies indicate MGMT methylation as a prognostic marker of better response to treatments [76, 77], leading to patient selection for appropriate treatments, MGMT significance as stratification biomarker still represents a matter of debates and requires more investigations because of both the variations in how the degree of methylation affects outcomes and the sensitivity of test analyzing the methylation status.

The oncogene BRAF encoding a serine threonine kinase involved in cell signaling, is frequently associated with high grade and diffuse glioma. The most common mutation in BRAF involves gene duplication that leads to a mutant protein with a kinase domain constitutively activated [75].

Finally, mutations of IDH enzymes represent intriguing biomarkers since occur early in the pathogenesis of diffuse glioma [68]. IDH enzymes are normally responsible for the decarboxylation of isocitrate to a-ketoglutarate, leading to reduced NADP in the Krebs cycle. Mutation in codon 132 disrupts the function of IDH1 to convert isocitrate to a-ketoglutarate, forming R (-)-2-hydroxyglutarate (2-HG), a metabolite which inhibits ketoglutarate-dependent dioxygenases, leading to aberrant histone and DNA methylation. IDH1 and IDH2 have been frequently found mutated in low gliomas and represent good prognostic marker for GBM transformation [75].

4.1.2 TSPO, translocator protein: a potential marker of glioma transformation

Translocator protein (TSPO), formerly known as the peripheral benzodiazepine receptor (PBR), is a 18-kDa mitochondrial membrane protein that forms, with other mitochondrial proteins such as the voltage dependent anion channel (VDAC) and adenine nucleotide transporter (ANT), a complex known as the mitochondrial permeability transition pore (MPTP) whose function is the regulation of the mitochondrial membrane potential. TSPO is mainly involved in the regulation of cholesterol transport into the inner mitochondrial membrane where it serves as a precursor for steroids and neurosteroids. Hence, TSPO is constitutively expressed in steroidogenic tissue such as adrenal gland, gonad and brain [106]. Forming part of the MPTP, TSPO is also involved in the regulation of the release of pro apoptotic and necrotic factors into the cytosol. It seems that the presence of ROS during pathological state would activate VDAC causing a collapse of the mitochondrial membrane potential, which is critical for the release of apoptotic factors from mitochondira and for initiating the apoptotic cascade. Moreover, since cellular proliferation is an energy intensive process

and requires mitochondrial resources, TSPO plays an important role in proliferation through the transport of pre-proteins needed for maturation.

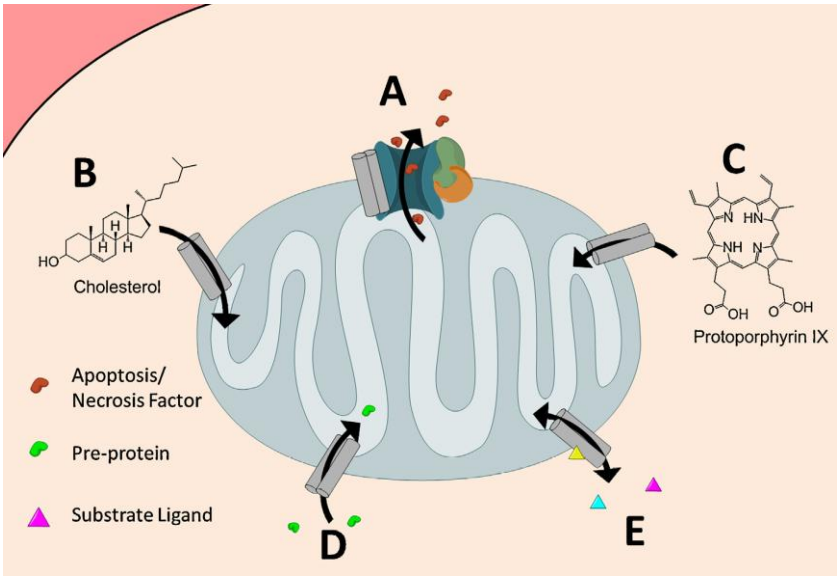

Figure 25 *Functions of the Translocator Protein. A) Release of apoptotic and necrotic factors into the cytosol; B) Transport of cholesterol into the mitochondria; C) Iron incorporation and heme synthesis; D) Transport of mitochondrial preproteins; E) Ligand of small molecules (i.g. Ca2+) (Austin CJD, The Internationa Journal of Biochemistry & Cell Biology 45 (2013) 1212-1216).*

Beyond TSPO expression in steroidogenic tissue, low TSPO expression has been found in normal central nervous system both in neurons and activated glial cells (microglia and astrocytes), but its expression seems to markedly increase after brain injury and inflammation [107].

It is widely known that TSPO expression is upregulated in brain tissue at the site of injury and inflammation as a consequence of neuropathological conditions such as stroke, encelephatitis and neurodegenerative disorders.

Overall these evidences make TSPO an ideal and sensitive marker to detect changes in neuroinflammatory disease. Nevertheless, although the significant increases in TSPO levels, the exact role of TSPO during inflammation is not still clear.

As described in the first chapter, TSPO ligands are established probes for PET imaging in brain inflammation [46]. Classical TSPO ligands such as PK and Ro mitigate proinflammatory responses of microglia to inflammation triggered by LPS (lipopolysaccharide) as demonstrated by several works [109, 110]. It seems that TSPO may help in enhancing the ability of cells and tissue to deal with ROS, playing a role in the monitoring of neurological damage. Moreover, it is likely that TSPO plays a role in the modulation of M2 macrophages polarization, regulating the anti inflammatory response.

TSPO overexpression has been also demonstrated in various human cancers such as ovary, colon, prostate and brain [107, 108]. Its role in cancer may be due to the ability of TSPO to transport cholesterol into mitochondria for the increased energy typically needed by cancer cells. Moreover, the involvement in cell

proliferation and survival as well as its anti apoptotic properties, would provide additional explanations to TSPO role in cancer. Indeed, a positive correlation between TSPO levels and the grade of malignancy has been found in both breast cancer and gliomas. In particular, several studies have showed the link between cancer progression and TSPO expression, demonstrating also that TSPO knocked down is able to decrease cell proliferation both in vitro and in vivo [108].

4.1.3 Hypoxia: a hallmark of GBM

Cancer cells are typically characterized by deregulated and high proliferation that leads to functionally abnormal blood vessels unable to provide adequate nutrient and oxygen supply. This imbalance between oxygen supply and consumption represents a common feature of solid tumors known as hypoxia [78]. Hypoxia acts on tumor cells in two opposite ways, either by impairing growth and causing cell death or helping cells to adapt to nutritive deprivation and become more aggressive [79].

The mechanism by which cells become more aggressive involves the regulation of the expression of various genes that have critical roles in cell proliferation, differentiation, glycolysis, angiogenesis and invasion. For these reasons, determining hypoxia levels in cancer may be predictive of metastasis, tumor recurrence, resistance to therapy, invasion and decreased patient survival. Moreover, cells become more resistant to standard treatments such as chemotherapies and radiotherapy in response to hypoxia.

The most important regulator of the cellular response to hypoxic stress is the hypoxia inducible factor 1 (HIF), whose overexpression has been associated with poor prognosis in many cancers, like brain, breast, ovary and uterus [78]. As described in the first chapter, HIF-1 is a αβ-heterodimeric transcription factor, consisting of a constitutively expressed HIF-1β subunit and a oxygen-sensitive subunit (HIF-1α). While in oxygen condition HIF-1α is hydroxylated and subsequently degraded by the proteasome complex, in condition of low oxygen proline hydroxylases is not able to hydroxylate HIF-1α and the successively degradation is inhibited. HIF-1α accumulates and translocates in the nucleus where dimerizes with the subunit β triggering the transcription of growth factor genes initiating an autocrine signalling pathway that could be crucial for tumour progression [78].

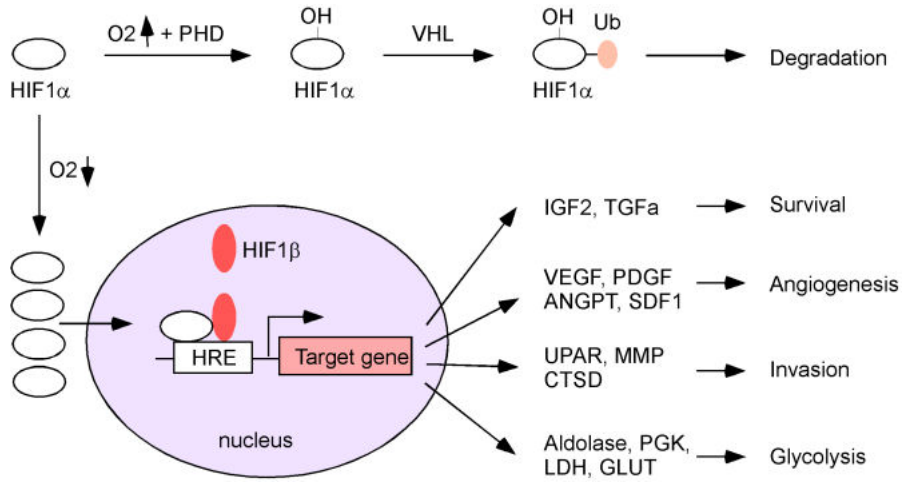

Figure 26 *Signalling and degradation of HIF-1α in normal and low oxygen conditions. In hypoxic conditions hydroxylation of HIF1α is inhibited causing its accumulation. Translocation of HIF1α in the nucleus determines its binding to the HIF responsive Element (HRE) of target genes activating their transcriptions (Province P et al, Hypoxia, Angiogenesis and Mechanisms for Invasion of Malignant Gliomas).*

Although the role of hypoxia in GBM is not fully understood, there are many evidences that demonstrate the impact of hypoxia on patient prognosis [80].

GBM is characterized by both necrosis and high rate of proliferation that requires enhanced supply of nutrient and oxygen. As for many other cancers, neo vascularization arising during rapid proliferation is often tortuous, with leak, abnormal and closed end blood vessels. This new microvasculature results very inefficient and contribute to the formation of hypoxic and necrotic areas within the tumor. Histologically GBM are characterized by the presence of central necrotic areas surrounded by pseudo-palisading tumor cells that have been shown to over-express HIF-1α and secrete other pro angiogenic factors in addition to VEGF like interleukin 8 (IL-8) [80, 81]. It seems that the combinations of hypoxia and tumor molecular biology are both responsible for the presence of pseudopalisading necrosis. Hypoxia, invasion and angiogenesis appear close interlinked in glioma through several pathways. The presence of low oxygen levels in the microenvironment activates cellular and molecular signalling pathways that promote an adaptive response of glioma cells. This response includes increasing motility and invasive properties with the aim to seek new oxygen supply through the initiation of angiogenic processes. GBM is one of the most vascularized tumors and it has been proposed that hypoxia caused by antiangiogenic therapy leads to the up regulation of alternative proangiogenic pathways and the recruitment of bone marrow-derived cells (BMDCs) with the ability to increase tumor growth [81].

The initiation, progression and recurrence of GBM are dependent on the presence of glioma stem cells (GSCs) that, like cancer stem cells (CSCs) have been found in functional niches closed to hypoxic regions. GSCs secrete high levels of VEGF promoting angiogenesis and sustain GBM cells survival and tumor growth. Many evidences suggest that hypoxia is able to maintain the stemness of GSCs even if the mechanism is still poorly understood. The expression of CD133 and the activation of transcription factors

such as Notch and Oct4 led by HIF-1 seem to control the self-renewal and multipotence ability of GSCs [80, 81].

The volume of hypoxic areas within glioma before radiotherapy is strongly associated with decreased overall survival. Indeed, since the beginning of the last century it has been known that the presence of hypoxic regions within the tumor decrease the efficacy of cytotoxic drugs and radiotherapy. It has been shown that the number of CD133-positive cells that increased in hypoxic areas correlated with increased radioresistance. The expression of HIF-1α in GBM can be affected by the activation of oncogenes and growth factors like epidermal growth factor receptor (EGFR), platelet-derived growth factor receptor (PDGFR) or the loss of tumor suppressors function like p53 or phosphatase and tensin homolog gene (PTEN). EGFR, for example, activates HIF through several pathways including the Phosphatidylinositol 3-kinase (PI3K) pathway. PDGF is thought to enhance the transcription of VEGF, contributing to both angiogenesis and hypoxia, while loss of function of PTEN is associated with increased expression of HIF-1α and tumor vascularization. Finally, p53 seems to enhance the degradation of HIF-1α which, in turns, stabilizes p53 by direct physical interaction.

The importance of hypoxia in GBM progression is also demonstrated by the effects due to the inhibition of HIF-1α activity, which is important for suppressing tumor angiogenesis and increasing cell apoptosis [81]. Therefore, decreasing HIF-1α levels in tumor cells becomes an intriguing option to treat aggressive tumor like GBM.

4.1.4 Molecular imaging strategies applied in GBM

Beyond the use of consolidated molecular biomarkers for GBM management, *in vivo* imaging based on clinical and preclinical procedures such as nuclear imaging, optical imaging and MRI represent a useful tool to identify biomarkers in a non-invasive manner and obtain information regarding tumor features and response to treatments.

Initial diagnosis of GBM is traditionally based on Computer Tomography (CT) or Magnetic Resonance Imaging (MRI) which provides excellent anatomic details and represents the gold standard for brain tumor imaging. While for low grade gliomas the role of MRI is mainly related to monitor disease progression and anaplastic transformation, its role in high grade lesions is required for the differentiation between recurrence and treatment-induced changes. Although the extensive use in clinical practice, MRI displays some limits, mainly due to the low accuracy in differentiating between radiation necrosis and post treatment recurrence and to the presence of the blood brain barrier (BBB) destruction that leads to the consequent leakage of contrast enhancement. Both high grade transformation and treatment lead to BBB disruption, rendering in this way difficult the discrimination of the origin of BBB breakdown. Moreover, when used to monitor tumor response to treatment, MRI can provide information only weeks after treatment beginning [82].

In the last decades, the development of new MRI technologies, able to provide physiological information, allows a better comprehension of tumor related changes. Proton magnetic spectroscopy (1H-MRS), perfusion/permeability MRI, diffusion/weighted MRI (DW-MRI) and Functional MRI (fMRI) show

promising results in distinguish cerebral necrosis from viable brain tumor and early detection of response to treatment. Magnetic resonance spectroscopy (MRS) represents an intriguing tool for the study of cellular metabolism, since it is able to visualize changes in the concentration of organic molecules different from water and composed by Carbon and Phosphor. The most commonly examined metabolites include lactate as the product of glycolysis and choline as an indicator of membrane turnover and, thus, cell proliferation. Increasing choline/creatinine ratios and lactate concentration correlate with tumor progression as demonstrated in several works. Moreover, the association of 1H MRS and FDG PET imaging has been shown to improve the detection of glioma recurrence [83].

Perfusion-weighted MRI involves the quantification of cerebral blood volume (CBV) after contrast administration. The frequent breakdown of the BBB caused by the presence of large tumor mass triggers extravasation and renders rCBV images analyses more difficult. Increased angiogenesis in high-grade gliomas correlated with higher rCBV and tumor aggressiveness and seems to occur prior to malignant transformation. Finally, DW-MRI plays an important role in tumor diagnosis since it enables the quantification of two parameters, apparent diffusion coefficient and fractional anisotropy, which provide information on tumor size [82].

MRI techniques as well as PET imaging continued to be refined in preclinical models to obtain functional measurements of tumor physiology and potential biomarkers of tumor response to treatment.

4.1.4.1 PET imaging

Providing information related to molecular targets with high sensitivity, PET represents a complementary tool to MRI for glioma patients' management. Since glioma cells, like other cancer cells, demonstrate high rate of glycolysis, FDG helps in differentiation between tumor and normal tissue and in differentiating between recurrent or residual tumor and radiation necrosis. A significant advantage of FDG PET is its ability to determine the metabolic state of tumor cells differently from MRI which is limited to evaluating changes in tumor size. Currently, FDG PET is not used for evaluating therapeutic response to treatment in high-grade gliomas, but it is widely used for staging and distinguishing tumor recurrence. Beyond [^{18}F]FDG whose use is also limited by the high cerebral background, PET tracers based on amino acids metabolism, since aminoacids transports is upregulated in malignant transformation. 1-[methyl-11C] methionine ([^{11}C]MET) and fluoro-3'-deoxy-3'-fluorothymidine ([^{18}F]FET display superior sensitivity in the detection of gliomas, distinguish tumor recurrence from radiation necrosis, monitoring response to treatment and in planning of radiotherapy [84].

As previously stated, nucleic acid tracers like [^{18}F]FLT have been proposed as marker of proliferation. [^{18}F]FLT has been extensively validate as a surrogate marker of proliferation since it targets the activity of the thymidine kinase 1 (TK-1) which is absent in quiescent cells and reaches its maximum activity in the late G1 and S phases if cell cycle of proliferating cells [42].

Successful results in the use of [^{18}F]FLT PET has been reported for diagnosis and assessment of glioma grading [85] and response to therapy assessment [85, 86, 87]. Different clinical and preclinical studies have

shown the possibility to use [^{18}F]FLT as an early biomarker of anti tumor therapy before morphological changes become measurable. It has been reported that the changes of [^{18}F]FLT uptake during treatment were more predictive of overall survival and progression-free survival than MRI in recurrent gliomas patients treated with antiangiogenic drugs [87]. Preclinical studies also reported the usefulness of [^{18}F]FLT PET in the early prediction of response to Temozolomide therapy [88, 89], demonstrating a significant reduction of [^{18}F]FLT uptake early after treatment beginning, when MRI was not able to distinguish any reduction.

Although these promising results, it is now clear that [^{18}F]FLT tumor uptake does not always correlate with the expression of histopathological proliferation markers such as Ki67 or TK1.

The presence of necrotic regions and hypoxic areas are known to contribute to lesion progression and treatment resistance particularly to radiotherapy [90]. Detecting hypoxic areas is of fundamental importance for GBM patients since hypoxia is proved to induce resistance to chemo- and radio-therapy thorough several mechanisms. PET tracers using radiopharmaceuticals with an oxygen-dependent mechanism of retention such as the nitroimidazoles compounds [18F]Fluoromisonidazolo ([^{18}F]FMISO) and [18F]Fluoroazomycin arabinoside ([^{18}F]FAZA) or [64Cu]ATSM. Nitroimidazoles enter in the cell by passive diffusion and undergo a selective bioreduction because of their instability. Nitroreductase mediates the bioreduction of nitroimidazole with formation of free radicals. In presence of oxygen, the anion of free radical is quickly reverted by oxygen in its original compound that can go out cell for passive diffusion. The oxidation speed depends on intracellular oxygen concentration. On the contrary, in hypoxic condition, the reduced compound undergoes further reduction steps which irreversibly entrapped the compound within the cell. The reactive fragments of imidazole ring react with macromolecular components of cell and, remaining trapped they accumulate into the cells.

Using PET and [^{18}F]MISO as radioligand, it has been shown that in patients with GBM, hypoxia strongly correlated with poor time to progression and survival [90].

Although the majority of clinical studies in patients were performed using [^{18}F]MISO as radioligand, [^{18}F]FAZA has been shown promising results with a high tumor to background ratio and with pharmacokinetic properties that overcome the limits of [^{18}F]FMISO.

Several studies have shown interesting results in the use of [^{18}F]FAZA as hypoxic tracer in clinical and preclinical studies, but nowadays only few works have investigated its role in glioma. In clinic, the role of [^{18}F]FAZA was evaluated in two studies with patients with head and neck cancer, in which it has been shown as a feasible and adequate method for imaging tumour hypoxia [91] and for planning radiation treatment [92]. In one only study, glioblastoma patients revealed high uptake of [^{18}F]FAZA and good tumor to background ratio, indicating [^{18}F]FAZA PET as a very promising agent for assessing hypoxic fraction [93]. Moreover, [^{18}F]FAZA PET has been shown a useful tool for the identification of hypoxic area within the tumor in a preclinical model of glioablastoma, revealing high tumor to background ratio [94].

4.1.5 GBM treatment

The high aggressiveness and invasiveness make GBM almost incurable and efforts to find new treatment approaches still represent a challenging aim. At present, the specific treatment of patients with high-grade gliomas is comprised of a maximally safe surgical resection, followed by radiation therapy and chemotherapy [95]. Despite the numerous advances in surgical, radiotherapeutic and chemotherapeutic modalities, primary brain tumours are considered resistant to the most commonly used antineoplastic agents. Invasive nature of gliomas and their anatomical localization within brain that is sensitive to disruption compromises the effectiveness of surgical treatment and complicates the delivery of effective doses of radiation to tumour cells. Furthermore, the strategies for systemic chemotherapy are limited by the presence of the blood brain barrier, although the continuity of it is occasionally not maintained because of the presence of extended areas of tumor. Alkylating chemotherapeutic drugs, including the chloroethylnitrosoureas (carmustine, lomustine and fotemustine), procarbazine and temozolomide (TMZ), are commonly administrated in patients suffering from high-grade gliomas [73].

The most widely implemented treatment regimen has been developed by the European Organisation for Research and Treatment of Cancer (EORTC) and is known as Stupp Protocol [73]. This therapeutic approach is based on the administration of TMZ chemotherapy in conjunction with radiotherapy followed by TMZ alone as maintenance.

TMZ is an oral alkylating agent and represents the standard chemotherapy used for GBM patients since 2005. It is rapidly absorbed and its cytotoxicity is mainly due to the methylation of DNA at several sites including the O6 position of guanine nucleotides. The methylation is known to form the O6-methylguanine adduct that determines the failure of the DNA mismatch repair system. The impossibility to remove the incorrect base-pairing of methyl-guanine and thymine causes an arrest of tumor cell in G2/M phase. Treatment with TMZ concurrent with ionizing radiation has been extensively demonstrated efficacy in several clinical studies, with a significant prolonged overall survival. Even though this efficacy has led to an extensive use of TMZ for GBM treatment, most patients that initially display a strong response recur and/or develop resistance after the first cycles of therapy [73], giving rise to many doubts about its effectiveness. The major determinant of chemoresistance to TMZ is the activity of a O6-methylguanine-DNA methyltransferase (MGMT). This enzyme rapidly removes methyl adducts at the O6 position of guanine, thus repairing alkylating agent-induced DNA damage. Epigenetic silencing of MGMT by promoter methylation was shown to be associated with low protein expression in a range of tumours including gliomas and with major tumour sensitivity to TMZ [76].

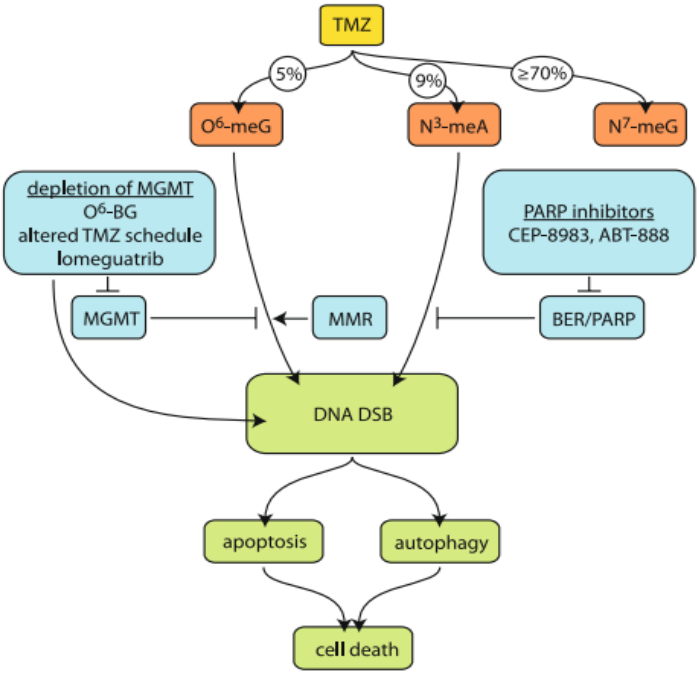

Figure 27 Temozolomide effects. *Schematic representation of TMZ action's mechanism and related involved pathways.*

Since the high variability of glioma response to TMZ treatment and the diffuse resistance, there is a clear need of effective treatments and finding new strategies to counteract tumor resistance. The increasing knowledge of the molecular biology of GBM has the potential to improve patients' survival both through the development of compounds that targets molecular pathways altered in cancer and through the better understanding of those pathways modulated by TMZ.

In this regard, the knowledge about the role of autophagy in cancer can provide an alternative target for new treatment approaches. Autophagy is considered a therapeutic target in cancer due to its ability to promote the survival of cancer cells in the response to metabolic and therapeutic stress. The role of autophagy in glioma has been demonstrated as an adaptive response to both radiation and TMZ. In particular, continuous dosing of TMZ or the combination with radiotherapy have been demonstrated to produce more sustained autophagy, thus representing a target that can be hit to enhance TMZ efficacy [96, 97]. Moreover, it has been demonstrated that beyond the well-known oxygen dependent degradation of HIF1α by the proteasome, HIF1α degradation may occur in the preoteasome thorough alternative oxygen independent pathways. HIF1α is in fact a chaperone-mediated autophagy target that can be degraded after Hsp70 recognition in the lysosomes [98]. Taking together these evidences should be of particular interest for glioma investigation since they can represent a link between the role of HIF1α as biomarker and TMZ response.

4.1.6 Preclinical models of glioblastoma

The development of accurate and reproducible animal models of disease able to recapitulate the key features of the human forms may provide a useful tool for both the investigation of molecular events triggering tumors and the evaluation of new therapies. Despite the use of preclinical models is still a source of controversial debates, some rodent models of glioma have been developed able to resemble human tumor progression kinetics and anti tumor immune response of spontaneous GBM. The most representative preclinical models of glioma can be achieved through the intracranial injection of tumor cells in specific cerebral areas by the use of stereotaxic instruments. In this way animals develop tumors in the proper area and can be monitored *in vivo* by the use of imaging techniques over time [25].

The main advantages in the use of animal models can be referred to the highly efficient gliomagenesis, reproducible growth rates and accurate knowledge of tumor location.

On the basis of the cell species used, preclinical models can be divided into syngeneic models, obtained using cells of the host without be affected by immunogenicity, or human xenograft models, achieved by the use of human cells in immunocompromised mice. Despite the lack of the immune response that occur during tumorigenesis and treatments administration, human xenograft are extensively used in translational research giving the possibility to test new therapies directly on human cells [25].

The U251 model represents one of the most studied human GBM xenograft. U251 cells implanted in the brain of immune-deficient mice give rise to detectable tumors in few days and display features resemble those of the human disease.

Histopathologically U251 model shows the presence of necrotic foci, glioma cells disposed in pseudopalisading pattern, microvascular and endothelial proliferation and strong positivity to GFAP that demonstrates the glial origin of this tumor cell type. Moreover GFAP positivity in non-neoplastic parenchyma is indicative of the infiltrative behaviour.

Regarding molecular features, the U251 model has been shown to display similarity with the human GBM, such as the presence of non-functional p53 and mutations in PTEN that, as stated previously, is a negative regulator of the PI3K/AKT pathway. PTEN mutation determines the hyper activation of the PI3K pathway and, subsequently, contributes to the stability, translocation and transcription of HIF1α. Since the fundamental role of HIF1α in glioma progression and resistance to therapy, the use of the engineered cell line U251-HRE cell line represents a tool for the study of HIF1α activity. U251 cell line and the relative intracranial tumor model mimicking the main features of human GBM both at histopathological and genetic level seem to be a good tool to investigate new therapies for GBM [99].

4.2 Materials and methods

4.2.1 Cell line

Engineered U251-pGL3 and U251-HRE human glioma cells were kindly provided by Dr Giovanni Melillo, national Cancer Institute Frederick (MD). U251-pGL3 cells have been engineered to express the luciferase reporter gene under the control of the SV40 constitutive promoter, while U251-HRE cells express the luciferase reporter gene under the control of three copies of an HRE sequence (pGL2-Tk-HRE). Cells were transfected using pCLL.PGK and mCherry.WPRE (PLW) lentivirus to obtain U251-pGL3-mCherry and U251-HRE-mCherry cell lines with the mCherry gene under the control of the constitutive promoter PGK.
Cells were routinely maintained in RPMI supplemented with 10% heat-inactivated fetal bovine serum, penicillin and streptomycin, glutamine in humidified condition of 5% CO2 at 37.The day of the surgery, cells were trypsinized, centrifuged, counted (with trypan blue) and resuspended at the final concentration of 10^5cells/2 µl of PBS (all reagents from Life Technologies).

4.2.2 In vivo animal studies

Studies were conducted in 7/8 weeks old female nude mice (Harlan Laboratories) with an approved animal protocol. The orthotopic murine model was obtained by the stereotaxic injection (coordinates: AP = 1.5, L = 0 and V = 3) of 1 x 10^5 human glioma cells (U251-pLG3, U251-HRE, U251-HRE-mCHerry). The skull was drilled and a 10 µl-Hamilton syringe was inserted in the hole for the injection of the cells in the established region. Cells were injected at the speed of 1 µl every minute and, after injection, the needle was left in place for additional 5 min and then slowly withdrawn; holes were sealed with bone wax and the incision was sutured. Following surgery, mice were reported in their cage and monitored until awakening from anaesthesia.

4.2.3 Study design

- Firstly, we characterized HIF-1α molecular processes related to hypoxia in the U251-HRE cellular model through *in vitro* experiments and *in vivo* longitudinal evaluation of tumor growth and hypoxia establishment with a multimodal imaging approach. Starting from cell implantation, a group of animal (n=20) performed weekly BLI scans until the end of protocol (30 days). In another group of animal (n=6) PET with [^{18}F]FDG, [^{18}F]FAZA and [^{18}F]FLT and MRI scans were carried out at intermediate and late time points as depicted in Figure 27.
- Relying on the characterization of the U251-HRE model, we performed a second study to assess HIF-1α activity modulation by Temozolomide (TMZ) treatment both *in vitro* and *in vivo* with the same multimodal imaging approach used in the characterization study. Mice bearing U251-HRE-mCherry tumors were divided into three groups (n=5 per group) and treated with two different TMZ regimens. Starting from the day 21 after cells injection mice were treated by oral gavage with 400

mg/kg of TMZ (acute regimen), 100 mg/kg of TMZ (metronomic regimen) for 4 consecutive days and with PBS as vehicle (control group).

Mice were monitored with BLI and FLI scans before and every day after TMZ treatment until sacrifice. Moreover, in order to study CAIX and integrine expression mice were also imaged with HipoxiSense680 and IntegriSense750 fluorescent probes before, during and at the end of treatment. Finally, MRI and [^{18}F]FLT PET were performed at three different time points: before, at an intermediate time point (2 days after treatment beginning) and at the end of treatment (Figure 28). At the end of the study mice were sacrificed and tumors collected for immunohistochemistry analyses.

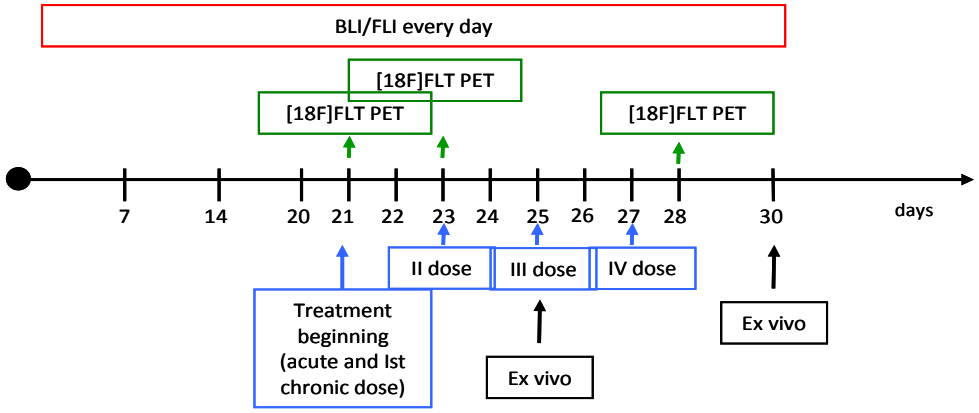

Figure 28 Study design. *Schematic representation of scheduling of in vivo treatment with TMZ and acquisition with optical imaging and PET.*

4.2.4 BLI/FLI studies

To detect luminescence anesthetized mice (4% chloral hydrate) were intraperitoneally injected with 150 mg/kg of luciferine. After 12 minutes of biodistribution, mice were positioned in the light-tight chamber (IVIS Spectrum/CT) and photons emission due to luciferase reaction was acquired for 2 minutes. For mCherry reporter gene, a correct filter was applied (two consequent acquisition at exc:570 nm and em:620 nm and exc:605 nm and em:660 nm) for mice acquisition. Animals were evaluated also with the IVIS Spectrum-CT (Caliper LifeSciences, Perkin Elmer) performing a Fluorescence Imaging Tomography (FLIT) with HypoxiSense680 fluorescent probe (PerkinElmer). For these studies animals were intravenously injected, 24 h before acquisition, with HypoxiSense680 and IntegriSense probes (2 nmol in 100 µl of sterile PBS) to target Carbonic Anhydrase IX (CAIX) and integrin. The day after mice underwent a FLIT acquisition. Images were analysed and scaled after completion of all acquisition using appropriate computer software (Living Image Software, PerkinElmer) and the same Region of Interest (ROI) was applied on BLI and FLI tumor images. Data were expressed as average radiance (photons/second/square centimetre/steradian) which is a calibrated measurement of photon emission. For FLI data were expressed as

average of radiant efficiency which is a further correction of the signal considering the intensity of the incident excitation light.

4.2.5 PET studies

At an intermediate (18-20 days) and at late time point (30 days) after cells injection, mice were evaluated using the YAP-(S)-PET II (I.S.E. s.r.l., Pisa, Italy) small animal tomograph with [^{18}F]FDG, [^{18}F]FLT and [^{18}F]FAZA for the evaluation of glucose metabolism, cell proliferation and tumor hypoxia, respectively. [^{18}F]FDG is routinely prepared in our facility for clinical use (European Pharmacopeia V ed.) while [^{18}F]FAZA and [^{18}F]FLT were obtained as previously described [100, 67] with minor modifications. All radiopharmaceuticals were injected with a radiochemical purity greater than 99%. After a slight anaesthesia with ether animals in fasting conditions were injected in a tail vein with 4.4 ± 0.2MBq of [^{18}F]FDG, 4.3 MBq± 0.2 of [^{18}F]FLT and 5.7 ± 0.3 MBq of [^{18}F]FAZA. During PET acquisition, mice were anesthetized with a mixture of isoflurane and air (1:2) and positioned prone on the tomograph bed with the head centred in the field of view. A special polystyrene support was used to ensure the correct positioning of mice and the co-registration of images obtained with the different radiotracers. Dynamic acquisition with [^{18}F]FDG and [^{18}F]FLT started 60 min after tracer injection and lasted for 30 min, whereas scans with [^{18}F]FAZA started 120 minutes after injection and lasted 15 minutes (three frames of five min each). PET data were acquired in list mode using the full axial acceptance angle of the scanner (3D mode) and then reconstructed with the expectation maximization (EM) algorithm.

4.2.6 Image analysis

Radioactivity concentration was corrected for physical decay and calibrated in order to transform counts per voxel values in MBq/ml. Radiotracers uptake was measured using Region of Interest (ROIs) analysis. A circular ROI was drawn on the tumour region using the automatic isocontour tool of the PMOD software. Background regions were defined manually drawing circular ROIs on three consecutive transaxial slices on a controlaetral region (vol 0.5 mm^3) for [^{18}F]FDG and on cerebellum for [^{18}F]FAZA and [^{18}F]FLT (9.7 mm^3). Automatically, maximum, mean and minimum uptake values and standard deviation were generated. The radiopharmaceutical distribution was calculated as maximum standardized uptake value (SUVmax) correcting for the injected dose and the animal weight. Moreover, tumour to background ratio (T/B ratio) was calculated dividing the SUVmax of the tumor by the SUVmean of the background region.

4.2.7 Immunohistochemistry

After the last acquisition animals were sacrificed and their brains retrived, fixed in 10% neutral buffered formalin and paraffin-embedded after dehydration with increasing concentrations of ethanol. Longitudinal sections of 4 um were cut and stained with hematoxylin and eosin for morphological evaluation. After antigen retrival using EDTA or citrate solutions and cooling, slides were washed in buffer and incubated with the following antibodies: monoclonal anti HIF-1α antibody, monoclonal anti CAIX antibody,

monoclonal mouse anti-human Ki67 antigen and anti-firefly luciferase antibody. Reactions were revealed using the Novolink Max Plymer detection system for 30 minutes and then with DAB for 8 minutes.

4.2.8 Statistical analyses

Data are presented as mean values ± standard deviation. Statistical analysis was performed using Prism 4 (GraphPad Software).

4.3 Results

4.3.1 Characterization of luciferase activity

The relationship between HIF1α and luciferase reporter gene expression has been previously evaluated in vitro, demonstrating that only U251-HRE cells expressed luciferase reporter gene in relation to HIF1α stabilization. On the basis of these results we decided to assess the dependence of reporter gene expression on HIF1α activity *in vivo* in mice bearing U251-HRE and U251-pLG3 glioma cells. Mice underwent *in vivo* BLI longitudinal studies weekly starting from cells injection until the end of the protocol to monitor hypoxia onset and progression. Luciferase activity was immediately detectable at the first scan in the U251-pLG3 model and it increased over time proportionally to tumor growth. On the contrary, in the U251-HRE model, an increase in luciferase activity was detectable only from the 18 day after cells injection and it was not maintained until the late time point. The sudden increase starting from day 18 have that has been observed in U251-HRE mice can be attributed to the establishment of hypoxia within the lesions underlining the dependence of luciferase expression on hypoxia (Figure 29). At the later time point U251-HRE mice were also imaged by FLIT acquisition with a HypoxiSense680 fluorescent probe. FLIT acquisition showed the presence of wide hypoxic areas co-localizing with the bioluminescent signal, suggesting that the bioluminescence signal observed could corresponded to hypoxic areas (data not shown).

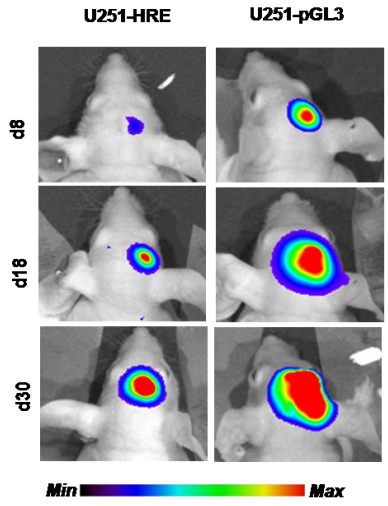

Figure 29 Optical imaging characterization. *Representative BLI images of U251-HRE and U25- pGL3 mice at 8, 18 and 30 days after cells implantation show a different Luciferase signal over time.*

4.3.2 MRI and PET studies of U251 glioma model features

Tumors localization and growth were monitored by MRI scans. MRI images performed 20 days after cells injection in U251-HRE mice revealed isointense or slightly hyperintense lesions. Small areas of necrosis were present that became larger at the last scan (30 days).

In order to define the role of [^{18}F]FDG, [^{18}F]FAZA and [^{18}F]FLT in imaging hypoxia and delineate other glioma features such as glucose metabolism and cell proliferation, U251-HRE mice were in vivo monitored with PET imaging at early time (18-20 days after cells implantation) and at later time (30 days after cells implantation). U251-HRE animals revealed hypo-glycolytic (T/B = 1.27 +/- 0.17; 1.08 +/- 0.06) but highly proliferative tumors since the first PET studies, while at the same time [^{18}F]FAZA uptake was observed only in few animals. Hypoxic areas became clearly detectable 30 days after cells injection as shown by [^{18}F]FAZA uptake (from T/B = 1.01 to T/B = 1.38). Moreover, a significant enhancement of cell proliferation was observed at the same time as depicted by the increase in [^{18}F]FLT uptake of 1.78 fold (from T/B = 1.33 to T/B = 2.38) (Figure 30).

A

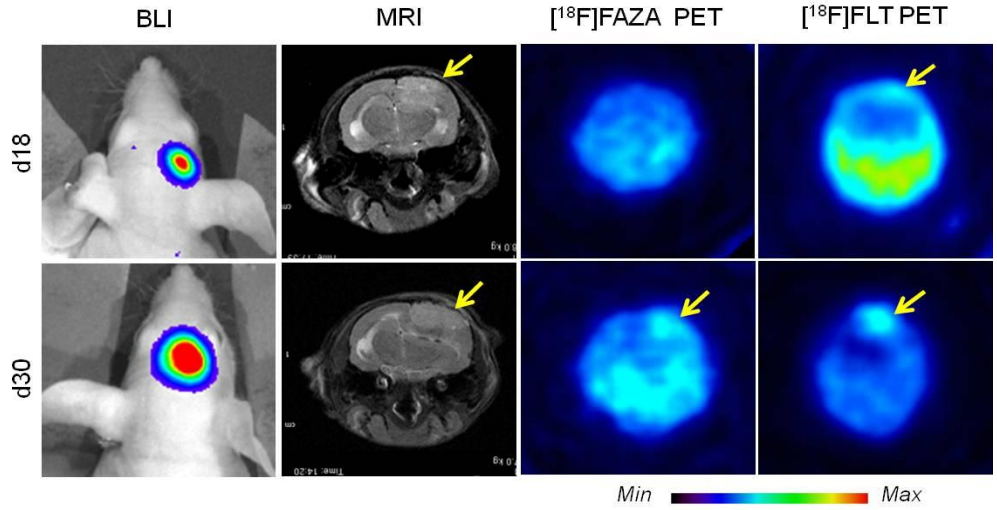

B

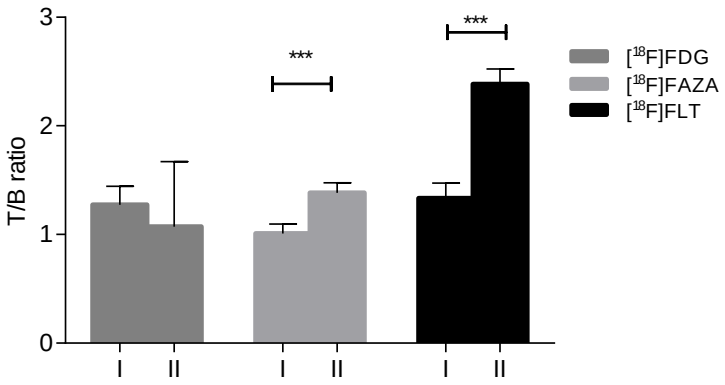

Figure 30 Multimodal imaging characterization of U251-HRE mice*. A)** *Representative images of mice orthotopically injected with U251-HRE cells. BLI images showed a detectable and progressive induction of luciferase activity starting at 18 days from cell implantation. PET analysis showed a high rate of proliferation and a moderate hypoxia uptake only at later time points. MRI provided morphological and a contribution for hypoxia determination.* **B)Quantification of FDG, FAZA and FLT PET images at 18-20 (I) and 30 (II) days after cells implantation. Radiotracers uptake is calculated as T/B ratios (*** $p < 0.005$).*

Imaging results were confirmed by immunohistochemical analyses performed on harvested brains. Morphological staining with H&E showed typical features of GBM: hypercellular proliferation, fusiform cells with atypical and pleomorphic nuclei, high mitotic activity and microvascular proliferation. IHC staining for HIF-1α showed a detectable nuclear accumulation and a strong expression of CAIX along the cell membranes, confirming the presence of hypoxia within the tumor. Ki67 staining corroborated the prominent proliferation characterizing U251-HRE tumor, as showed *in vivo* by [^{18}F]FLT PET (Figure 31).

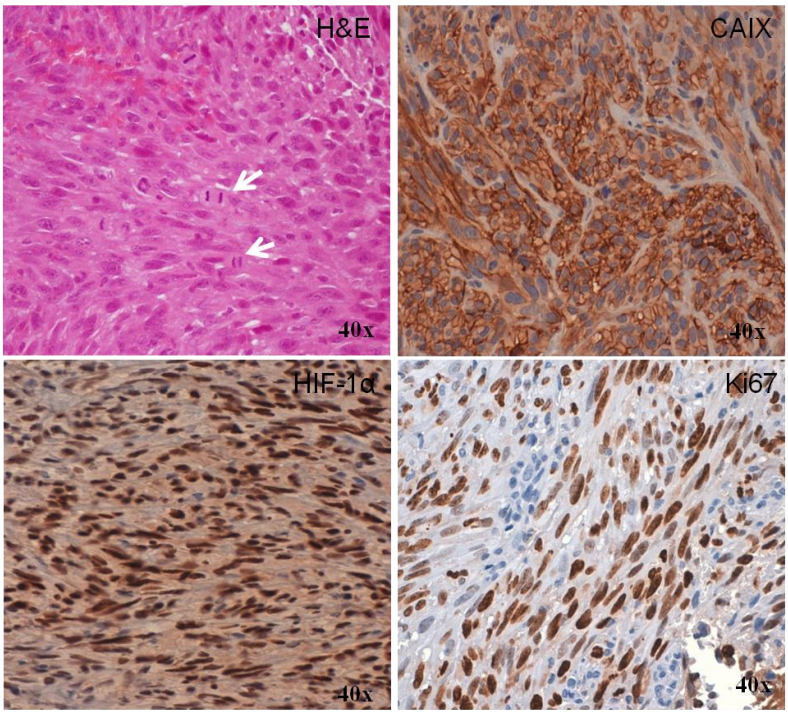

Figure 31 Ex vivo analyses. *H&E and IHC staining for CAIX, HIF-1a and Ki67. H&E revealed the typical morphology of GBM (arrows indicates mitotic activity). IHC staining showed the presence of hypoxic areas and high rate of proliferation.*

4.3.3 Assessment of HIF-1α activity modulation after TMZ treatment

4.3.3.1 BLI and FLI studies

TMZ activity has been previously tested in vitro on U251-pGL3-mCherry and on U251-HRE-mCherry cells at different time points. Results showed a different behaviour in luciferase activity between the two cell lines, displaying a decrease of luciferase activity only at later time points for U251-pGL3-mCherry and a massive decrease of luciferase activity at earlier time point in the U251-HRE-mCherry cells. In addition, in vitro results revealed a similar decrease of mCherry signal in the two cell lines, indicating that luciferase activity is selectively modulated by TMZ treatment as a consequence of HIF-1α modulation and that TMZ action on HIF-1α precedes the cytotoxic effect.

On the basis of these data, we chose to investigate luciferase modulation *in vivo* in nude mice orthotopically injected with U251-HRE-mCherry glioma cells and treated with two different TMZ regimens: acute regimen and metronomic regimen (4 doses). Mice were monitored with a multimodal imaging approach before, during and at the end of TMZ administration.

Mice revealed high BLI and FLI signals that co-localized before TMZ treatment. Two days after treatment beginning (at the end of acute regimen and after two doses of metronomic treatment), tumors of treated animals displayed a significant reduction of luciferase signal that was more marked in the acute regimen group. At the same time mCherry signal of treated animals was comparable to that of control group. On the contrary, a strong reduction of both luciferase and mCherry signals were observed at the end of treatment in treated animals when compared to controls as depicted in Figure 32.

FLI studies were performed also using two different fluorescent probes to detect hypoxia (HypoxiSense) and integrine expression (IntegriSense) 4 days and 1 week after TMZ administration. At the earlier time point we observed a decrease in HypoxiSense probe signal, while IntegriSense signal remains comparable to the baseline. At the later time point, a decrease of both probes' signal have been observed, suggesting a decrease of hypoxia markers and integrins involved in neo angiogenesis. Control animals, on the contrary, showed a progressive increase of both signals over time.

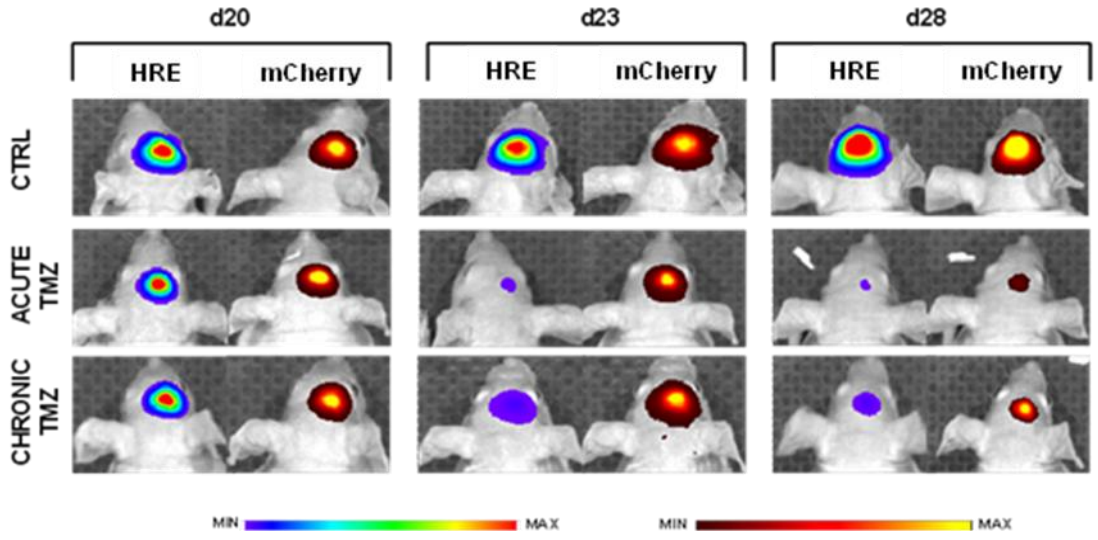

Figure 32 BLI and FLI imaging. *In vivo detection of luciferase activity in orthotopic U251-HRE glioma models.Representative image of mCherry (red) and Luciferase (yellow) signal in a implanted mouse in a 3D acquisition performed by merging of Luciferase and mCherry on CT scan. 2D Luminescent (rainbow scale) and Fluorescent (red-yellow scale) images of control U251-HRE tumors and TMZ treated mice at different time point.*

4.3.3.2 PET imaging

The possibility to investigate tumor response to therapy with PET or MR imaging allow a rapid translation of obtained results from preclinical setting to clinical practice. For this reason U251-HRE-mCherry tumors

bearing mice were monitored for TMZ effects with [^{18}F]FLT-PET and MRI. To evaluate the feasibility of [^{18}F]FLT to predict glioma response to TMZ, animals performed PET scans before, during and after the end of TMZ treatment. In mice treated with metronomic regimen of TMZ no differences in [^{18}F]FLT uptake expressed as T/B ratio were detected after 2 days of treatment compared to the baseline. On the contrary controls and acute regimen mice displayed an increase of tracer uptake. At the end of TMZ treatment, we observed an increased in [^{18}F]FLT uptake in all control mice compared to the baseline. Treated animals displayed a stable or decreased uptake of [^{18}F]FLT regardless the regimen of treatment if compared with the pre-treatment one. Regarding tumor volume measured with [^{18}F]FLT, control animals displayed an increase over time as expected (Figure 33). Treated animals showed a progressive decrease of tumor volume regardless treatment regimen displaying a trend similar to that observed with FLI analysis.

A

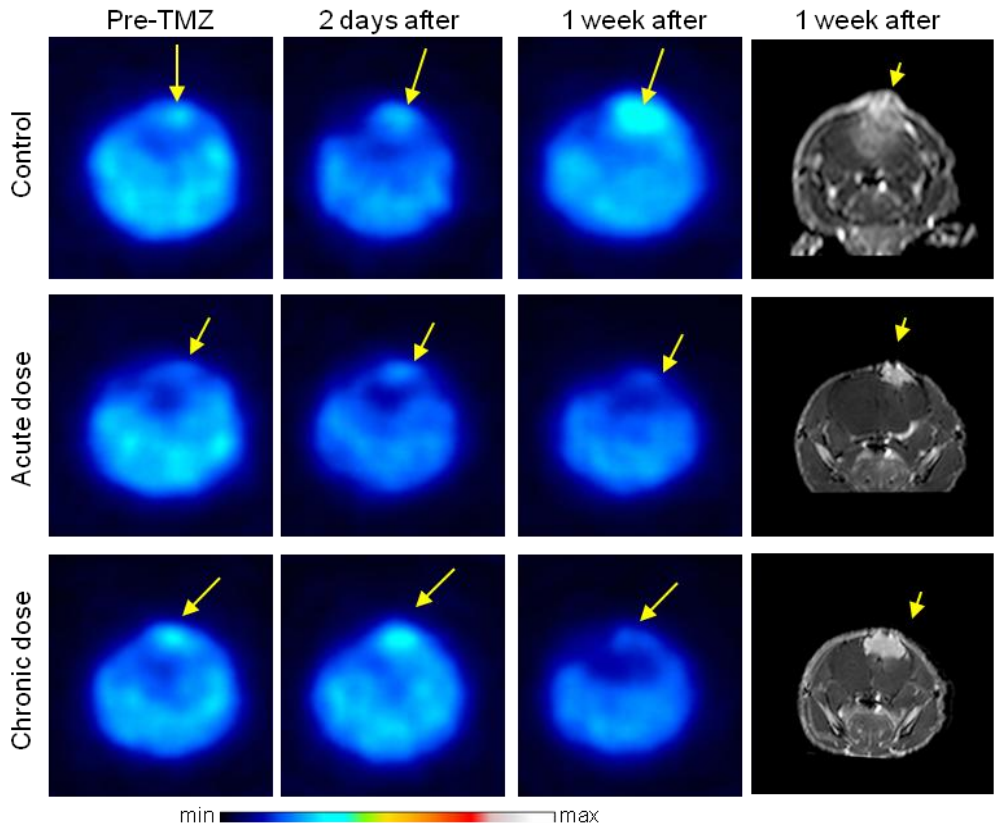

B

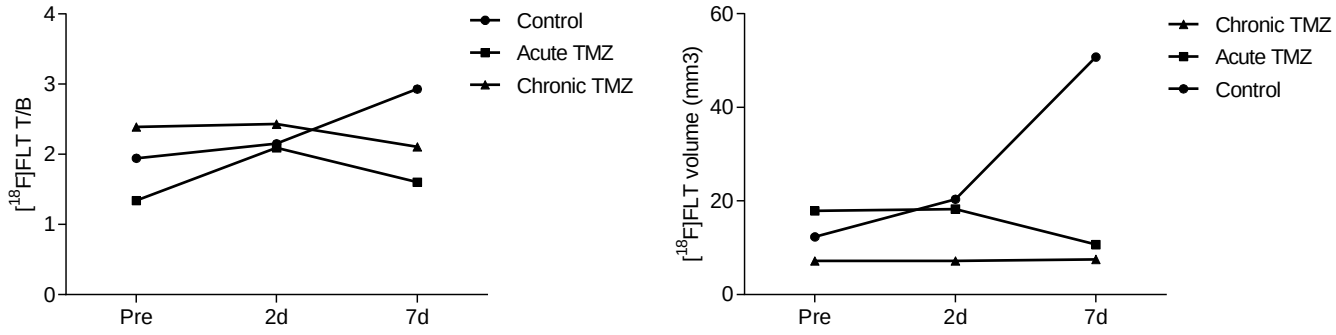

Figure 33 PET and MRI imaging. **A**) *In vivo representation of PET and MRI analyses. Representative transaxial [^{18}F]FLT PET and MRI images of U251-HRE-mCherry animal model performed at baseline and at 2 days and 1 week after treatment (acute and metronomic dose). Yellow arrows indicate tumors. Images were presented with the same scale, and were corrected for injected dose and animal weight.* **B)** *Quantification of [^{18}F]FLT uptake, expressed as tumour to background ratio and uptake volume (mm3) over time during treatment.*

Immunohistochemical analyses performed on explanted brains confirm imaging data. In particular, untreated U251-HRE-mCherry tumors displayed distinctive features of GBM. HIF-1α nuclear labelling in treated animals seemed strongly reduced compared to control as well as Ki67 and CAIX (Figure 34).

A **B**

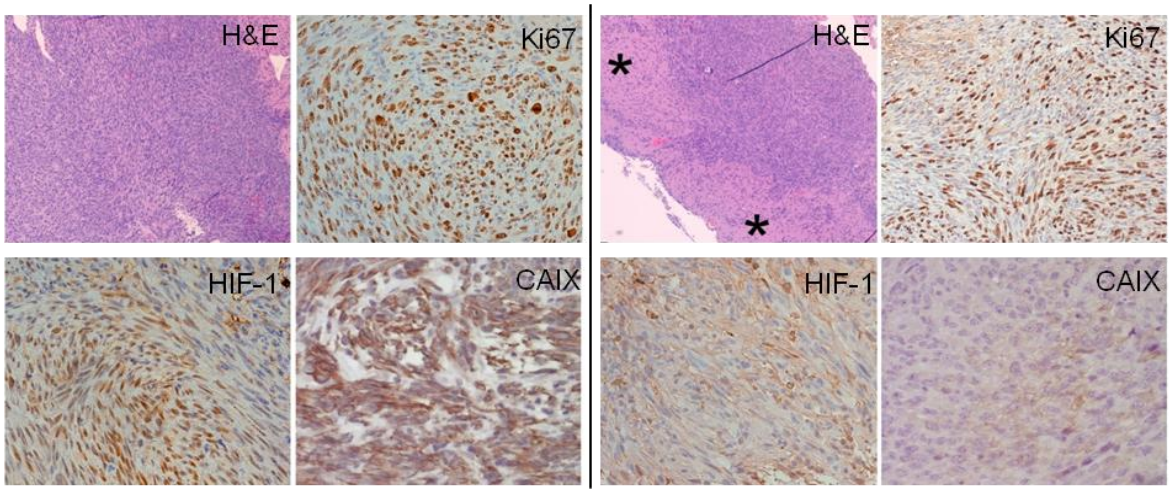

Figure 34 Ex vivo analyses. *H&E and IHC staining for Ki67, HIF-1α and CAIX of representative control (A) and TMZ-treated mice (B).*

4.4 Assessment of the role of TSPO as a marker of glioma progression

Aim of this part of the work was the investigation of the potential role of TSPO as prognostic marker of anaplastic transformation in human gliomas. Through the evaluation of TSPO expression levels we aim to stratify patients eligible for surgical resection or TSPO targeted treatment. Moreover, in this way we aim to provide important information about differential TSPO expression in low grade gliomas for the following use of PET with TSPO tracers in the management of these patients.

To this aim, patients diagnosed for low or high grade gliomas have been involved in the study on the basis of structural and perfusion MRI scans. Tumor samples derived from biopsy or surgical resection have been used for immunohistochemistry (IHC), double immunofluorescence (DFI) and molecular analyses.

The expression of TSPO in neoplastic and non-neoplastic cells, the extent of glioma associated microglia and macrophages (GAMs), astrocytosis and microvascular proliferation were evaluated using IHC and DIF with antibodies directed against TSPO, the calcium-binding adapter molecule 1 (Iba1) for GAMs and glial acid fibrillary protein (GFAP). DIF was used to distinguish TSPO-positivity in neoplastic and non-neoplastic cells.

4.4.1 Materials and methods

4.4.1.1 Histopathological studies

DNA from paraffin embedded human tissue was extracted using the DNA Miniprep Kit from Quiagen following the manufacturer's instructions; DNA samples were stored at -20°C until further use. DNA concentration and purity was assessed by spectrophotometry (NanoDrop ND1000; NanoDrop Technologies, Delaware, USA). Pyrosequencing analysys are now ongoing.

For IHC experiments, following antigen unmasking, endogenous peroxidase was quenched with 1% hydrogen peroxide in methanol at -20°C for 15 min. After rinsing in phosphate buffered saline (PBS), the sections were incubated overnight at room temperature with the primary antibody. The SuperSentitive IHC detection system from BioGenex was used to visualize antibody binding. Finally sections were counterstained with Mayer's Haemalum before being dehydrated and coverslipped. To further characterize TSPO expression in the different cell populations present in gliomas and distinguish TSPO-positive neoplastic cells from GAMs, astrocytes and endothelial cells, we used double immunofluorescence. The primary anti-TSPO antibody was mixed with anti-Iba1 and anti-$IDH1^{R132H}$ antibodies in donkey serum buffer. A cocktail of these antibodies was applied into sections and incubated overnight. After repeated washings in PBS, the slides were incubated with a secondary biotinylated anti-goat antibody and a complex of biotin and streptavidin conjugated Alexa Fluor 546 to detect TSPO and with the donkey anti-rabbit AlexaFluor 488 to detect Iba1 and $IDH1^{R132H}$. Secondary antibodies were incubated for 45 minutes and the avidin-biotin complex for 1 hour. Sections were then incubated with DAPI in PBS for 30 minutes, rinsed and coverslipped using mountant for fluorescence microscopy. Images were captured by fluorescent microscopy using the LEICA TCS SP5 II confocal microscope with integrated application suite.

4.4.2 Results

TSPO-positive cells showed cytoplasmic, granular TSPO immunolabelling consistent with mitochondrial location. TSPO-positive cells were evenly distributed in the tumor mass as well as in its peripheral, infiltrative component. The number of TSPO-positive neoplastic cells increased with the WHO grade even if without statistical significance. When grouped by grade and histotype, the average value significantly increased with grade, being higher in high grade gliomas than low grade gliomas, indicating the TSPO expression as a potential marker to help in distinguishing gliomas histotype and grade (Figure 35).

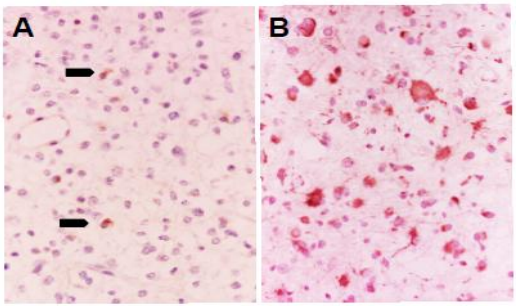

Figure 35 *Tissue analysis of TSPO expression in different tumor histotypes and grades using IHC. Examples shown are a low grade oligodendroglioma (A) and an anaplastic astrocitoma (B) in TSPO immunoperoxidase IHC, ×20. Neoplastic cells in low grade gliomas show a rim of positive cytoplasm (black arrows) while neoplastic cells in the case of high grade gliomas show large, intensely positive cytoplasm reflecting a higher TSPO content.*

Gliomas are heterogeneous tumors and contain non-neoplastic cell populations that are known to express TSPO. In particular, TSPO-positive GAMs may represent a confounder in the evaluation of PET-imaging findings.

For this reason, IHC analyses have been also conducted for the evaluation of TSPO and Iba1 expression and to identify their possible co-localization (Figure 36). The density of TSPO-positive cells and Iba1-positive glioma associated macrophages (GAMs) of each tumor was quantified and represented as the value of percentage of positive cells against overall cell density × 0.25mm^2.

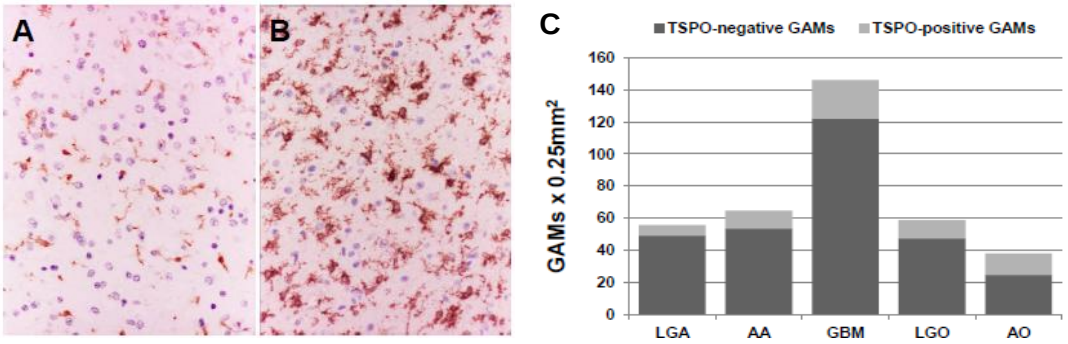

Figure 36 *Overall distribution of GAMs and TSPO-positive GAMs in different tumor histotypes and grades. Examples shown are a low grade (A) and a high grade glioma (B) in Iba1 immunoperoxidase IHC, ×20. Less Iba1-positive stain is observed in the low than the high grade glioma, indicating the increase of GAMs with tumor grade. (C) Density (per*

0.25mm^2) of TSPO-positive and TSPO-negative GAMs in different tumor histotypes and grades. (LGA = low-grade astrocytoma; LGO = low-grade oligodendroglioma; AA = anaplastic astrocytoma; AO = anaplastic oligodendroglioma; GBM = glioblastoma multiforme).

We also quantified the number of TSPO-positive microglia in each tumor using double immunofluorescence (DFI). Sections were stained for TSPO (red) and GAMs using IDH1 and Iba antibodies (green) (Figure 37A and B). Images from 5 to 10 randomly selected fields were captured using a fluorescence microscope with a digital camera. Combined red and green digitized images were analyzed using Image J. The number of cells that co-localized TSPO and Iba1 was counted by manual tagging.

DIF experiments demonstrated that TSPO was predominantly expressed in neoplastic cells. GAMs accounted for 7.5% to 44.4% of the overall cell density and their density also showed a trend to increase with the WHO grade. Moreover, DIF demonstrated that only a small proportion of GAMs expressed TSPO and that TSPO-positive GAMs accounted for a minority of overall TSPO cell population. No TSPO expression was identified in reactive astrocytes, while endothelial and smooth muscle cells of normal vessels entrapped in neoplastic tissue were TSPO positive irrespective of tumor histotype and grade. In contrast, TSPO expression was low to absent in newly formed vessels seen in the cases of GBM (Figure 37C and D).

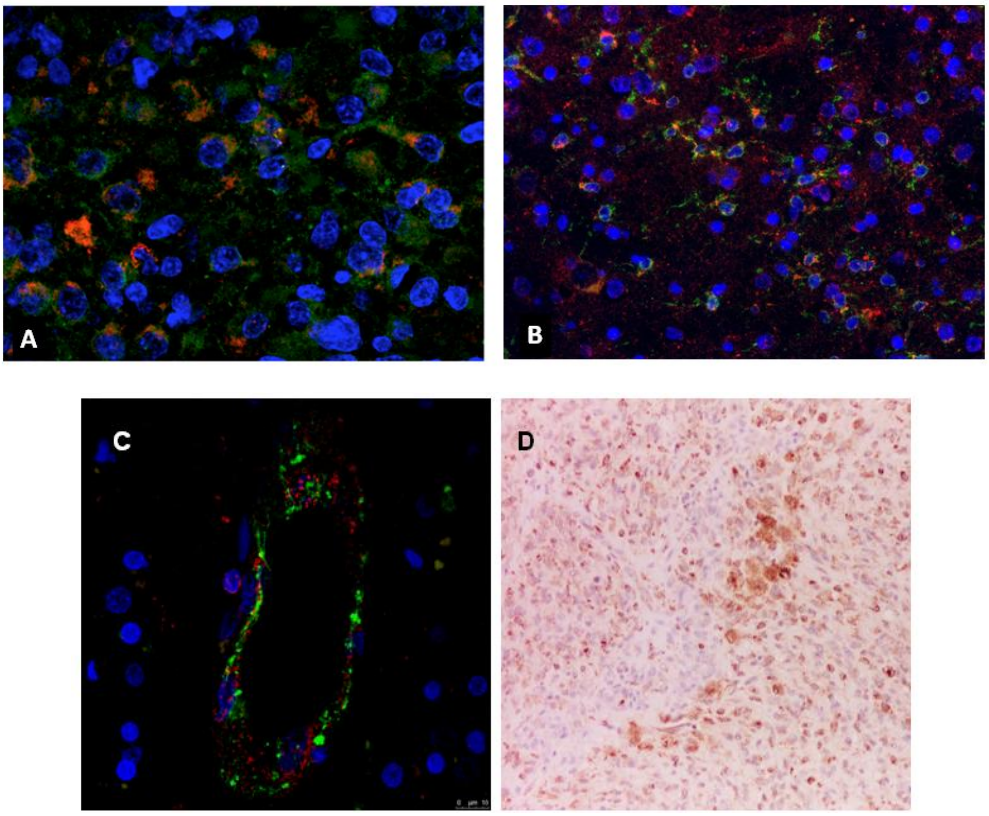

Figure 37 ***A)*** *Double immunofluorescence for IDH1^{R132H} (green) and TSPO (red) demonstrates predominant TSPO expression in neoplastic cells (A, LGA, ×40).* ***B)*** *Double immunofluosescence for Iba1 (green) and TSPO (red) shows that only a minority of GAMs are TSPO-positive (×20).* ***C)*** *TSPO is expressed in endothelia and smooth muscle cells of normal vessels entrapped in tumor tissue (CD34 green and TSPO red, ×20);****D)*** *endothelium of newly formed vessels shows negligible TSPO expression when assessed with immunoperoxidase (×20).*

Low- and high-grade gliomas (LGG – HGG) are the most common primary brain tumors in adults. Their outcome depends on patients' age, tumor location, histotype and grade. Moreover, the optimal management of glioma patients, especially those diagnosed as LGGs, remains uncertain. In particular, the timing and extent of resection and its impact on survival are controversial. In this view the possibility to find a biomarker able to predict anaplastic transformation appears of great interest since it allows a better stratification and management of patients with significant improvements in their survival. Further experiments are needed to confirm the role of TSPO as predictive marker of transformation. In particular, we are assessing TSPO expression both as protein and mRNA levels in low grade glioma patients samples who recurred over time to better investigate if the higher expression would correlate with anaplastic transformation.

4.5 TSPO in neuroinflammation

BV2 are an immortalised murine microglial cell line that has been shown to exhibit both phenotypic and functional properties of reactive microglial cells. BV2 cells have been shown to express functional properties of activated microglia on endotoxin stimulation and thus provide a suitable model for studying inflammation. LPS is the most widely used molecule for M1 macrophage-like cells activation and it is able to simulate the activation of microglia. The use of LPS stimulation on BV2 cells have been demonstrated to be a good cellular model for screening potential therapeutic compounds for neuroinflammatory disorders.
The main aim of this preliminary study is to establish whether TSPO is directly linked with the presence of the M1 classification of microglial phenotype induced with LPS treatment using the BV2 cell line as model.

4.5.1 Materials and methods

4.5.1.1 Cell line culture and reagents

The transformed C57BL/6 mouse microglial cell line (BV2) was purchased from the Biological Bank and Cell Factory in Genoa, Italy (accession number ICLC ATL03001). Cells were cultured in Dulbecco's modified Eagle's medium (DMEM) supplemented by 10% of filtered heat inactivated foetal bovine serum (FBS), sodium pyruvate (1 mM), L-glutamine (2 mM), streptomycin (50 μg/mL) + penicillin (50U/mL) in a humidified incubator at 37°C with 5% CO_2.

4.5.1.2 Cell line experiments

Experiments were conducted between the 3rd and the 7th passages. Cells were plated at 5 x 10^6 per 25 cm^2 flask for 24 hours and left to adhere. On the next day, the media was changed to DMEM culture media without serum after 2 washes with sterile PBS (Phosphate Buffered Saline) and incubated for another 24 hours. Simulation with 0.5μg/mL of LPS (Lipopolysaccarides; Escherichia coli 0111:B4; from SIGMA,

Saint-Louis, Missouri, USA), mouse Interferon-γ (INF-γ; Miltenyi Biotec UK, Bisley, UK) or 50µg of PK11195 (SIGMA) were started the following day. Cells were stimulated for 4 hours. After stimulation, the cells were scrapped off instead of being trypsinised and washed twice before the pellet was snap frozen on dry ice and store at -20°C for RNA extraction. Media from experiments was also collected for ELISA.

4.5.1.3 RNA isolation and Quantitative Real Time PCR (qPCR)

RNA from BV2 cells was extracted using the Absolutely RNA Miniprep Kit from Agilent following the manufacturer's instructions; RNA samples were stored at -20°C until further use. Total RNA was extracted from dissected snap-frozen human tissue (< 100 mg) according to an optimised protocol (Durrenberger et al., 2010) using the RNeasy® tissue lipid mini kit (Qiagen Ltd, Crawley, UK) and samples were stored at -80°C. RNA concentration and purity was assessed by spectrophotometry (NanoDrop ND1000; NanoDrop Technologies, Delaware, USA). RNA integrity was further assessed using the Agilent 2100 Bioanalyzer. Sample concentration, the 28S/18S ribosomal ratio, and the RIN values were automatically calculated with the system software. Expression of murine TSPO and TNF was assessed with the two-step real-time reverse transcriptase quantitative polymerase chain reaction (qPCR). qPCR was performed using the QuantiTect® reverse transcription kit including genomic DNA removal step and the Brillant® II QPCR master mix. For each sample, 20 µl reactions were set up in duplicate, with each reaction containing 10 µl of 2X master mix, 2 µl of primetime assay, 7 µl of RNase-free water and 1 µl template cDNA. Reactions were carried out with the following cycling protocol: 95°C for 10 min, then 50 cycles with a 2-step program (95°C for 15 s, 60°C for 60 s). Fluorescence data collection was performed during the annealing step. Expression levels of target genes were normalised to the levels of the novel Xpnpep1 [X-prolyl aminopeptidase (aminopeptidase P) 1] reference gene and the more commonly used normaliser gene GAPDH and calibrated utilising a standard curve method for quantitation. The standard curve was used to determine relative quantity expression values for each target gene after qPCR analysis of each test specimen.

4.5.1.4 siRNA transfection

Antisense oligonucleotide sequences for Tspo silencing are reported in Table 2 and were purchased from SIGMA. Manufacturers' protocol was followed. Efficiency of each antisense and the three antisense in pool was first established (data not shown). Cells were plated at 1 x 10^5/wells in a 6-plate-well cultured to 50-70% confluency. Culture media was removed and cells were washed twice with serum-free and antibiotics-free MEM. DNA/liposome (EscortTM IV Transfection Reagent from SIGMA) complex was prepared 45 minutes prior application at a ration 1:1 in serum-free and antibiotics-free MEM and left to incubate for 5 hours under standard culture conditions. Standard culture media was then added and cells were left to incubate overnight. The cells were assayed over a period of days post-transfection (1 to 5 days). Reporter gene product expression was evaluated at regular interval (each day) to assess the efficiency of silencing and the optimal interval to perform experiments. Scrambled control siRNA (MISSION siRNA Universal Negative Control SIC-001; SIGMA) and a positive control (Gapdh) were used.

4.5.2 Results

4.5.2.1 Assessment of baseline Tspo expression

We first evaluated cell proliferation rate under conditions using various concentration of fetal bovine serum (0, 2, 5 and 10 % respectively) over a 4-day culture time course (0, 1, 2, 3 and 4 days). The use of 10% of foetal bovine serum (FBS) led to most rapid growth over 4 days, while 5% and 2% led to respectively less. There was no growth with 0% FBS. At the 3-day time-point, we measured TSPO mRNA expression at the following FBS concentration 10%, 5% and 2% using BV2 cells cultured in 10% FBS at time-point 0 as a baseline. TSPO expression levels remained constant over 3 days with a 10% FBS supplemented media. However, reduced FBS concentrations (5% and 2%) showed a reduction in TSPO expression levels compared to 10%. The purpose of this experiment was not to establish a link between TSPO endogenous levels and cell proliferation, but to highlight in BV2 cells TSPO expression levels fluctuations due to experimental manipulations. We opted to use TSPO expression levels at time point 0 cultured with 10% FBS as baseline for our first experiment.

4.5.2.2 TSPO expression following activation with LPS and INF-γ

We first treated BV2 cells with LPS at the concentration of 0.5µg/mL for 0.5, 2, 4 and 8 hours to determine optimal expression of TSPO and TNF mRNA level. TNF mRNA expression significantly increased after LPS stimulation with a peak at 2 hours. Levels remained high for 8 hours but decreased gradually over the time (Figure 38). TNF levels without LPS stimulation remained constant over the time course although lower than the cells in growth media.

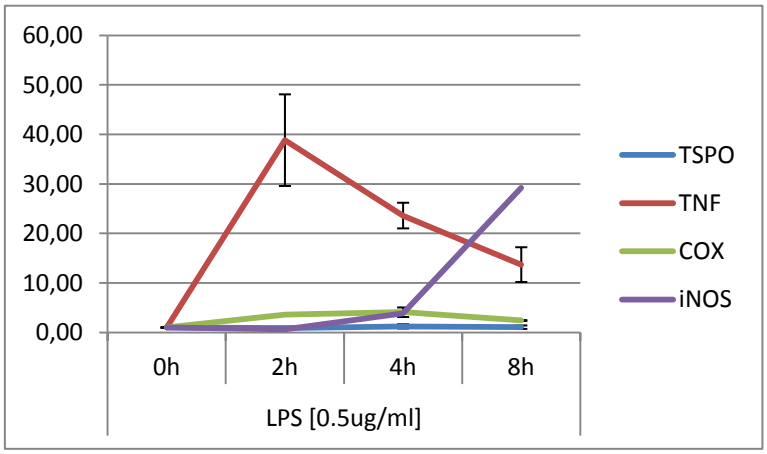

Figure 38 *Temporal TSPO, TNF, COX and iNOS mRNA expression profiling after LPS activation of BV2 microglial cells.*

In contrast, TSPO expression (Figure 37) was not significantly altered by LPS stimulation over time as no difference in TSPO expression was also detected between LPS treated cells and non-LPS treated cells.

We tested another commonly used stimulator agent within the M1 classical activation model: INF-γ. To establish most effective interferon-γ dose, we stimulated BV2 cells for 4 hours with 0, 1, 5, 25 and 125 ng/mL. Although some differences in the mean of TSPO expression levels were detected between serum conditions, the difference was no statistically significant. Similarly, no individual differences on TNF expression were detected despite a weak overall significant effect.

4.5.2.3 PK11195 and LPS treatment

The TSPO antagonist PK11195 was previously found to reduce TNF in a model of human embryonic microglia [109]. We therefore aimed to investigate the effect of PK11195 on TNF expression in BV2 cells. Presence of FBS (10%) did not interfere with mRNA expression level of TNF and TSPO. Expression levels of mRNA remained unchanged following LPS stimulation but also with the presence of PK11195 (Figure 37). TNF mRNA expression levels confirmed that the BV2 cells responded as expected since our findings were similar as those found in human embryonic microglia [109]. PK11195 did not have any modulatory effect on TSPO nor on TNF mRNA expression in BV2 murine microglia. Similar results were found with interferon-γ treatment (Figure 38).

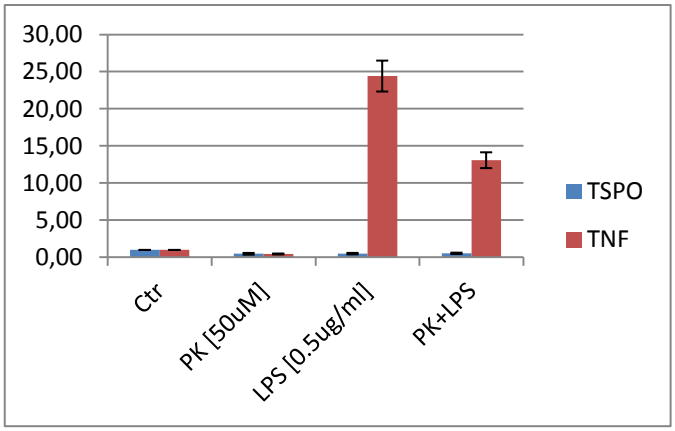

Figure 38 *TSPO and mRNA expression levels after LPS activation of BV2 microglial cells cultured in presence of PK11195.*

4.5.2.4 TSPO expression following siRNA silencing

To understand if TSPO plays a role in the regulation of neuroinflammation, we silenced TSPO using siRNA. We first conducted a time course to establish the efficiency over time of the knockdown. To that effect, we transfected cells plated in 6-well plates and measured TSPO mRNA expression levels one, 2, 3, 4 and 5 days post-transfection. TSPO mRNA remained reduced for 3 days post transfection before recovering to near basal levels (Figure 39A).

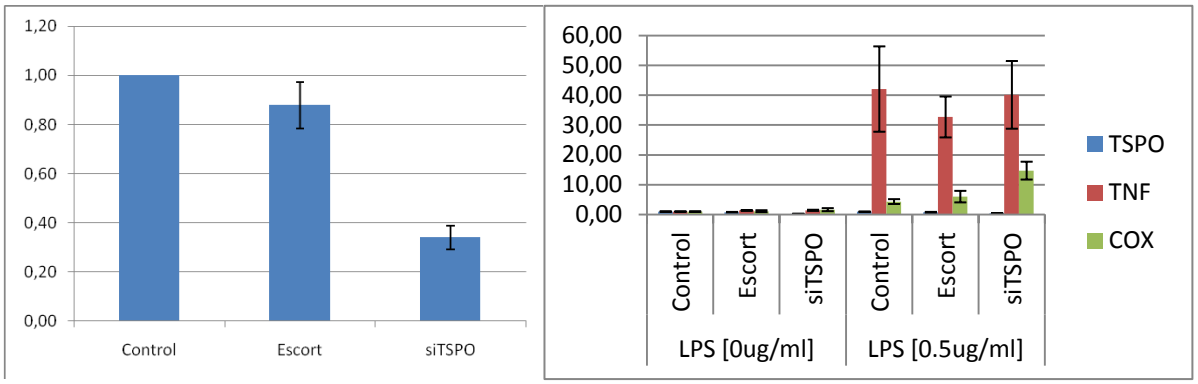

Figure 39 A) *TSPO expression levels after silencing.* ***B)*** *TSPO, TNF and COX mRNA expression profiling after TSPO silencing and LPS activation of BV2 microglial cells.*

After LPS stimulation, TSPO showed no increase in controls. On the contrary, TNF mRNA expression levels increased dramatically after LPS stimulation as previously demonstrated herein and were not statistically altered when TSPO was silenced, suggesting that TNF expression may be not directly regulated by TSPO.

From these preliminary results it seems that TSPO after LPS stimulation does not show the response curve as the classical M1 pro-inflammatory cytokine release. Moreover, TNF increase in the same way in presence or in absence of TSPO after LPS treatment. Further experiments are needed in particular to investigate TSPO modulation after prolonged exposure to LPS. Indeed, as demonstrated by others, when BV2 cells are treated with LPS for 24 hours TSPO mRNA expression levels significantly increase [109]. For this reason, our results may suggest that PET with TSPO tracers is not always representative of the M1 inflammatory response but have to be better elucidated with more experiments that are now ongoing.

4.6 Discussion

Hypoxia plays a crucial role in tumor growth and progression and is involved in the development of aggressive phenotype and therapy resistance. Hence, hypoxia is considered a promising target for therapies of several human cancers characterized by the presence of hypoxic and necrotic areas, such as glioblastoma. The master regulator of hypoxia is represented by HIF-1α and its activity has been strictly related to hypoxia onset in malignant tissues contributing to cancer growth and progression.

Molecular imaging techniques - based on the use of optical imaging, MRI and PET - allow the non-invasive investigation of cancer-related processes in preclinical models through longitudinal studies, providing a direct link between *in vitro* and clinical studies. In this way, *in vivo* techniques represent an intriguing way to investigate biomarkers of tumor responses to therapies, allowing to stratify patients that really benefit from a specific treatment and avoid ineffective drug administration. The possibility of combining techniques directly transferable in clinical settings, as MRI and PET to optical imaging, augments the usefulness of molecular imaging as a unique tool to investigate cancers.

In this study, the glioblastoma model obtained using a glioma cell line expressing luciferase enzyme under the control of HRE and mCherry under the control of a constitutive promoter has been characterized both *in vitro* and *in vivo*.

U251-HRE glioblastoma model is a brain tumor model that reproduces the biological behaviour of human GBM and is therefore of particular interest for the preclinical evaluation of novel therapeutic approaches. The multimodal imaging approach used in this study allows in first instance to further evaluate different GBM features and, subsequently, to assess hypoxia modulation and cell proliferation as potential biomarkers of tumor response to TMZ therapy.

The link between luciferase activity and hypoxia in U251-HRE cells have been already demonstrated by Rapisarda et al [101]. Both our *in vitro* and *in vivo* BLI and FLI data confirmed these findings, demonstrating that luciferase activity in U251-HRE cell line is strictly dependent on HIF-1α activation, differently from U251-pLG3.Post mortem analyses were also performed to further validate the model, revealing the presence of luciferase and HIF-1α positive staining co localizing in adjacent sections.

MRI and PET imaging with [^{18}F]FDG, [^{18}F]FLT and [^{18}F]FAZA have been performed to better characterize the glioma model investigating glucose metabolism, proliferation and hypoxia and, at the same time, exploiting the potential transferability of these techniques in clinical setting. It is well known that in clinical research and practice glioblastoma lesions display high glucose metabolism and [^{18}F]FDG uptake positively correlates with tumor grade. Differently from this typical glioma behaviour previously shown also in preclinical models [88], in our study [^{18}F]FDG PET revealed poor glycolytic lesions as depicted by the low levels of uptake close to normal brain tissue. This discrepancy can be probably related to the low spatial resolution of the tomograph in detecting tracers with high background in the brain.

On the contrary, GBM lesions displayed high proliferative tumors, with a clearly detectable uptake of [^{18}F]FLT already from the early time point. The high proliferation rate of tumors was also confirmed by IHC staining with Ki67 marker.

Finally, PET with [^{18}F]FAZA has been performed to better assess hypoxia within tumors. [^{18}F]FAZA PET revealed large hypoxic areas only at the later time point with a good T/B ratio. Although the majority of clinical studies in patients were performed using [18F]MISO as radioligand, [^{18}F]FAZA has been already used on patients with GBM, reporting T/B ratio values ranging between 1.9 and 15.6 and in few preclinical models, including GBM, revealing a good ability to detect lesions with high T/B values [102, 94].

Combining TMZ and radiotherapy represents the gold standard for GBM treatment and seems to improve patients' survival, as demonstrated in several clinical studies. Although the large use of TMZ for GBM treatment, tumor frequently recurs and mortality is still high. For these reasons, further efforts to better investigate TMZ effects and the pathways involved in its action are needed.

Our preliminary *in vitro* data suggested that TMZ treatment results in a modulation of HIF-1α activity, as already presented by Persano and colleagues. Moreover, although the underlying mechanism is not still clear, it has been postulated that counteracting HIF-1α stability would enhance TMZ sensitivity. In the current study, mice orthotopically injected with U251-HRE-mCherry glioma cells were evaluated *in vivo* to investigate HIF-1α modulation after two different regimens of TMZ. Optical and fluorescence imaging were associated to MRI and [^{18}F]FLT PET performed at different time points after cells injection. HIF-1α activity resulted clearly decreased already after two days of treatment, as depicted by BLI analyses. On the other hand, mCherry revealed a decrease of fluorescence signal only at later time, suggesting the role of HIF-1α-dependent Luciferase activity as a potential biomarker of TMZ efficacy in this GBM model. Moerover, by using HypoxiSense probe FLI imaging revealed a decrease of signal from the early time point and a later decrease of integrine expression as observed using IntegriSense probe.

To further verify the role of HIF-1α as a prognostic marker of response to TMZ with a direct applicability in clinic, PET with [^{18}F]FLT was performed assessing cell proliferation over time in comparison to HIF-1α-dependent Luciferase activity. PET tracers based on precursor of DNA synthesis, as [^{18}F]FLT, act as surrogate markers of proliferation, measuring the activity of the TK-1 enzyme in the salvage pathway for nucleotides production. Many studies revealed the usefulness of [^{18}F]FLT PET in the early detection of tumor response to therapy with a good correlation with the histological marker of proliferation Ki67. The presence of the *de novo* thymidine pathway utilization may determine an underestimation of the proliferation rate and it have to be kept into account when FLT is used to evaluate proliferation. In fact, as demonstrated by Mc Kinley and colleagues [103], de novo pathway is complementary to salvage pathway and is able to provide all the thymidine needed for DNA synthesis through the activity of the thymidylate synthase (TS). However, [^{18}F]FLT PET has been demonstrated a good imaging biomarker for an early readout of tumor response to TMZ therapy in glioma models [88, 89, 104]. Corroyer-Dulmont and colleagues demonstrated the highest sensitivity of [^{18}F]FLT PET in detecting changes due to the anti-proliferative treatment compared

to MRI [88]. Moreover, in other glioblastoma models, [^{18}F]FLT is shown a good prognostic indicator for the variation of the tumor size seen at later time points [89].

In the current study, [^{18}F]FLT images revealed a decrease of proliferation at the late time point correlating with mCherry data and thus providing a comparison between cell viability and proliferation index. Our insights are corroborated by the work of Mittra and colleagues, which demonstrated BLI as a more sensitive tool to detect tumor onset and predict glioma response to therapy earlier than [^{18}F]FLT PET [105].

Moreover, we choose to use [^{18}F]FLT PET to investigate the modulation triggered by TMZ instead of a specific hypoxia marker that could be easier to compare with the other imaging techniques used. In fact, at the temporal window chosen to perform treatments, hypoxia modulation was finely monitored *in vivo* by BLI while [^{18}F]FAZA uptake was poor and not representative of hypoxia levels. Moreover, since [^{18}F]FLT is extensively validated and used in clinic to monitor glioma grading and early response to treatment, the use of this tracer as an indicator of tumor response to therapy appears more specific.

This different ability to detect TMZ effects during time outlined by BLI and [^{18}F]FLT PET is given by the fact the optical imaging reports directly about HIF-1α activity, while [^{18}F]FLT SUV is related to cell proliferation. Taking this in mind, our results suggest that the reduction of HIF-1α activity is an earlier event compared to the reduction of cell viability and proliferation. Indeed, HIF-1α is closely linked to proliferation since it is known that HIF-1α is responsible of leading tumor malignant progression and has a key role in increasing proliferation.

Overall, this study indicates BLI and PET as two complementary *in vivo* techniques useful to characterize the U251-HRE-mCherry cell model and evaluate HIF-1α activity and cell proliferation after treatment, allowing the identification of HIF-1α and FLT as potential biomarkers of tumour response to anti-cancer treatments.

Moreover, the preliminary results obtained on human samples demonstrated a potential role of TSPO expression as marker of glioma transformation. The differential TSPO expression in low and high grade gliomas can be exploited for PET imaging with TSPO tracers in the management of these patients.

5. CONCLUSION

In conclusion, this thesis proposes PET imaging as sensitive and useful technique for the early assessment and monitoring of changes in metabolic processes due to treatments in cancer.

We define the feasibility of the use of [^{18}F]FDG and [^{18}F]FLT PET as a sensitive method to monitor the metabolic alterations occurring in NIH-RAS fibroblasts, an established cell model of transformation, with the final aim to use this model for treatment effects evaluation.

Firstly, we monitored tumor growth over time with caliper measurement and longitudinal PET scan acquisitions. NIH-RAS cells gave rise to fast growing and aggressive tumors in all mice considered. We observed a sudden increase in glucose metabolism over time and a stable and constant uptake of [^{18}F]FLT, confirming, even if indirectly, the glutamine's dependence for growth of NIH-RAS cells found *in vitro*. Subsequently, taking advantage from these observations, we investigated the role of PET imaging in early detection of tumor response to therapy. Mice bearing NIH-RAS tumors were treated with a glutaminase inhibitor and an autophagy blocker for 48 hours focusing on the time window characterized by the increased glucose uptake. The association of treatments provided a slight slowdown of tumor growth if compared to not treated animals, but no differences in glucose metabolism and cell proliferation were found with [^{18}F]FDG and [^{18}F]FLT PET. Further studies will be essential to better investigate the discrepancy between *in vivo* and *in vitro* results. Proteomic and metabolomic studies may be useful to understand treatments mechanism and validate PET data and, thus, connect molecular changes to metabolic processes. We postulated that NIH-RAS cells being representative of highly aggressive human tumors displaying ras mutations, represent a good model to study treatments effects over time, but may need higher doses of drugs.

In this thesis we also investigated the modulation of HIF-1α after treatment in a glioblastoma model obtained through the intra cranial injection of U251-HRE-mCherry glioma cell lines expressing Luciferase under the control of HRE and mCherry under the control of a constitutive promoter with a multimodal imaging approach involving optical imaging, magnetic resonance and PET. Tumor progression monitored comparing bioluminescence, fluorescence and PET with [^{18}F]FAZA and [^{18}F]FLT revealed the presence of proliferating tumors displaying large areas of hypoxia establishing progressively over time. Temozolomide treatment triggered a decrease of HIF-1α-dependent Luciferase activity at early time after Temozolomide administration as depicted by BLI images, while mCherry fluorescence and [^{18}F]FLT uptake decreased only at the end of treatments, supporting the hypothesis that cell death after Temozolomide is a delayed event preceded by the modulation of several intracellular pathways involving HIF-1α activity. This study suggests that the U251-HRE-mCherry cell model can be employed to evaluate HIF-1α activity and treatment effects in *in vivo* studies. Further analyses will be carried out on other or patient-derived cell lines to assess if the reduction of HIF-1α activity after TMZ treatment is detected also in these cells in relation to treatment response.

BIBLIOGRAPHY

1. Hanahan D, Weinberg RA. *The hallmarks of cancer*. Cell. 2000;100(1):57-70.
2. Hanahan D, Weinberg RA. *Hallmarks of cancer: the next generation*. Cell. 2011;144(5):646-74.
3. White E, DiPaola RS. *The double-edged sword of autophagy modulation in cancer*. Clin Cancer Res. 2009;15(17):5308-16.
4. Grivennikov SI, Greten FR, Karin M. *Immunity, inflammation, and cancer*. Cell. 2010;140(6):883-99.
5. Raynaud CM, Hernandez J, Llorca FP, et al. *DNA damage repair and telomere length in normal breast, preneoplastic lesions, and invasive cancer*. Am J Clin Oncol. 2010;33(4):341-5.
6. Hanahan D, Folkman J. *Patterns and emerging mechanisms of the angiogenic switch during tumorigenesis*. Cell. 1996;86(3):353-64.
7. Baeriswyl V, Christofori G. *The angiogenic switch in carcinogenesis*. Semin Cancer Biol. 2009;19(5):329-37.
8. Ward PS, Thompson CB. *Metabolic reprogramming: a cancer hallmark even Warburg did not anticipate*. Cancer Cell. 2012;21(3):297-308.
9. Gatenby RA, Gawlinski ET, Gmitro AF, Kaylor B, Gillies RJ. *Acid-mediated tumor invasion: a multidisciplinary study.* Cancer Res. 2006 May 15;66(10):5216-23.
10. Vander Heiden MG, Cantley LC, Thompson CB. *Understanding the Warburg effect: the metabolic requirements of cell proliferation*. Science. 2009;324(5930):1029-33.
11. Riganti C, Gazzano E, Polimeni M, Aldieri E, Ghigo D. *The pentose phosphate pathway: an antioxidant defense and a crossroad in tumor cell fate*. Free Radic Biol Med. 2012;53(3):421-36.
12. DeBerardinis RJ, Lum JJ, Hatzivassiliou G, Thompson CB. *The biology of cancer: metabolic reprogramming fuels cell growth and proliferation. Cell Metab*. 2008;7(1):11-20.
13. Moreno-Sánchez R, Rodríguez-Enríquez S, Marín-Hernández A, Saavedra E. *Energy metabolism in tumor cells*. FEBS J. 2007;274(6):1393-418.
14. DeBerardinis RJ, Cheng T. *Q's next: the diverse functions of glutamine in metabolism, cell biology and cancer*. Oncogene. 2010;29(3):313-24.
15. Sciacovelli M, Gaude E, Hilvo M, Frezza C. *The metabolic alterations of cancer cells*. Meth Enzymol. 2014;542:1-23.
16. Fendt SM, Bell EL, Keibler MA, et al. *Reductive glutamine metabolism is a function of the α-ketoglutarate to citrate ratio in cells*. Nat Commun. 2013;4:2236.
17. Metallo CM, Gameiro PA, Bell EL, et al. *Reductive glutamine metabolism by IDH1 mediates lipogenesis under hypoxia*. Nature. 2012;481(7381):380-4.
18. Vivanco I, Sawyers CL. *The phosphatidylinositol 3-Kinase AKT pathway in human cancer*. Nat Rev Cancer. 2002;2(7):489-501.
19. Vaupel P, Mayer A. *Hypoxia in cancer: significance and impact on clinical outcome.*Cancer Metastasis Rev. 2007 Jun;26(2):225-39. Review.

20. Semenza GL. *Defining the role of hypoxia-inducible factor 1 in cancer biology and therapeutics*. Oncogene. 2010;29(5):625-34.
21. Semenza GL. *HIF-1: upstream and downstream of cancer metabolism*. Curr Opin Genet Dev. 2010;20(1):51-6.
22. Wise DR, DeBerardinis RJ, Mancuso A, et al. *Myc regulates a transcriptional program that stimulates mitochondrial glutaminolysis and leads to glutamine addiction*. Proc Natl Acad Sci USA. 2008;105(48):18782-7.
23. Konstantinopoulos PA, Karamouzis MV, Papavassiliou AG.*Post-translational modifications and regulation of the RAS superfamily of GTPases as anticancer targets.*Nat Rev Drug Discov. 2007 Jul;6(7):541-55.
24. Rudin M, Weissleder R. *Molcular Imaging in drug discovery and development.* Nature Reviews. 2013.
25. De Jong M, Essers J, Weerden WM. *Imaging preclinical tumor models: improving translational power*. Nature Reviews, 2014.
26. Cherry SR. *The 2006 Henry N. Wagner Lecture: Of mice and men (and positrons)--advances in PET imaging technology*. J Nucl Med. 2006;47(11):1735-45.
27. Gambhir SS. *Molecular imaging of cancer with positron emission tomography*. Nat Rev Cancer. 2002;2(9):683-93.
28. Basu S, Kwee TC, Surti S, Akin EA, Yoo D, Alavi A. *Fundamentals of PET and PET/CT imaging*. Ann N Y Acad Sci. 2011;1228:1-18.
29. Peng BH, Levin CS. *Recent development in PET instrumentation*. Curr Pharm Biotechnol. 2010;11(6):555-71.
30. Bar-Shalom R, Valdivia AY, Blaufox MD.*PET imaging in oncology.*Semin Nucl Med. 2000 Jul;30(3):150-85.
31. Lucignani G, Schmidt KC, Moresco RM, Striano G, Colombo F, Sokoloff L, Fazio F. *Measurement of regional cerebral glucose utilization with fluorine-18-FDG and PET in heterogeneous tissues: theoretical considerations and practical procedure.*J Nucl Med. 1993 Mar;34(3):360-9.
32. Kristian A, Revheim ME, Qu H, et al. *Dynamic (18)F-FDG-PET for monitoring treatment effect following anti-angiogenic therapy in triple-negative breast cancer xenografts*. Acta Oncol. 2013;52(7):1566-72.
33. Munk Jensen M, Erichsen KD, Björkling F, et al. *Imaging of treatment response to the combination of carboplatin and paclitaxel in human ovarian cancer xenograft tumors in mice using FDG and FLT PET*. PLoS ONE. 2013;8(12):e85126.
34. Brepoels L, Stroobants S, Verhoef G, De groot T, Mortelmans L, De wolf-peeters C. *(18)F-FDG and (18)F-FLT uptake early after cyclophosphamide and mTOR inhibition in an experimental lymphoma model*. J Nucl Med. 2009;50(7):1102-9.
35. Krause BJ, Herrmann K, Wieder H, Zum büschenfelde CM. *18F-FDG PET and 18F-FLT PET/CT for assessing response to therapy in esophageal cancer*. J Nucl Med. 2009;50 Suppl 1:89S-96S.

36. Farwell MD, Pryma DA, Mankoff DA. *PET/CT imaging in cancer: Current applications and future directions*. Cancer. 2014.
37. Garcia C, Gebhart G, Flamen P.*New PET imaging agents in the management of solid cancers.*Curr Opin Oncol. 2012 Nov;24(6):748-55.
38. Barthel H, Cleij MC, Collingridge DR, et al. *3'-deoxy-3'-[18F]fluorothymidine as a new marker for monitoring tumor response to antiproliferative therapy in vivo with positron emission tomography*. Cancer Res. 2003;63(13):3791-8.
39. Salskov A, Tammisetti VS, Grierson J, Vesselle H. *FLT: measuring tumor cell proliferation in vivo with positron emission tomography and 3'-deoxy-3'-[18F]fluorothymidine*. Semin Nucl Med. 2007;37(6):429-39.
40. Keen H, Pichler B, Kukuk D, Duchamp O, Raguin O, Shannon A, Whalley N, Jacobs V, Bales J, Gingles N, Ricketts SA, Wedge SR. *An evaluation of 2-deoxy-2-[18F]fluoro-D-glucose and 3'-deoxy-3'-[18F]-fluorothymidine uptake in human tumor xenograft models.*Mol Imaging Biol. 2012 Jun;14(3):355-65.
41. Everitt SJ, Ball DL, Hicks RJ, Callahan J, Plumridge N, Collins M, Herschtal A, Binns D, Kron T, Schneider M, MacManus M. *Differential 18F-FDG and 18F-FLT Uptake on Serial PET/CT Imaging Before and During Definitive Chemoradiation for Non-Small Cell Lung Cancer*.J Nucl Med. 2014 May 15;55(7):1069-1074.
42. Chen W, Cloughesy T, Kamdar N, et al. *Imaging proliferation in brain tumors with 18F-FLT PET: comparison with 18F-FDG.* J Nucl Med. 2005 Jun;46(6):945-52.
43. Pio BS, Park CK, Pietras R, et al. *Usefulness of 3'-[F-18]fluoro-3'-deoxythymidine with positron emission tomography in predicting breast cancer response to therapy*. Mol Imaging Biol. 2006;8(1):36-42.
44. Zhang CC, Yan Z, Li W, Kuszpit K, Painter CL, Zhang Q, Lappin PB, Nichols T, Lira ME, Affolter T, Fahey NR, Cullinane C, Spilker M, Zasadny K, O'Brien P, Buckman D, Wong A, Christensen JG. [*(18)F]FLT-PET imaging does not always "light up" proliferating tumor cells.*Clin Cancer Res. 2012 Mar 1;18(5):1303-12.
45. Wester HJ. *Nuclear imaging probes; from bench to bedside.* Clin Cancer Research 2007; 12(12).
46. Wu C, Li F, Niu G, Chen X. *PET imaging of inflammation biomarkers.* Theranostics, 2013; 3(7):448-466.
47. Konstantinopoulos PA, Karamouzis MV, Papavassiliou AG. *Post-translational modifications and regulation of the RAS superfamily of GTPases as anticancer targets*. Nat Rev Drug Discov. 2007;6(7):541-55.
48. Kompier LC, Lurkin I, Van der aa MN, Van rhijn BW, Van der kwast TH, Zwarthoff EC. *FGFR3, HRAS, KRAS, NRAS and PIK3CA mutations in bladder cancer and their potential as biomarkers for surveillance and therapy*. PLoS ONE. 2010;5(11):e13821.

49. Kim MJ, Woo SJ, Yoon CH, et al. *Involvement of autophagy in oncogenic K-Ras-induced malignant cell transformation*. J Biol Chem. 2011;286(15):12924-32.
50. Levine B, Kroemer G. *Autophagy in the pathogenesis of disease*. Cell. 2008;132(1):27-42.
51. Guo JY, Chen HY, Mathew R, et al. *Activated Ras requires autophagy to maintain oxidative metabolism and tumorigenesis*. Genes Dev. 2011;25(5):460-70.
52. Bossù P, Vanoni M, Wanke V, et al. *A dominant negative RAS-specific guanine nucleotide exchange factor reverses neoplastic phenotype in K-ras transformed mouse fibroblasts*. Oncogene. 2000;19(17):2147-54.
53. Chiaradonna F, Gaglio D, Vanoni M, Alberghina L. *Expression of transforming K-Ras oncogene affects mitochondrial function and morphology in mouse fibroblasts*. Biochim Biophys Acta. 2006a;1757(9-10):1338-56.
54. Gaglio D, Soldati C, Vanoni M, Alberghina L, Chiaradonna F. *Glutamine deprivation induces abortive s-phase rescued by deoxyribonucleotides in k-ras transformed fibroblasts*. PLoS ONE. 2009;4(3):e4715.
55. Gaglio D, Metallo CM, Gameiro PA, et al. *Oncogenic K-Ras decouples glucose and glutamine metabolism to support cancer cell growth*. Mol Syst Biol. 2011;7:523.
56. Alberghina L, Gaglio D, Gelfi C, Moresco RM, Mauri G, Bertolazzi P, Messa C, Gilardi MC, Chiaradonna F, Vanoni M. Cancer cell growth and survival as a system-level property sustained by enhanced glycolysis and mitochondrial metabolic remodeling.Front Physiol. 2012 Sep 12;3:362.
57. Oldiges M, Lütz S, Pflug S, Schroer K, Stein N, Wiendahl C. *Metabolomics: current state and evolving methodologies and tools.*Appl Microbiol Biotechnol. 2007 Sep;76(3):495-511.
58. Gallagher FA, Kettunen MI, Day SE, Lerche M, Brindle KM. *13C MR spectroscopy measurements of glutaminase activity in human hepatocellular carcinoma cells using hyperpolarized 13C-labeled glutamine.*Magn Reson Med. 2008 Aug;60(2):253-7.
59. Qu W, Oya S, Lieberman BP, Ploessl K, Wang L, Wise DR, Divgi CR, Chodosh LA, Thompson CB, Kung HF. *Preparation and characterization of L-[5-11C]-glutamine for metabolic imaging of tumors.*J Nucl Med. 2012 Jan;53(1):98-105.
60. Shukla K, Ferraris DV, Thomas AG, et al. *Design, synthesis, and pharmacological evaluation of bis-2-(5-phenylacetamido-1,2,4-thiadiazol-2-yl)ethyl sulfide 3 (BPTES) analogs as glutaminase inhibitors*. J Med Chem. 2012;55(23):10551-63.
61. Emadi A, Jun SA, Tsukamoto T, Fathi AT, Minden MD, Dang CV. *Inhibition of glutaminase selectively suppresses the growth of primary acute myeloid leukemia cells with IDH mutations*. Exp Hematol. 2014;42(4):247-51.
62. Le A, Lane AN, Hamaker M, Bose S, Gouw A, Barbi J, Tsukamoto T, Rojas CJ, Slusher BS, Zhang H, Zimmerman LJ, Liebler DC, Slebos RJ, Lorkiewicz PK, Higashi RM, Fan TW, Dang CV.*Glucose-independent glutamine metabolism via TCA cycling for proliferation and survival in B cells.* Cell Metab. 2012 Jan 4.
63. Lozy F, Karantza V. *Autophagy and cancer cell metabolism*. Semin Cell Dev Biol. 2012;23(4):395-401.

64. Morgan MJ, Gamez G, Menke C, Hernandez A, Thorburn J, Gidan F, Staskiewicz L, Morgan S, Cummings C, Maycotte P, Thorburn A. *Regulation of autophagy and chloroquine sensitivity by oncogenic RAS in vitro is context-dependent.*Autophagy. 2014 Oct 1;10(10):1814-26.
65. Amaravadi RK, Yu D, Lum JJ, et al. *Autophagy inhibition enhances therapy-induced apoptosis in a Myc-induced model of lymphoma*. J Clin Invest. 2007;117(2):326-36.
66. Kaneko M, Nozawa H, Hiyoshi M, et al. *Temsirolimus and chloroquine cooperatively exhibit a potent antitumor effect against colorectal cancer cells*. J Cancer Res Clin Oncol. 2014;140(5):769-81.
67. Martin SJ, Eisenbarth JA, Wagner-Utermann U, Mier W, Henze M, Pritzkow H, et al. *A new precursor for the radiosynthesis of [18F]FLT*. Nucl Med Biol 2002;29:263-73.
68. Gross MI, Demo SD, Dennison JB, Chen L, Chernov-Rogan T, Goyal B, Janes JR, Laidig GJ, Lewis ER, Li J, Mackinnon AL, Parlati F, Rodriguez ML, Shwonek PJ, Sjogren EB, Stanton TF, Wang T, Yang J, Zhao F, Bennett MK. *Antitumor activity of the glutaminase inhibitor CB-839 in triple-negative breast cancer.*Mol Cancer Ther. 2014 Apr;13(4):890-901.
69. Ratikan JA, Sayre JW, Schaue D. *Chloroquine engages the immune system to eradicate irradiated breast tumors in mice.* Int J Radiat Oncol Biol Phys. 2013 Nov 15;87 (4):761-8.
70. Zinn RL, Gardner EE, Dobromilskaya I, et al. *Combination treatment with ABT-737 and chloroquine in preclinical models of small cell lung cancer*. Mol Cancer. 2013;12:16.
71. Seront E, Boidot R, Bouzin C, Karroum O, Jordan BF, Gallez B, Machielis JP, Feron O. *Tumor hypoxia determines the potential of combining mTOR and autophagy inhibitors to treat mammary tumors.* Br J Cancer 2013 Nov 12;109(10):2597-606.
72. E.A. Maher, F.B. Furnari, R.M. Bachoo, D.H. Rowitch, D.N. Louis, W.K. Cavenee, *et al. Malignant glioma: genetics and biology of a grave matter* Genes Dev, 15 (2001).
73. Stupp R, Mason WP, van den Bent MJ, Weller M, Fisher B, Taphoorn MJ, Belanger K, Brandes AA, Marosi C, Bogdahn U, Curschmann J, Janzer RC, Ludwin SK, Gorlia T, Allgeier A, Lacombe D, Cairncross JG, Eisenhauer E, Mirimanoff RO; European Organisation for Research and Treatment of Cancer Brain Tumor and Radiotherapy Groups; *Radiotherapy plus concomitant and adjuvant temozolomide for glioblastoma.*National Cancer Institute of Canada Clinical Trials Group. N Engl J Med. 2005 Mar 10;352(10):987-96.
74. Camara-Quintana JQ, Nitta RT, Li G. *Commonly monitored glioblastoma markers: EGFR, EGFRvIII, PTEN, and MGMT*. Neurosurg Clin N Am 23 237-246, 2012.
75. Siegal T. *Clinical impact of molecular biomarkers in gliomas***.** J Clin Neurosci. 2014 Dec 18.
76. Melguizo C, Prados J, González B, Ortiz R, Concha A, Alvarez PJ, Madeddu R, Perazzoli G, Oliver JA, López R, Rodríguez-Serrano F, Aránega A. .*MGMT promoter methylation status and MGMT and CD133 immunohistochemical expression as prognostic markers in glioblastoma patients treated with temozolomide plus radiotherapy.* J Transl Med. 2012 Dec 17.

77. Rivera AL, Pelloski CE, Gilbert MR, Colman H, De La Cruz C, Sulman EP, Bekele BN, Aldape KD. *MGMT promoter methylation is predictive of response to radiotherapy and prognostic in the absence of adjuvant alkylating chemotherapy for glioblastoma.*Neuro Oncol. 2010 Feb;12(2).
78. Semenza GL, Nejfelt MK, Chi SM. *Hypoxia-inducible nuclear factors bind to an enhancer element located 3' to the human erythropoietin gene.* Proc Natl Acad Sci U S A.1991, 88(13):5680-4.
79. Vaupel P. *Hypoxia and aggressive tumor phenotype: implications for therapy and prognosis.* Oncologist, 2008;13 Suppl 3:21-6.
80. Yang L, Lin C, Wang L, Guo H, Wang X. *Hypoxia and hypoxia-inducible factors in glioblastoma multiforme progression and therapeutic implications.* Exp Cell Res. 2012 Nov 15.
81. Jensen RL. *Hypoxia in the tumourigenesis of gliomas and as a potential target for therapeutic measures.* Neurosurg Focus. 2006, 20(4):E24.
82. Ahmed R, Obroski MJ, Hwang M, Lieberman FS, Mountz JM. *Malignant gliomas: current perspectives in diagnosis, treatment, and early response assessment using advanced quantitative imaging methods.* Cancer management and research 2014:6 149-170.
83. Imani F, Boada FE, Lieberman FS, Davis DK, Deeb LK, Mountz JM. *Comparison of proton magnetic resonance spectroscopy with fluorine-18 2-fluoro-deoxyglucose positron emission tomography for assessment of brain tumors progression.* J Neuroimaging 2012;22(2) 184-190.
84. la Fougère C, Suchorska B, Bartenstein P, Kreth FW, Tonn J-C. *Molecular imaging of gliomas with PET: opportunities and limitations.* Neuro-oncology 13(8):806-819, 2011.
85. Yamamoto Y, Ono Y, Aga F, Kawai N, Kudomi N, Nishiyama Y. *Correlation of 18F-FLT uptake with tumor grade and Ki-67 immunohistochemistry in patients with newly diagnosed and recurrent gliomas.*J Nucl Med. 2012 Dec;53(12):1911-5.
86. Zhao F, Cui Y, Li M, Fu Z, Chen Z, Kong L, Yang G, Yu *Prognostic value of 3'-deoxy-3'-18F-fluorothymidine ([(18)F] FLT PET) in patients with recurrent malignant gliomas.*J. Nucl Med Biol. 2014 Sep.
87. Schwarzenberg J, Czernin J, Cloughesy TF, Ellingson BM, Pope WB, Geist C, Dahlbom M, Silverman DH, Satyamurthy N, Phelps ME, Chen W. *3'-deoxy-3'-18F-fluorothymidine PET and MRI for early survival predictions in patients with recurrent malignant glioma treated with bevacizumab.*J Nucl Med. 2012 Jan;53(1):29-36.
88. Corroyer-Dulmont A, Pérès EA, Petit E, Durand L, Marteau L, Toutain J, Divoux D, Roussel S, MacKenzie ET, Barré L, Bernaudin M, Valable S. *Noninvasive assessment of hypoxia with 3-[18F]-fluoro-1-(2-nitro-1-imidazolyl)-2-propanol ([18F]-FMISO): a PET study in two experimental models of human glioma.* Biol Chem. 2013 Apr;394(4):529-39.
89. Viel T, Schelhaas S, Wagner S, Wachsmuth L, Schwegmann K, Kuhlmann M, Faber C, Kopka K, Schäfers M, Jacobs AH. *Early assessment of the efficacy of temozolomide chemotherapy in experimental glioblastoma using [18F]FLT-PET imaging.*PLoS One. 2013 Jul 4;8(7):e67911.

90. Spence AM, Muzi M, Swanson KR, O'Sullivan F, Rockhill JK, Rajendran JG, Adamsen TC, Link JM, SwansonPE, Yagle KJ, Rostomily RC, Silbergeld DL, Krohn KA. *Regional hypoxia in glioblastoma multiforme quantified with [18F]fluoromisonidazole positron emission tomography before radiotherapy: correlation with time to progression and survival.* Clin Cancer Res. 2008 May 1;14(9):2623-30.
91. Souvatzoglou M, Grosu AL, Röper B, Krause BJ, Beck R, Reischl G, Picchio M, Machulla HJ, Wester HJ, Piert M. *Tumour hypoxia imaging with [18F]FAZA PET in head and neck cancer patients: a pilot study.* Eur J Nucl Med Mol Imaging. 2007 Oct;34(10):1566-75.
92. Grosu AL, Souvatzoglou M, Röper B, Dobritz M, Wiedenmann N, Jacob V, Wester HJ, Reischl G, Machulla HJ, Schwaiger M, Molls M, Piert M. *Hypoxia imaging with FAZA-PET and theoretical considerations with regard to dose painting for individualization of radiotherapy in patients with head and neck cancer.*Int J Radiat Oncol Biol Phys. 2007 Oct 1;69(2):541-51.
93. Postema EJ, McEwan AJ, Riauka TA, Kumar P, Richmond DA, Abrams DN, Wiebe LI. *Initial results of hypoxia imaging using 1-alpha-D:-(5-deoxy-5-[18F]-fluoroarabinofuranosyl)-2-nitroimidazole (18F-FAZA).*Eur J Nucl Med Mol Imaging.2009 Oct.
94. Belloli S, Brioschi A, Politi LS, Ronchetti F, Calderoni S, Raccagni I, Pagani A, Monterisi C, Zenga F, Zara G, Fazio F, Mauro A, Moresco RM. *Characterization of biological features of a rat F98 GBM model: a PET-MRI study with [18F]FAZA and [18F]FDG.* Nucl Med Biol. 2013 Aug;40(6):831-40.
95. Wen PY, Kesari S. *Malignant gliomas in adults.* N Engl J Med. 2008 Jul 31;359(5):492-507.
96. Kanzawa T, Germano IM, Komata T, Ito H, Kondo Y, Kondo S. *Role of autophagy in temozolomide-induced cytotoxicity for malignant glioma cells.* Cell Death Differ. 2004, Apr;11(4):448-57.
97. Natsumeda M, Aoki H, Miyahara H. *Induction of autophagy in temozolomide treated malignant gliomas.* Neuropathology. 2011;31(5):486-93.
98. Persano L, Pistollato F, Rampazzo E, Della Puppa A, Abbadi S, Frasson C et al. *BMP2 sensitizes glioblastoma stem-like cells to Temozolomide by affecting HIF-1α stability and MGMT expression.*Cell death and disease. 2012.
99. Radaelli E, Ceruti R, Patton V, Russo M, Degrassi A, Croci V, Caprera F, Stortini G, Scanziani E, Pesenti E, Alzani R. *Immunohistopathological and neuroimaging characterization of murine orthotopic xenograft models of glioblastoma multiforme recapitulating the most salient features of human disease.*Histol Histopathol. 2009 Jul;24(7):879-91.
100. Piert M, Machulla HJ, Picchio M, Reischl G, Ziegler S, Kumar P, Wester HJ, Beck R, McEwan AJ, Wiebe LI, Schwaiger M. *Hypoxia-specific tumor imaging with 18F-fluoroazomycin arabinoside.*J Nucl Med. 2005 Jan;46(1):106-13.
101. Rapisarda A, Zalek J, Hollingshead M, Braunschweig T, Uranchimeg B, Bonomi CA et al. *Schedule-dependent inhibition of hypoxia-inducible factor-1alpha protein accumulation, angiogenesis, and tumor growth by topotecan in U251-HRE glioblastoma xenografts*. Cancer Res. 2004, 64(19):6845-8.

102. Valtorta S, Belloli S, Sanvito F, Masiello V, Di Grigoli G, Monterisi C, Fazio F, Picchio M, Moresco RM. *Comparison of 18F-fluoroazomycin-arabinofuranoside and 64Cu-diacetyl-bis(N4-methylthiosemicarbazone) in preclinical models of cancer.*J Nucl Med. 2013 Jul;54(7):1106-12.

103. McKinley ET, Ayers GD, Smith RA, Saleh SA, Zhao P, Washington MK et al. *Limits of [18F]-FLT PET as biomarker of proliferation in oncology*. PLoS One. 2013, 8(3):e58938.

104. Rueger MA, Ameli M, Li H, Winkeler A, Rueckriem B, Vollmar S, Galldiks N, Hesselmann V, Fraefel C, Wienhard K, Heiss WD, Jacobs AH. *[18F]FLT PET for non-invasive monitoring of early response to gene therapy in experimental gliomas.*Mol Imaging Biol. 2011 Jun;13(3):547-57.

105. Mittra ES, Fan-Minogue H, Lin FI, Karamchandani J, Sriram V, Han M, Gambhir SS.*Preclinical efficacy of the anti-hepatocyte growth factor antibody ficlatuzumab in a mouse brain orthotopic glioma model evaluated by bioluminescence, PET, and MRI.* Clin Cancer Res. 2013 Oct 15;19(20):5711-21. Epub 2013 Aug 27.

106. Chen MK, Guilarte TR. *Translocator protein 18 kDa (TSPO): molecular sensor of brain injury and repair*. Pharmacology & Therapeutics 118 (2008) 1-17.

107. Batarseh A, Papadopoulos V. *Regulation of translocator protein 18 kDa (TSPO) expression in health and disease states.* Molecular and cellular endocrinology 327 (2010) 1-12.

108. Austin CJD, Kahlert J, Kassiou M, Rendina ML. *The translocator protein (TSPO): a novel target for chemotherapy.*The international journal of biochemistry & cell biology 45 (2013) 1212-1216.

109. Choi J, Ifuku M, Noda M, Guilarte TR. *Translocator protein (18 kDa)/peripheral benzodiazepine receptor specific ligands induce microglia functions consistent with an activated state.* Glia 59:219-230 (2011).

ABSTRACTS AND PUBLICATIONS

Proceedings at National and International meetings:

- *25th European Association of Nuclear Medicine Congress (EANM) Milan (Italy) 27-31 Ottobre 2012*: S. Valtorta, R.M. Moresco, **I. Raccagni**, G. Di Grigoli, M. Curtarello, G. Nardo, E. Zulato, S. Todde, C. Monterisi, S. Indraccolo, F. Fazio. Evaluation of response to therapy in ovarian cancer models with different glycolytic phenotype using in-vivo imaging PET.
- *25th European Association of Nuclear Medicine Congress (EANM) Milan (Italy) 27-31 Ottobre 2012*: Belloli S, Bogni A, Valtorta S, Tortoreto M, Pascali C, **Raccagni I**, Zaffaroni N, Crippa F, Fazio F, Daidone MG, Moresco RM , Bombardieri E. Monitoring preclinical model of breast cancer with [^{18}F]FLT and [^{18}F]FDG-PET
- *26th Congresso of the European Association of Nuclear Medicine Congress (EANM) Lione (Francia) 19-23 Ottobre 2013*: **I. Raccagni**, D. Gaglio, S. Valtorta, S. Belloli, G. Di Grigoli, M. Vanoni, F. Mastroianni, S. Todde, L. Alberghina, R.M. Moresco. Assessing cancer metabolic remodelling in animal models using PET imaging.
- *8th European Molecular Imaging Meeting (EMIM) Torino (Italia) 26-28 Maggio 2013.* S Valtorta, **I Raccagni**, M Curtarello, G Di Grigoli, G Nardo, E Zulato, S Todde, C Monterisi, S Indraccolo, RM Moresco. Influence of glycolytic phenotype on anti-angiogenic therapy response in ovarian cancer xenograft models evaluated by PET imaging
- *8th European Molecular Imaging Meeting (EMIM) Torino (Italia) 26-28 Maggio 2013.* S Belloli, A Bogni, S Valtorta, M Tortoreto, C Pascali, **I Raccagni,** N Zaffaroni , F Crippa, MG Daidone, RM Moresco, E Bombardieri. Monitoring preclinical model of breast cancer with [18F]FLT and [18F]FDG-PET**.**
- *European Molecular Imaging Meeting 2014, 4th-6th June 2014, Antwerp:* Belloli S, Zanotti L, Di Grigoli G, Mazzon C, Politi LS, Wang L, **Raccagni I**, Monterisi C, Masiello V, Pagani A, Moresco RM. Neuroinflammation assessment in a MS mouse model with [^{18}F]VC701-PET.
- *European Molecular Imaging Meeting 2014, 4th-6th June 2014, Antwerp*: Valtorta S, **Raccagni I,** Orsisi F, Pagliarin R, Coccetti P, Moresco RM. Validation of a new combretastatin A-4 (CA-4) analogue in a colon cancer mouse model using PET imaging.

Publications:

- *Lo Dico A, Valtorta S, Martelli C, Belloli S, Gianelli U, Tosi D, Bosari S, Degrassi A, Russo M, **Raccagni I**, Lucignani G, Moresco RM, Ottobrini L.* Validation of an Engineered Cell Model for In Vitro and In Vivo HIF-1α Evaluation by Different Imaging Modalities. Mol Imaging Biol. 2013 Sep 4.

- Belloli S, *Brioschi A, Politi LS, Ronchetti F, Calderoni S,* ***Raccagni I****, Pagani A, Monterisi C, Zenga F, Zara G, Fazio F, Mauro A, Moresco RM.* Characterization of biological features of a rat F98 GBM model: a PET-MRI study with [18F]FAZA and [18F]FDG. Nucl Med Biol. 2013 Aug;40(6):831-40.
- *Lo Dico A., Martelli C., Valtorta S.,* ***Raccagni I****., Diceglie C., Belloli S., Gianelli U., Vaira V., Politi L., Bosari S., Lucignani G., Moresco R.M, Ottobrini L.* Identification of imaging biomarkers for the assessment of tumour response to different treatments in a preclinical glioma model. Submitted to: European Journal of Nuclear Medicine and Molecular Imaging.